Stress concentrations in riveted plate girders due to fatigue loading

defining a new stress range parameter to accurate describe the life prediction of riveted bridge girders

Gremmen, Tom A.W.

Award date:
2021

Department of Built Environment
Architecture, Building and Planning

Stress Concentrations in Riveted Plate Girders due to Fatigue Loading

Defining a new stress range parameter to accurate describe the life prediction of riveted bridge girders

Ing. T.A.W. Gremmen

Supervisors:

Prof. Dr. Ir. J. Maljaars
Dr. Ir. D. Leonetti

version 3.0

Eindhoven, July 2021

Colophon

Subject: Fatigue in Rivet Connected Plate Girders.
Document: Main Thesis
University: TU/e
Author: Ing. T.A.W. Gremmen
Student number: 1244270
Graduation Committee:

First chair:
Prof. Dr. Ir. J. (Johan) Maljaars
Eindhoven University of Technology
Full Professor
Chair of Aluminum Structures

Second chair:
Dr. Ir. D. Leonetti
Eindhoven University of Technology
Assistant professor

Third chair:
Ing. R. van der Zwan
ProRail

Version 3.0

Preface

Before you lies the document containing the thesis for the graduation project *"Stress Concentration in Riveted Plate Girders due to Fatigue Loading"*. This thesis is the final document of the master Structural Engineering and Design at the Eindhoven University of Technology.

The research has been conducted under supervision of prof. dr. ir. J. Maljaars and dr. ir. D. Leonetti. I would like to thank my supervisors for their guidance and support during this research, especially for their cooperation during unprecedented times with obligated remote working.

Futhermore i'd like to thank my colleague and fellow student I. Vidimlic for the lengthy discussions to make deliberate decisions on the trajectory of the research.

I hope you enjoy your reading,

Tom Gremmen

Eindhoven, 2021

Abstract

This research main focus is fatigue of riveted bridge girders. These girders are build up of a web plate with four l-profiles serving as flange profiles. The web plate and the flange profiles are connected through rivets. When assessing fatigue data from full scale tests on riveted girders a large variance in fatigue strength can be observed. Fatigue strength is defined as the numbers of cycles to failure of the beam under a specific stress range. When there is a large variance in stress range for a set numbers of cycles to failure the fatigue life prediction also has a large variance. The aim of this research is to define a new stress range parameter which has a smaller variance in stress range, and thus can describe the fatigue life prediction in a more precise manner.

Fatigue data from existing full scale tests is collected in the literature study. In these full scale tests, the stress range is mostly defined as the net section stress range at the most outer fibre of the beam. In the research documents of these full scale tests it can be seen that the majority of the beams fail at the location where the rivet connects the plate to the flange profile, with crack initiation mostly occurring at the notches of the rivet hole.

Failure at the notches of the rivet hole can be explained by stress concentrations around these holes. The stress concentrations consists of three main components, namely bypass loading, pin loading and friction. Stress concentrations due to bypass loading is caused by disturbance of the flow of forces through the section. This disturbance is the rivet hole, causing stress concentrations at the notches of the rivet holes. Stress concentrations due to pin loading is caused by force transfer of the rivet from the web plate to the flange profile causing ovalization of the rivet hole. Friction is caused by clamping force of the hot rivet. The friction causes stress concentrations at the notches of the rivet holes due to the plates having direct force transfer through friction.

To process the collected data of full scale tests, a parametric analytical model is made. This model calculates the stress concentrations at the notches of the rivet holes of a riveted bridge girder. In this model, the dimensional parameters and forces acting on the beam of the full scale tests are filled in. The model then calculates, at each of the rivet hole notches in the beam, the maximum occurring stress. This model includes the effects of the stress concentration due to bypass loading, due to pin loading, and due to the friction between the web and the flange.

Calculation steps in the analytical model as follows. The nominal stress in the beam is calculated through Euler–Bernoulli beam theory. In this step, full cooperation between the web and the flange profile is assumed. The next step is the calculation of the distribution of forces among the rivets. All of the stress in the flange profile is transferred through the rivets. To calculate the stress concentration due to pin loading, the force transfer of each rivet is calculated. Calculation of the forces through matching the displacement of the flange profile to the web profile and calculating the forces corresponding with said displacements. After this the friction is taken into consideration. Friction is present between the web and the flange profile due to the clamping force of the hot rivet. The friction between the web and the flange will facilitate partial force transfer direct from the web to the flange instead of through the rivet. This effect is taken into account in the analytical model by lowering the force transfer in the rivet by a calculated percentage, and partially adding this transfer to the bypass loading.

After calculating the net section stress, the force transfer in the rivets, and the contribution of the friction, the effects of the stress concentrations are taken into account. For the calculation of the stress concentration at the notches, formulas proposed in Peterson's Stress Concentration Factors [20] are used. These formulas give a ratio between the nominal stress in a section, and the stress concentration around notches, taking into account the dimensions of the section and the rivet hole. The stress concentrations are calculated for each rivet.

Several numerical models are set up in ANSYS to validate the analytical model. Firstly, a global model simulating a quarter of the beam, and is used to validate the force transfer in the rivets calculated in the analytical model. This model is set up with an semi-arbitrarily chosen set of dimensions. These same dimensions are then computed in the analytical model. The force transfer of the analytical model is then validated against the results gained from the analytical model.

Secondly, a sub-model is made from the global model. In this model, a row of six rivets is sliced out of the global model, where boundary conditions from the nodes in the sub-model are imported from the global model. In this FEM analysis the rivets are modelled as full solid parts, and the mesh density is increased. In this model, the stress concentrations at the notches are validated against the results gained from the analytical model.

After validation of the analytical model, the data-set collected in the literature study is processed. Processing the data meaning: converting the existing stress range from the paper to the newly defined stress range parameter. In the collected data-set, most of the papers use the net section stress range at the most outer fiber of the beam. The analytical model calculates the stress, including stress concentrations, at each of the notches of the rivet holes. From all of these locations, the rivet hole with the highest stress concentration is taken as the new stress range. The data with the existing numbers of cycles to failure is then plotted with the newly calculated stress range parameter.

Two types of statistical analysis are conducted on the old and new data set. Firstly, the correlation coefficient between the two data-sets is computed. The unprocessed data-set, with the net section stress range parameter, has a correlation coefficient of r=-0,468. The processed data-set, with the new stress range parameter has a correlation coefficient of r=-0,446. This is a neglectable increase in correlation strength. Secondly a linear regression analysis is conducted on the two data-sets. For the unprocessed data-set, using the net section stress range, the standard deviation of C is 0,093. For the processed data-set, using the new stress range parameter, the standard deviation of C is 0,118. From the linear regression analysis it can be concluded that the data-set containing the new stress range parameter has less coherence than the old data-set using the net section stress range.

Contents

List of Figures

List of Tables

Chapter 1

Introduction

Rivets are one of the oldest types of fasteners, having been found in archaeological findings dating back to the bronze age. Rivets where the most popular fasteners during the first half of the 20th century. Currently in the construction field, riveted connections are not as common anymore, demanded manpower needed to realize these types of connections is high, and with this the costs of these connections. The use of riveted connections has steadily declined since the introduction of high-strength bolts and welding [10]. Although these types of connections are currently not used anymore in the structural field, these connections still hold a high relevance. Many old structures, mainly bridges, are built my means of these riveted connections. built in the 50's, there is a high possibility of needed maintenance of these structures due to aging and increase in loading on the bridges.

Regarding bridges, one of the most typical uses of riveted connections is for assembling plate girders. These beams are mainly used in bridges and are suitable for short to medium spans [16]. Plate girders are a type of beam that is built from different plates or profiles which are connected by rivets. In the situation of riveted plate girders., a web profile is connected to four L-profiles with rivets. This situation is shown on figure 1.1.

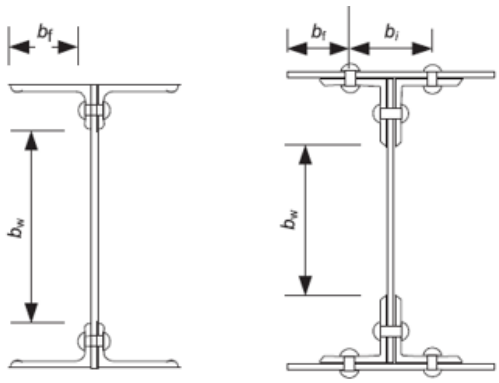

Figure 1.1: Build-up girders

The left hand graph of 1.1 shows a girder where the L-profiles form the flange of the girder, in the right hand graph there is an additional flange plate connected to the L-profiles. Both situations, with and without additional flange plate, will be assessed in this research. The focus in this research is on four point bending of beams. At some of the rivets, the beam will be loaded in pure bending, and at some of the rivets the beam will be loaded in a combination of shear and bending.

1.1 Problem definition

When assessing existing fatigue data from full scale tests of riveted girders, there is a large variance in fatigue strength. Fatigue strength is defined as the numbers of cycles to failure under a specific stress range, the specification of the stress range is an important factor in this definition. The results of fatigue tests on beams with different geometries reveal that there is a large variance of results for number of cycles to failure for set stress ranges. The problem with the large variance of numbers of cycles to failure is the remaining fatigue life cannot be predicted in a precise manner.

The most widely used definition for checking the fatigue strength of rivet location in a riveted beam is the net section stress in the most outer fibre of the beam, or the net section stress at the rivet location.

$$\Delta\sigma = \frac{\Delta M}{I \cdot z} \tag{1.1}$$

where z is the distance of the neutral line to the most outer fiber. The large variance of this data can be explained by looking at the failure of the beams which are tested. A large percentage of the beams fail by crack initiation near the rivet holes in the flange profiles, where the stress state is different compared to the outer most fiber due to the region around the rivet hole being a disturbed zone for the flow of forces.

1.2 Objective

Objective for this research is to find a more suitable stress range parameter to describe the occurring maximum stress concentrations for fatigue verification of riveted built-up beams. By determining the occurring stress concentrations at the rivet holes, and finding the most extreme case for each built-up beam. An analytical model will be made incorporating the force range, and the geometrical properties of the web profile and flange profiles and processing this data to a more precise stress range definition. This new stress range parameter should lead to a more accurate fatigue life assessment of such beams compared to the current state-of-the-art.

1.3 Methodology

To find the new stress parameter the research is divided into several steps. These steps are a literature study, collecting data of tests on riveted girders, the set up of an analytical model, the set up of several numerical models, and finally processing the data.

1.3.1 Literature study

A literature study is conducted on riveted built-up beams. This part will mainly focus on the stress state occurring around the notches of the beam. These locations will be mainly around the holes drilled in the plate and L-profile for the riveted connection. By finding the stress in these high loaded zones, a new stress range will be determined.

1.3.2 Collecting data

Fatigue test results data is collected from papers describing full scale tests on girders. the S-N data of every beam is collected, and additional geometrical properties of the tested riveted girders. The used stress range parameter in these papers is an important factor. These properties of the beam will be used in the next step by the numerical model to process the new stress range.
Through the literature review and analysing of the data, the governing locations on the beam and the local stress concentrations in the disturbed regions of the beam are determined.

1.3.3 Analytical model

An analytical model is set up to derive a suitable stress definition for fatigue of riveted beams, based on mechanical principles. This new stress definition is used to assess the data collected in the second step. This model requires numerical integration which is done in excel and parametrically set up to process the data from the practical tests. In this sheet, using the geometrical properties of the beam and the force range used in the test, the newly proposed stress method is used to compute the stress ranges at all rivet holes in the flange profiles.

1.3.4 Numerical model

Using ANSYS workbench numerical models are set up. The models are used to validate the results of the analytical model. By using finite element modelling for a beam with the same geometrical properties as in the analytical model, the results between these models are checked. The analytical model is validated when the results gained from the analytical model, using the same geometrical properties, are in accordance with the numerical model.

The first check is the force transfer in the rivets. This validation is made using a global model of the beam. In this global model the complete beam is modelled, with simplified modelling of the riveted connections.
The second check is the prediction of the stress concentrations at the rivet holes. Using the sub-modeling technique, a portion of the global geometry in which failure is expected to occur is modelled more accurately for determining the stress concentration at the notches set up in ANSYS, where a row of several rivets is modelled in detail. In the sub-model the rivets are modelled using solids, and the connection between elements is defined using contacts. This model will simulate the stress state at the rivet holes in more detail, thus giving a more accurate result regarding the stress at the edge of the rivet hole.

1.3.5 Processing data

The data collected in Chapter 1.3.2 is processed using the analytical model as described in Chapter 1.3.3. The analytical model calculates the values of stress concentration at each of the rivet locations for the specific geometries and test conditions of the beams. From these rivet locations, the maximum peak stress of all rivet holes is taken as the new stress range parameter for the fatigue verification.

This is done for each of the suitable tests for processing. Not every test described in the literature study provides enough information to process the data, or has a different test set up not suitable for processing using this specific analytical model.

After processing all of the suitable data, the data of the old and new stress range is compared. The correlation of the old data-set using the net section stress range is compared to the correlation of the data-set using the new stress range parameter. The correlation of the S-N data will provide insight in whether the spread of the data is lessened, and thus whether the new stress range parameter gives better a better estimation of the fatigue life of riveted bridge girders.

Chapter 2

Literature review

2.1 Fatigue loading and failure

Fatigue is localised damage, eventually resulting in failure of a component or a structure, in a material that is subject to fluctuating loading. This means that the structure is loaded and unloaded over time. The only way to obtain a quantitative measure of fatigue strength is to carry out fatigue test under controlled conditions [11]. Within these controlled conditions there are three basic types of cyclic loading illustrated in Figure 2.1 [17].

- (a) Reversing (smin = negative, Smax = positive)
- (b) Pulsating (smin = 0, Smax = positive)
- (c) Fluctuating (smin = postivie, Smax = positive)

This loading cycle is characterized by the stress range and the variable R, this is the stress ratio (S_{min}/S_{max}). R=0 corresponds to a pulsating load, a negative R with reversing and a positive R with a fluctuating cyclic load, these cyclic loads are shown on Figure 2.1 [17].

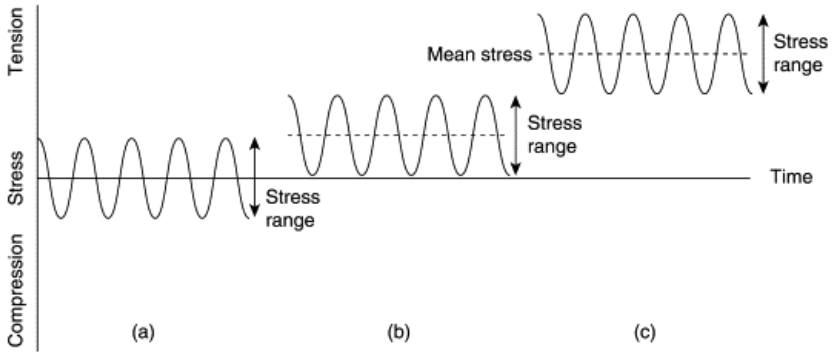

Figure 2.1: Types of cyclic loading

Fatigue failure under constant amplitude loading, the fatigue life is defined as a number of cycles to failure under the effect of a specific stress range. Where the stress range is defined as $\sigma_{max} - \sigma_{min}$ for a fluctuating load.
With regard to the collected data set, all of the tests are conducted using the fluctuating stress range. The minimum stress for all of these tests is still a positive value, in such a way that there is always a load acting on the beam.

2.2 Test data

S-N test data is collected from the papers as described in Table 2.1. As explained in the problem definition, the stress range in conducted tests is mostly defined as the stress of the net section in the most outer fibre of the beam.

Table 2.1: Collected tests dataset

Paper	Type of test	Dimensions	Stress range
Fisher [10]	4 point bending	Yes	Net section stress
Bruhwiller [4]	4 point bending	Yes	Unknown
Adamsson [12]	4 point bending	Yes	Strain gauges
Baker [3]	Tensile	Yes	Strain gauges
DiBattista [6]	Tensile	Yes	Strain gauges
Akesson [22]	4 point bending	Yes	Net section stress
Al-Emrani [2]	4 point bending	Yes	Net section stress
Out [19]	4 point bending	Yes	Unknown
Abe [13]	4 point bending	No	Unknown
Mang [13]	4 point bending	No	Unknown

In Table 2.1 several tests describe using strain gauges to calculate the stress range. These strain gauges are placed at the outer face of the beam. In essence, this method gives the same value as using the net section to calculate the stress range. The papers with unknown methods to calculate the given stress are assumed to use the net section to calculate the stress range.

The fatigue data from these tests is plotted in Figure 2.2. The horizontal axis in this plot is the numbers of cycles to crack initiation. The vertical axis is the stress range based on the net section of the beam.

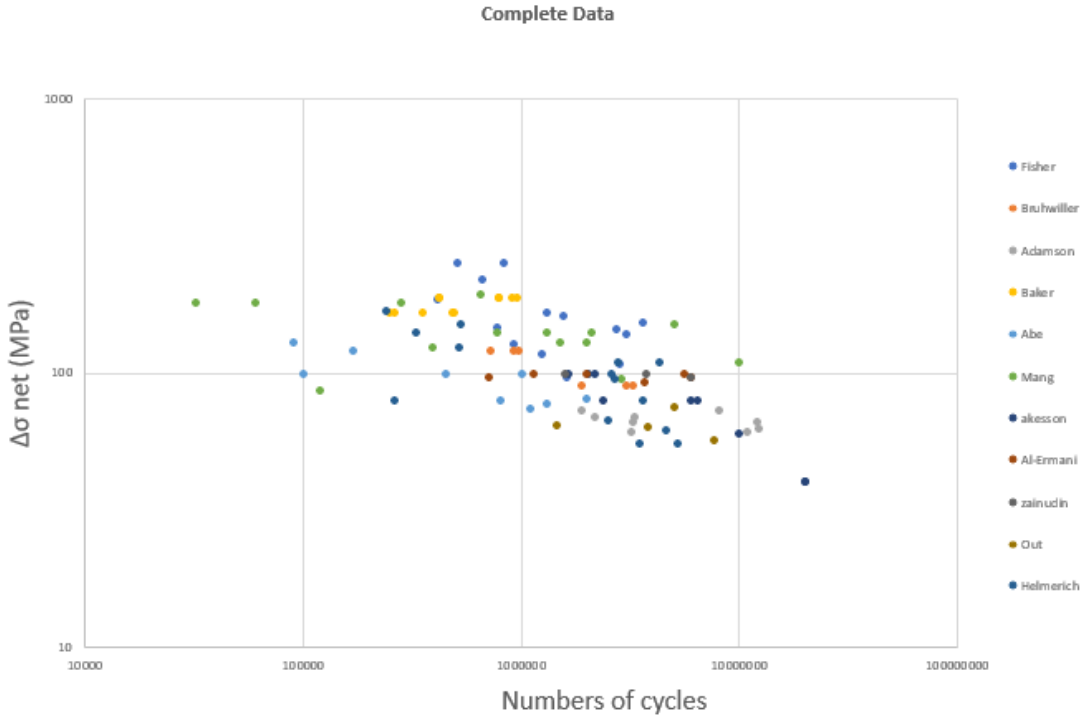

Figure 2.2: Plot of the complete collected dataset

2.3 Stress concentrations at a rivet hole

With the objective to define a stress parameter suitable for fatigue verification, that is based on the principles of applied mechanics, the governing locations with the corresponding stress concentrations need to be found. Stress concentrations at the governing locations have three different contributions. The influence of the bypass loading caused by bending of the beam, the influence of the pin loading from the force transfer of the rivet, and friction caused by the clamping force of the rivet.

2.3.1 Bypass loading

The stress concentration factor due to bypass loading for symmetrical configurations are calculated using [20]:

$$K_{tn} = 2 + (1 - \frac{d}{H})^3 \tag{2.1}$$

This formula describes the bypass loading without a rivet in the hole. The factor of stress concentration due to bypass loading is lower when a rivet is present in the hole. The difference between a non-filled rivet hole and a filled rivet hole is described by introducing the factor α. Values for this parameter described in a forthcoming paragraph.

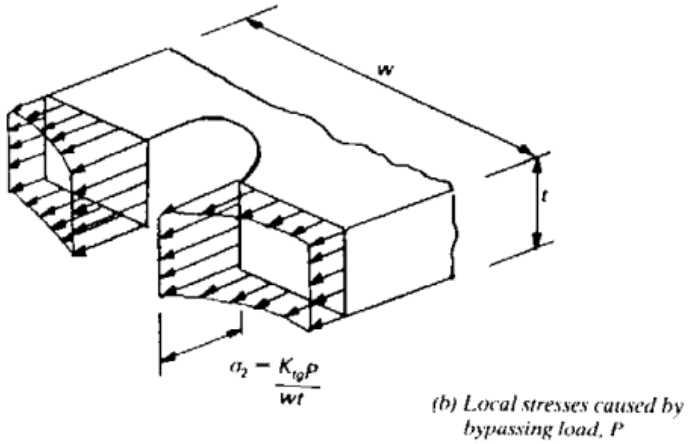

Figure 2.3: Stress concentrations due to bypass load

Figure 2.3 [20] shows the state of the stress concentration due to the bypass loading. The stress concentration due to bypass loading is given in Formula 2.2. This factor is the ratio between the nominal stress in the section due to bending and the peak stress at the notches of the rivet hole.

$$\sigma_{bypass} = \frac{K_{tg}P}{wt} \tag{2.2}$$

Where $\frac{P}{w \cdot t}$ is the nominal stress in the section due to bending.

Two different situations can be defined, these two situations are visualized in Figure 2.4 [20]. Where the figure on the left hand side shows a situation with two finite area's at each side of the rivet hole. On the right side a situation with one finite and one semi-infinite area side. The situation with the asymmetrical placed rivet hole will cause the edge at the finite side of the rivet hole (A) to have a higher stress concentration compared to the other edge of the rivet hole (B).

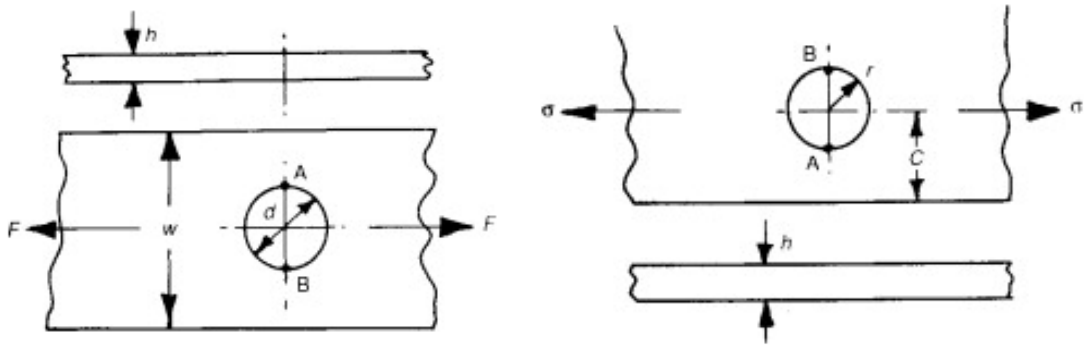

Figure 2.4: Two situations of bypass loading

The stress concentration of the bypass loading for the symmetrical situation are calculated using the following formula [20].

$$K_{tn} = 2 + 0,284 \cdot (1 - \frac{d}{H}) - 0,6 \cdot (1 - \frac{d}{H})^2 + 1,32 \cdot (1 - \frac{d}{H})^3 \tag{2.3}$$

where K_{tn} is the factor of stress concentration, d the diameter of the rivet hole and H he width of the profile. K_{tn} is the factor of stress concentration factor between the peak stress at the edge of the rivet hole and the net section stress.

The stress concentration of the bypass loading of the asymmetrical situation is calculated using the formula [20].

$$K_{tg} = 3 + 0,08 \cdot (\frac{d}{C}) + 7,342 \cdot (\frac{d}{C})^2 - 38,05 \cdot (\frac{d}{C})^3 + 106,04 \cdot (\frac{d}{C})^4 - 130,13 \cdot (\frac{d}{C})^5 + 65,07 \cdot (\frac{d}{C})^6 \tag{2.4}$$

Which is the factor of stress concentration between the peak stress at the edge of the rivet hole on the finite side of the plate compared to the gross section stress.

2.3.2 Pin Loading

Stress concentrations due to pin loading are caused by the rivet transferring force from the web to the flange profile. This means that the stress concentrations in the plate are based on the force transfer in the rivet. Stress concentration factors regarding pin loading can be determined using two different approaches. Nominal stress based on the net section, and nominal stress based on the bearing area [21] which is defined as the thickness of the plate multiplied by the rivet hole diameter.

Within the range of $0,15 \leq d/H \leq 0,75, c/H \geq 1,0$ the following equations are used to calculate the stress concentration factors for the net section in Equation 2.5 [20].

$$K_{tnd} = 12,882 - 52,741(\frac{d}{H}) + 89,762(\frac{d}{H})^2 - 51,667(\frac{d}{H})^3 \tag{2.5}$$

And the bearing stress concentration factor section in Equation 2.6 [20].

$$K_{tnb} = 0,2880 - 8,820(\frac{d}{H}) - 23,169(\frac{d}{H})^2 + 29,167(\frac{d}{H})^3 \tag{2.6}$$

This same approach of calculation of the bearing stress is stated by Niu in 1998 [18]. The stress bearing factor in this paper is determined with a curve following the same formula as in Equation 2.9. This formula determines the stress concentrations on the locations shown in Figure 2.5.

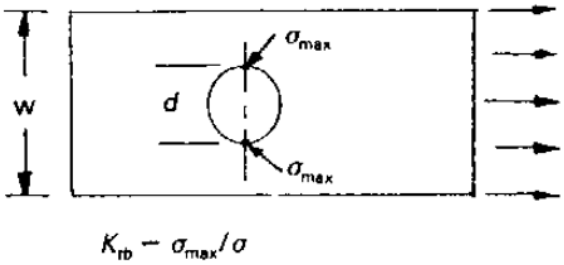

Figure 2.5: Location of the stress concentrations due to bearing

Both of the methods for determining the stress concentrations in the plate use the force transfer of the fastener as a basis to calculate the concentrations. In contrary to the bypass loading, which uses the reference stress in the profile.
Once the force transfer for each of the rivet is known, the stress caused by the rivets can be calculated. Stress around the rivet hole due to the force of the rivet acting on the section, with concentrations at the notches of the hole. Stress state is visualized in Figure 2.6.

The formula describing stress concentrations due to pin loading is shown in Equation 2.7. The equation describes the factor of stress increase over the net section of the profile.

$$K_{tnd} = 12,882 - 52,741(\frac{d}{H}) + 89,762(\frac{d}{H})^2 - 51,667(\frac{d}{H})^3 \tag{2.7}$$

The stress concentration factor K_{tnd} describes the relation between the occurring stress at the edges of the rivet hole and the nominal stress in the section. The used definition for the nominal stress in this case is given below, where 'w' is the width of the section and t is the thickness of the section [20].

$$\sigma_d = \frac{\Delta P}{w \cdot t} \tag{2.8}$$

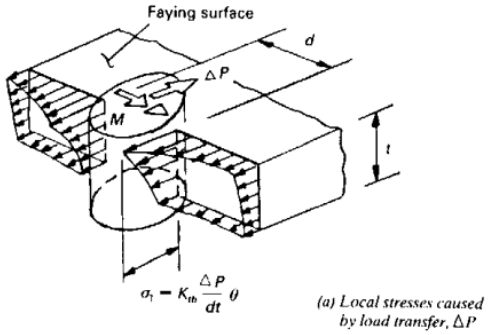

Figure 2.6: Stress concentrations due to the load transfer

A second method to calculate the stress concentrations is by calculating the stress concentrations based on the bearing stress caused by the force transfer in the rivet [20].

$$K_{tnb} = 0,2880 - 8,820(\frac{d}{H}) - 23,169(\frac{d}{H})^2 + 29,167(\frac{d}{H})^3 \tag{2.9}$$

Where the stress concentration is described by the relation between the occurring stress at the edges of the rivet hole and the stress in the bearing section. The stress in the bearing section is determined using.

$$\sigma_b = \frac{\Delta P}{d \cdot t} \tag{2.10}$$

For both of these cases, the maximum stress due to the pin load is calculated using.

$$\sigma_{max} = K_{tn} \cdot \sigma_{nom} \tag{2.11}$$

2.3.3 Combined bearing and bypass load

Looking at the loading situation in Figure 2.7 [9], the two loading situations around the rivet hole are shown.

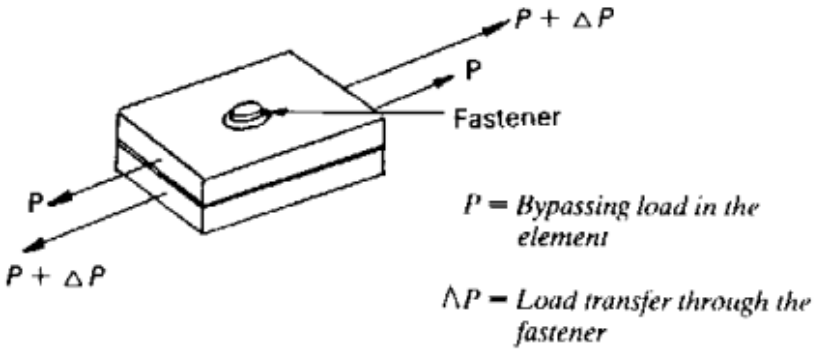

Figure 2.7: Loading situation rivet hole [9]

The two occurring stress concentrations factors around these holes are calculated in Formula 2.1 for K_{tn} and Formula 2.7 for K_{tb}. The total stress concentration around the rivet hole is calculated through the use of the following formula [9].

$$K_t = \frac{\sigma_{max}}{\sigma_{ref}} = \frac{\alpha\beta}{\sigma_{ref}}(K_{tb}\frac{\Delta P}{dt} + K_{tg}\frac{P}{wt}) \tag{2.12}$$

Rewritten for maximum stress value, the formula becomes:

$$\sigma_{max} = \alpha\beta(K_{tb}\frac{\Delta P}{dt} + K_{tg}\frac{P}{wt}) \tag{2.13}$$

In this formula, three more variables are introduced, namely α: the hole condition factor, β: the hole filling factor, and θ: the bearing distribution factor. When conditions during production of the beam are not known, it is suggested to use a factor of 1,0 for the hole condition factor [9]. For β the following values, shown in Table 2.2 are suggested [9]. The hole filling factor takes into consideration the hindrance of ovalization of the rivet hole due to the rivet being present in the hole, reducing the stress concentration in the notches.

Table 2.2: Suggested β factors

mean life	effective β, Rivets	Effective β, bolt
$5 * 10^4$ cycles	0,78	0,83
$1 * 10^5$ cycles	0,67	0,73
$1 * 10^6$ cycles	0,67	0,77

in Formula 2.12 the factor theta represents the bearing distribution factor. This means the effects of local bending on the bearing stress distribution. This factor is mentioned in the AIAA paper [5] where a detailed method for generating this factor is derived from test data. An other method for obtaining a value for theta is the, more conservative, single shear curve used by NIU [18].

2.3.4 Friction

The friction of the plate elements has an influence on the force transfer in the rivet, for a percentage of the force transfer will be directly from the web plate to the L-profile. The force transfer in the beam is dependent on two factors. The clamping force of the rivet, and the friction coefficient of the material. The maximum clamping stress of a rivet ($\sigma_{c,0}$) according to Eurocode 1-8 [1] is 0,70 of the yield strength of the rivet [15].

$$\sigma_{c,0} = 0,7 * f_{yr} = 165MPa \tag{2.14}$$

In the paper "Rivet clamping force of as-built hot-riveted connections in steel bridges" [14], the clamping force from hot-riveted connections are analysed. In the paper the clamping stress in the riveted connection are set out against a function of the ratio between the grip length (g) over the rivet diameter (d). The collected data gives the graph as seen in Figure 2.8 [14].

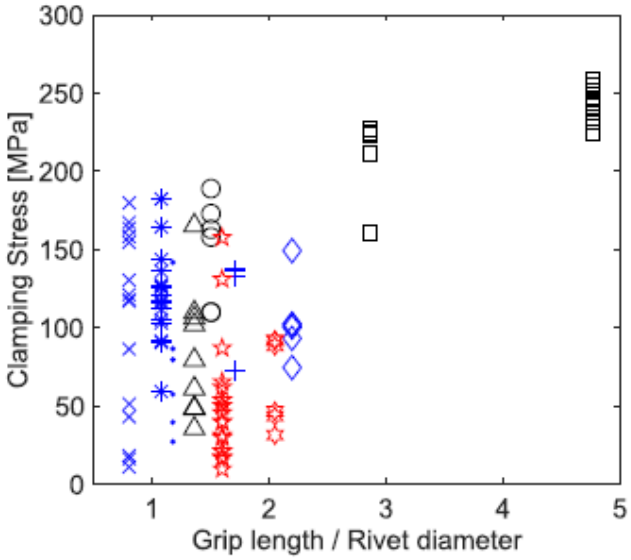

Figure 2.8: Clamping stress as a function of g/d

As can be seen from the graph, the theoretical maximum value of 165 MPa is around the same value as the maximum value's seen in the graph. Since it is not possible to know the real value of the clamping stress, and thus the friction in the build-up beams, a theoretical value must be chosen. For this research it is chosen to use this theoretical maximum value as described in the eurocode.

Two options for an analytical approach to Stress concentrations due to friction are presented in *Stress Intensity Factors of cracked riveted joints* [15] These methods are based on the theoretical bearing ratio β. Given in Equation 2.15. With μ is the friction coefficient and n is the number of rivets.

$$\beta = \frac{F - F_{c,0} * n * \mu}{F} \tag{2.15}$$

For $\beta = 0$, there is no bearing transfer, and $\beta = 1$ there is a full transfer via bearing.

$$\begin{aligned} K_{tb} &= K_{tb,friction} \qquad for \beta = 0 \\ K_{tb} &= K_{tb,pin} \qquad for \beta = 1 \end{aligned} \tag{2.16}$$

In this situation, a linear relation between β and the distribution is assumed. Combining these equations into Equation 2.17.

$$K_{tb}(\beta) = \beta * K_{tb,pin} + (1 - \beta) K_{tb,friction} \tag{2.17}$$

From this point, two different approaches are given [**?**]. Firstly, a solution where the distribution transferred by friction is equally distributed over the plate. Secondly a solution where prying occurs. For the solution with a equally distributed stress over the plate in contact with the rivet head, the following conditions are in place. $K_{t,g,friction} = 0,5 K_{t,n,bypass}$.

$$K_{tb}(\beta) = K_{tb,pin}(\beta) + 0,5 K_{tb,bypass}(1 - \beta) \tag{2.18}$$

The solution with prying is based on the condition $K_{tg,friction} = 0,5 * Ktn, bypass$ for $\beta = 0$ and $K_{tg,friction} = Ktg, pin$ for $\beta = 1$

$$K_{tb}(\beta) = K_{tb,pin}(2\beta - \beta^2) + 0,5 K_{tb,bypass}(0,5 - \beta + 0,5\beta^2) \tag{2.19}$$

When the β factor determines the amount of stress decreasing the pin load stress concentration factor, and increasing the bypass loading stress concentration factor.

Chapter 3

Analytical model

The analytical model is used to parametrically describe the stress state in the beam. The calculations made in the model can be divided into two parts. In the first part, the nominal stress state of the beam and the distribution of forces among the rivets are determined. In the second part the occurring stress concentrations at the notches of the rivet holes are determined, these stress concentrations are dependant on the nominal stress state and the force transfer in the beam. The nominal stress range multiplied by the stress concentrations in the notches are proposed as the new stress range parameter for fatigue verification.

3.1 Model description

Two analytical models are made, the difference between these two models is in the configuration of the rivets. One of the models will assume a symmetrical spacing of the rivet in the middle of the flange profile. The second model consists of two rows of rivets, with an asymmetrical spacing of the rivets. These two configurations are shown in Figure 3.1.

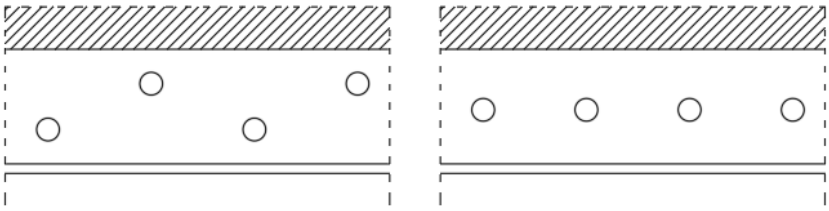

Figure 3.1: Two configurations of beams

For the configuration on the right hand side, the mechanical scheme is the same as the situation in the figure. The standardized formulas regarding stress concentrations for symmetrical bodies can be used in this situation. For the configuration on the left hand side, an extra step of simplification is made before calculating the stress concentrations. This step assumes all of the rivets on a single line, where the top row of rivets is lowered to the location of the bottom row of rivets in such a way that all of the rivets are on the same line. Using this simplification, the pre-defined asymmetric stress concentration factors can be used, where the highest stress concentration occurs at the bottom of the rivet hole.

3.1.1 Set up of the model

The analytical analysis can be divided into two parts. the first part of the analysis is determining the nominal stress state of the beam, and the force transfer in each of the rivets from the web profile to the flange profile. the second part of the analysis is calculating the peak stresses occurring at the edges of the rivet holes, and determining the governing location of these peak stresses.

Dimensional parameters are incorporated into the excel sheet, such as the dimensions of the plate, the dimensions of the L-profiles, the height and length of the section. Two distinct sheets are set up, one for the symmetrical configuration, and one for the asymmetrical situation. The difference in these two calculations is the method used to calculate the stress concentrations when the nominal stress and the force transfer in the rivets is known. Due to the different configuration in rivet location, the nominal stress and the pin loading have different effects on the stress concentrations at the notches.

In the analytical model, the numbering of the rivets is as shown in Figure 3.2, where rivet number 1 is the rivet closest to the symmetry plate at mid-span of the girder.

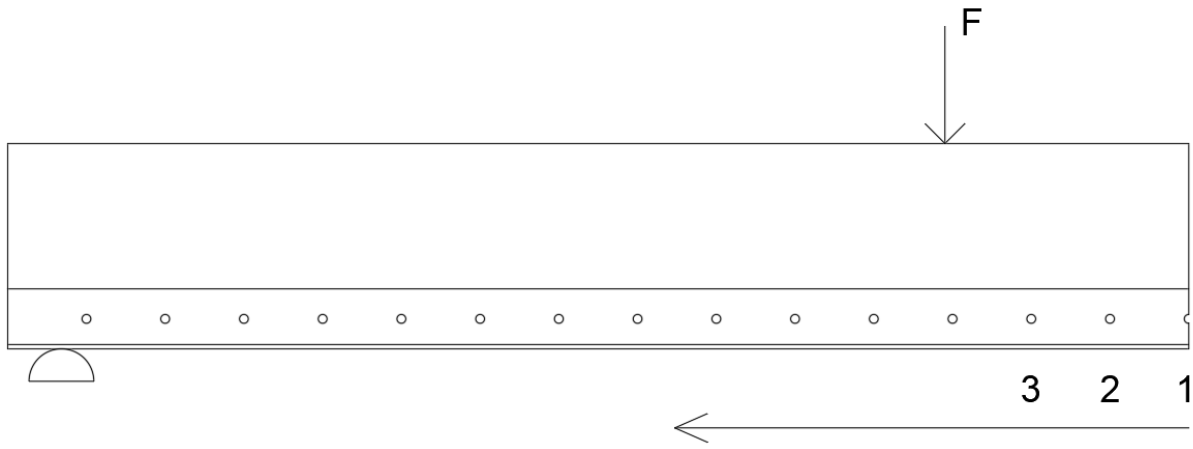

Figure 3.2: Numbering of rivets in analytical model

3.2 Steps in calculations

The first step in the numerical analysis is the determination of the stress distribution within the section according to Bernoulli's beam theory. Using the moment of inertia of the web and the shifted moment of inertia from the L-plate according to Steiners parallel axis theorem, the stress distribution at any given height of the section is determined.

After force distribution over the beam is determined, the riveted girder is simplified into the following basic situation as seen on Figure 3.3 [9].

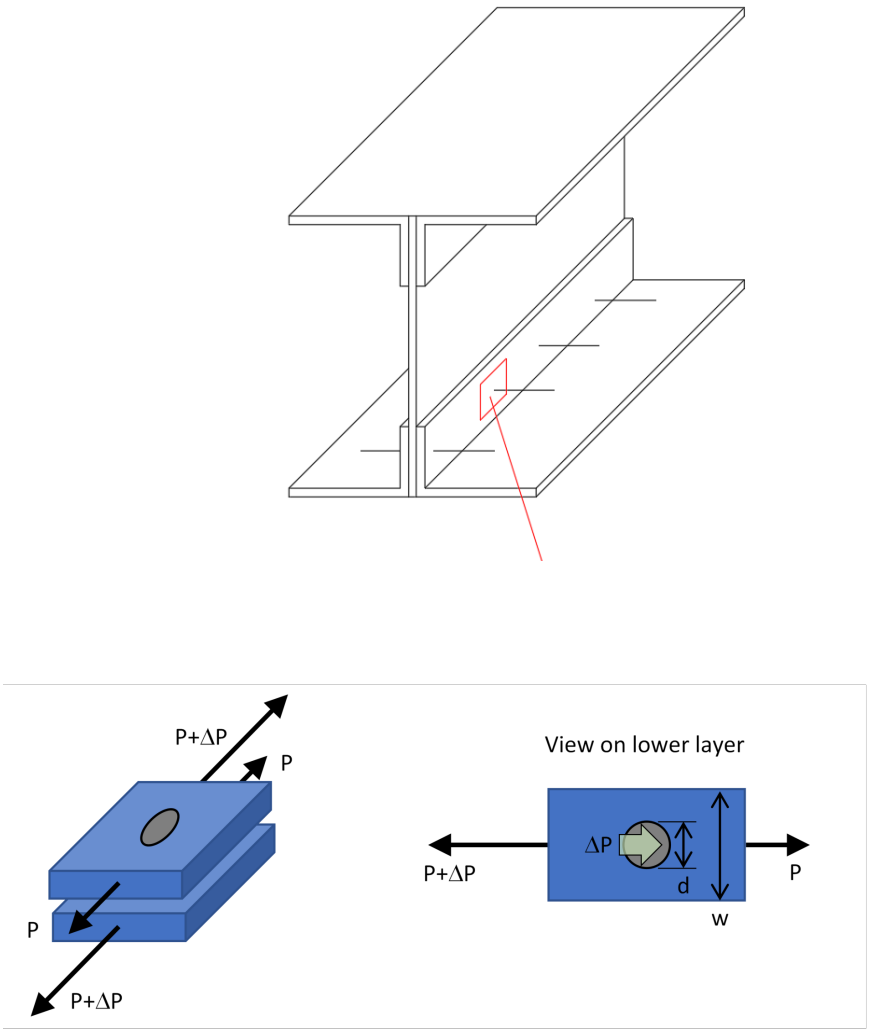

Figure 3.3: Basic loading situation

The blue model in the bottom of Figure 3.3 represents the cut out part of the beam shown in the top the figure where one plate is the web profile, one plate is part of the L-profile, and the gray circle represents the rivet.

In this model P represents the bypass loading and ΔP the transfer of load per fastener. Translated to the riveted girder, this means that P is the force through the L-profile and ΔP is the force transfer of a single rivet.

3.2.1 Load distribution among rivets

Shear flow

The first method determining load transfer in the rivets is through the shear flow in the beam. The shear flow in this case describes the longitudinal shear in bending. The shear flow is calculated through the use of Formula 3.1.

$$q = \frac{V_y * Q_x}{I_x} \tag{3.1}$$

where the first moment of area is taken as the area of the L-profile. Using the L-profile area as the shearing plane, the shear flow can be determined between these two elements. The shear flow is a unit given in force divided by length, multiplying the shear flow with the spacing between the rivets. The force transfer per rivet can then be determined.

As shown in Formula 3.1 the shear flow has a linear relation with the shear force. Considering the static system of a fully cooperating built-up beam, there is no shear force in the constant moment region. When all of the fasteners are 100 percent stiff, this would mean that the fasteners in the constant moment region transfer no force from the plate to the L-profile. However, the riveted connections in the built-up girders are not fully stiff, causing a different force distribution over the rivets. From the observations in the full scale tests it can be seen that the majority of the girders fail at a rivet hole in the constant moment zone, near the point of force application. This observation does not concur with these rivets not transferring force. When all of the rivets in the constant moment zone transfer no force, the crack initiation could happen at any arbitrary rivets in the constant moment zone, since there is no difference in stress state in between these locations.

Known displacement method

The second method to determine the force transfer in the rivet is by using the known displacements of the web profile to determine the unknown forces in the rivets. The force transfer in the rivets is due to the flange profile following the displacement of the web profile. For this method the displacements for the rivet locations of the complete beam are determined. After the displacement of the full beam is known, the forces needed for the flange profile corresponding with the same displacement can be determined using the constitutive relation between the displacement and the applied force. Using this relation, a set of forces among the rivets is determined which will result into the same deflection or displacement on the flange profile as calculated on the whole beam.

For the force transfer in the vertical direction the displacement of the locations of the rivets are determined by deriving the deflection formula. Using this formula, the deflection on each coordinate of the beam can be determined. Equation 3.2 describes the derivation of the deflection formula of the four point bending beam. The beam is divided into three parts. Segment 1: from support to first force, Segment 2: in between the two forces, and Segment 3: from second force to second support. The variables used in the derivation are shown in Figure 3.4.

In the calculations of the horizontal force transfer, it is assumed that the rivet hole location is located in the neutral axis of the flange profile. This means that the force transfer from the rivet to the flange profile only causes an axial force in the profile. In reality, the rivet hole is located outside of the neutral axis, meaning each force transfer causes an additional bending moment in the flange profile. There is a possibility this additional bending moment in the flange profile alters the distribution of forces among the rivets. This is not further investigated in this research.

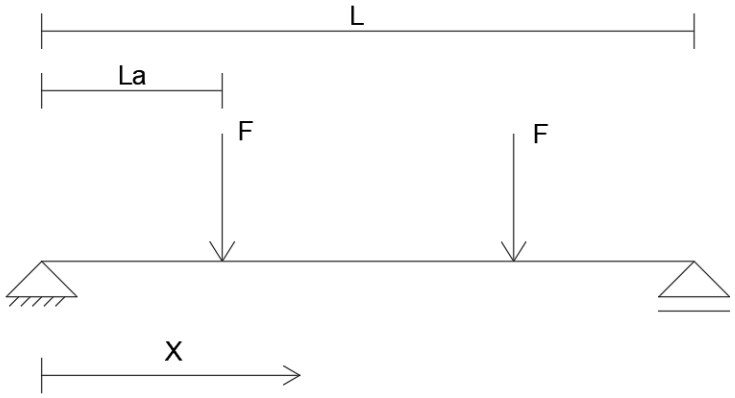

Figure 3.4: Variables for derivation

Derivation of displacement equations

Derivation for $X \leq L_a$.

$$M = F \cdot x \tag{3.2}$$

$$\kappa = \frac{1}{EI} \cdot F \cdot x \tag{3.3}$$

This gives the following beam equations with unknown integration constants C_1 and C_2.

$$\frac{dw_1^2}{d^2x} = \frac{1}{EI} \cdot F \cdot x \tag{3.4}$$

$$\frac{dw_1}{dx} = \frac{1}{2EI} \cdot F \cdot x^2 + C_1 \tag{3.5}$$

$$w_1(x) = \frac{1}{6EI} \cdot F \cdot x^3 + C_1 \cdot x + C_2 \tag{3.6}$$

Boundary conditions for this segment of the beam are: $w_1(0) = 0$ and $w_1(L_a) = w_2(L_a)$.
With the first boundary condition C_2 can be solved to $C_2 = 0$

Derivation for $x > L_a$ and $X < L - L_a$.

$$M = F \cdot L_a \tag{3.7}$$

$$\kappa = \frac{1}{EI} \cdot F \cdot L_a \tag{3.8}$$

This gives the following system of beam equations. Consisting of the deflection equation. The first derivative, the rotation equation, and the second derivative, the curvature equation. This set of equations have the unknown integration constants C_3 and C_4.

$$\frac{dw_2^2}{d^2x} = \frac{1}{EI} \cdot F \cdot L_a \tag{3.9}$$

$$\frac{dw_2}{dx} = \frac{1}{EI} \cdot F \cdot L_a \cdot x + C_3 \tag{3.10}$$

$$w(x) = \frac{1}{2EI} \cdot x^2 + C_3 \cdot x + C_4 \tag{3.11}$$

The boundary conditions for this section of the beam are $\phi_2(\frac{1}{2}L) = 0$ and $w_1(L_a) = w_2(L_a)$. $\phi_2(\frac{1}{2}L) = 0$ gives a value for C_3 shown in Equation 3.12.

$$C_3 = -\frac{F \cdot L_a \cdot L}{2 \cdot EI} \tag{3.12}$$

The boundary condition $w_1(L_a) = w_2(L_a)$. $\phi_2(\frac{1}{2}L) = 0$ for both equations. The beam equations at this stage are.

$$w_1(x) = \frac{F \cdot x^3}{6 \cdot EI} + C_1 \cdot x \tag{3.13}$$

$$w_2(x) = \frac{F \cdot L_a}{2 \cdot EI} \cdot x^2 - \frac{F \cdot L_a \cdot L}{2 \cdot EI} \cdot x + C_4 \tag{3.14}$$

This gives the equation

$$\frac{F \cdot L_a^3}{6 \cdot EI} + C_1 \cdot L_a = \frac{F \cdot L_a \cdot L_a^2}{2 \cdot EI} - \frac{F \cdot L_a \cdot L \cdot L_a}{2 \cdot EI} + C_4 \tag{3.15}$$

which can be reduced to the equation

$$C_1 = \frac{F \cdot L_a^2}{3 \cdot EI} - \frac{F \cdot L_a \cdot L}{2 \cdot EI} + \frac{C_4}{L_a} \tag{3.16}$$

The next boundary condition is the restraint of the rotation of the beam at the intersection point of the two different cut outs of the beam equation. This means the second derivative of the beam equation evaluated at $L = L_a$ are equal for section 1 and 2.

$$\frac{dw_1}{dx} = \frac{dw_2}{dx} \quad |_{x=L_a} \tag{3.17}$$

The following beam equations are current in this stage .

$$\frac{dw_1}{dx} = \frac{F \cdot x^2}{2 \cdot EI} + \frac{F \cdot L_a^2}{3 \cdot EI} - \frac{F \cdot L_a \cdot L}{2 \cdot EI} + \frac{C_4}{L_a} \tag{3.18}$$

$$\frac{dw_2}{dx} = \frac{F \cdot L_a \cdot x}{EI} - \frac{F \cdot L_a \cdot L}{2EI} \tag{3.19}$$

This can be reduced to the following value for C_4.

$$C_4 = \frac{F \cdot L_a}{6 \cdot EI} \tag{3.20}$$

Filling in C_4 in Equation 3.16 gives the following value for C_1

$$C_1 = \frac{F \cdot L_a^2}{3 \cdot EI} - \frac{F \cdot L_a \cdot L}{2 \cdot EI} + \frac{F}{6 \cdot EI} \tag{3.21}$$

Filling in the C_1 and C_4 value in Equation 3.13 and Equation 3.14 gives the final beam equations for the four point bending.

$$w_1(x) = \frac{F \cdot x^3}{6 \cdot EI} + \frac{F \cdot L_a^2 \cdot x}{3 \cdot EI} - \frac{F \cdot L_a \cdot L \cdot x}{2 \cdot EI} + \frac{F \cdot x}{6 \cdot EI} \tag{3.22}$$

$$w_2(x) = \frac{F \cdot L_a}{2 \cdot EI} \cdot x^2 - \frac{F \cdot L_a \cdot L}{2 \cdot EI} \cdot x + \frac{F \cdot L_a}{6 \cdot EI} \tag{3.23}$$

These beam equations are incorporated in the analytical model to calculate the vertical displacement of each location of a rivet. For the horizontal displacement of the rivet, the strain at the height of the rivet over the section is calculated. For this firstly the curvature of the beam is calculated through the use of Equation 3.24.

$$\kappa = \frac{M}{EI} \tag{3.24}$$

Where the bending moment of each rivet location is known. From the curvature the strain at a vertical distance z from the neutral axis is determined with Equation 3.25.

$$\epsilon = \kappa \cdot z \tag{3.25}$$

With the curvature at the location of the rivet known, the curvature is multiplied with the distance from the centre to determine the displacement in horizontal direction.

Determining vertical force transfer

The deflection equations as determined are used to find the displacement of each of the rivet locations along the x-axis. These displacements are calculated using the bending stiffness of the beam under full cooperation between the web and flange elements using Equation 3.22 and 3.23. These deflections are calculated using the earlier derived equations. Using these deflections the corresponding forces for only the flange profile to follow the web profile are determined, as explained hereafter.

For determining the corresponding vertical forces in the flange profile the mechanical scheme shown in 3.5 is used. This mechanical scheme represents only the flange profile. The fixed end on the right hand side of the mechanical scheme is the midpoint of the flange profile. In this situation, the fixed support is at the maximum deflection of the beam.

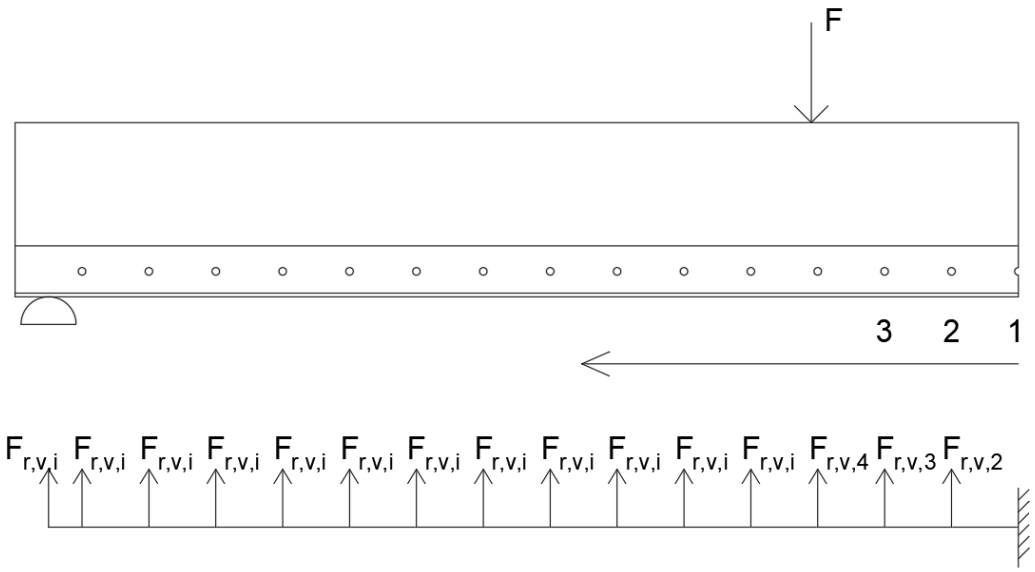

Figure 3.5: Mechanical scheme flange profile

A set of equations is set up for determining the force of each location to get an equivalent displacement of the flange profile as determined in the complete beam. The effects of each force is shown in Figure 3.6.

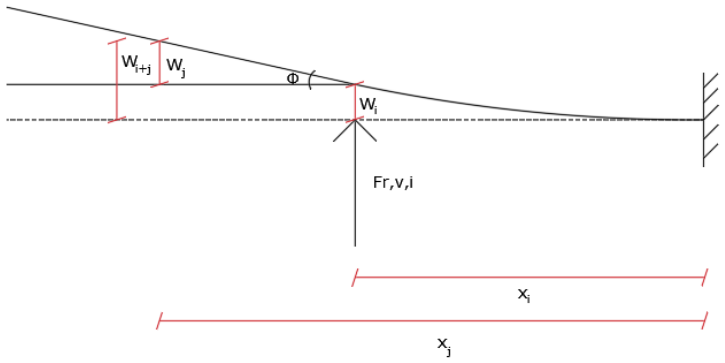

Figure 3.6: Variables for deflection

This figure gives the effects of one force on all of the rivet locations. Every location on the right hand side of the force undergoes a deflection equal to the deflection derived from the beam equation of a cantilever. The deflection of the force itself on the location of the force can be calculated through deflection formulas. On the left side of the force, the deflection is linear from the point shown in figure 3.6 and calculated with $W_{x+j} = W_i + \phi_i \cdot (x_j - x_i)$ where x_i and x_j are the length between the support and the point of calculation.

These calculations are made for each force on the beam. The number of forces acting on the flange profile is equal to the number of rivets in this section. On each location there is a deflection of the summation of all of the effects of the forces. These calculations are incorporated into the analytical model in a table which represents a system of equations.

An example of this system of equations is given in Figure 3.7. The columns in the table represent the acting force, the rows in the column represent the location on which the acting force causes deflection. The green squares are the effects of the force on it's location itself, thus using the deflection equations for a cantilever beam. On the left side of the green diagonal, the deflection is calculated by using the x-location in the deflection equation. On the right side of the green diagonal, the deflection is calculated using the rotation and beam length, as shown in Figure 3.6.

		Loc.	100	300	500	700	900	1100	1300	1500	1700	1900	2100	2300	2500	2700	2900	
F(v)	Loc.	Riv. Num	1	2	3	4	5	6	7	8	9	10	11	12	13	14	15	Rot.
1000,00	100	1	0,000103	0,000103	0,000103	0,000104	0,000104	0,000104	0,000104	0,000105	0,000105	0,000105	0,000106	0,000106	0,000106	0,000107	0,000107	1,54E-09
1000,00	300	2	0	0	0	0	0	0	0	0	0	0	0	0	0	0	0	0
1000,00	500	3	2,15E-06	1,66E-05	3,85E-05	6,16E-05	8,46E-05	0,000108	0,000131	0,000154	0,000177	0,0002	0,000223	0,000246	0,000269	0,000292	0,000315	1,15E-07
1000,00	700	4	9,03E-06	7,31E-05	0,000181	0,00031	0,000442	0,000575	0,000708	0,000841	0,000973	0,001106	0,001239	0,001371	0,001504	0,001637	0,00177	6,64E-07
1000,00	900	5	2,15E-05	0,000178	0,000454	0,000809	0,001204	0,001606	0,002007	0,002408	0,00281	0,003211	0,003613	0,004014	0,004415	0,004817	0,005218	2,01E-06
1000,00	1100	6	3,28E-05	0,000277	0,000718	0,001307	0,001995	0,002731	0,003476	0,004221	0,004966	0,005711	0,006456	0,007201	0,007945	0,00869	0,009435	3,72E-06
1000,00	1300	7	3,42E-05	0,000292	0,000766	0,001413	0,002189	0,003052	0,003958	0,004872	0,005785	0,006699	0,007612	0,008526	0,009439	0,010352	0,011266	4,57E-06
1000,00	1500	8	2,29E-05	0,000197	0,000521	0,000971	0,00152	0,002144	0,002819	0,003518	0,004222	0,004925	0,005629	0,006333	0,007036	0,00774	0,008444	3,52E-06
1000,00	1700	9	5,13E-06	4,43E-05	0,000118	0,000221	0,000349	0,000497	0,000659	0,000831	0,001008	0,001186	0,001364	0,001542	0,00172	0,001898	0,002076	8,9E-07
1000,00	1900	10	1,61E-05	0,00014	0,000373	0,000704	0,001117	0,001599	0,002136	0,002715	0,003321	0,003941	0,004563	0,005185	0,005808	0,00643	0,007052	3,11E-06
1000,00	2100	11	6,04E-05	0,000526	0,001413	0,002675	0,004263	0,006133	0,008236	0,010527	0,012958	0,015482	0,018054	0,020633	0,023212	0,025791	0,02837	1,29E-05
1000,00	2300	12	0,000152	0,001329	0,003579	0,006795	0,01087	0,015697	0,021168	0,027176	0,033613	0,040373	0,047347	0,054428	0,061527	0,068627	0,075726	3,55E-05
1000,00	2500	13	0,000243	0,002128	0,005746	0,01094	0,017552	0,025425	0,034402	0,044324	0,055034	0,066374	0,078187	0,090315	0,102601	0,114913	0,127226	6,16E-05
1000,00	2700	14	0,000304	0,002669	0,007225	0,013788	0,022176	0,032206	0,043697	0,056466	0,070329	0,085105	0,100612	0,116665	0,133084	0,149685	0,166317	8,32E-05
1000,00	2800		0,002044	0,017951	0,048633	0,092908	0,149593	0,217507	0,295467	0,382292	0,476801	0,577809	0,684137	0,794602	0,908021	1,023214	1,081106	0,000579
		total	0,00305	0,025924	0,069868	0,133004	0,213459	0,309384	0,418969	0,540449	0,672102	0,812228	0,959141	1,111167	1,26669	1,424194	1,524427	
		max - tot	-1,49695	-1,47408	-1,43013	-1,367	-1,28654	-1,19062	-1,08103	-0,95955	-0,8279	-0,68777	-0,54086	-0,38883	-0,23331	-0,07581	0,024427	
		Residual	0,01	0,01	0,01	0,00	0,00	0,00	0,01	0,01	0,01	0,01	0,01	0,00	0,00	0,00	0,02	
		Res sqr.	0,00	0,00	0,00	0,00	0,00	0,00	0,00	0,00	0,00	0,00	0,00	0,00	0,00	0,00	0,00	

Figure 3.7: Table with equations for analytical model

The bottom row of the table is the sum of a column, which is the deflection of a single point under the influence of all forces.

This is shown in Figure 3.8 and Figure 3.9 where the blue line represents the deflection of the beam obtained through Equation 3.22 and Equation 3.23, and the orange line represents the displacement calculated with the matrix seen in Figure 3.7, i.e. the calculated forces. In the first example Figure 3.8, all forces are set to 1 kN, in the second example Figure 3.9 the forces are calculated minimising the residual between the deflections gained from the beam equations of the fully cooperating beam and the deflections from the deflection matrix. Now the forces are known corresponding with the known deflection

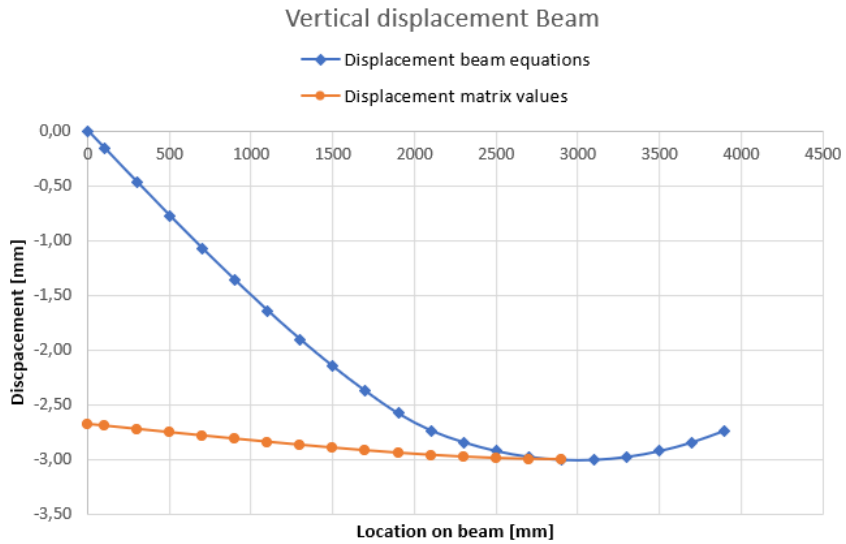

Figure 3.8: Deflection for $F_{r,v,i} = 1kN$

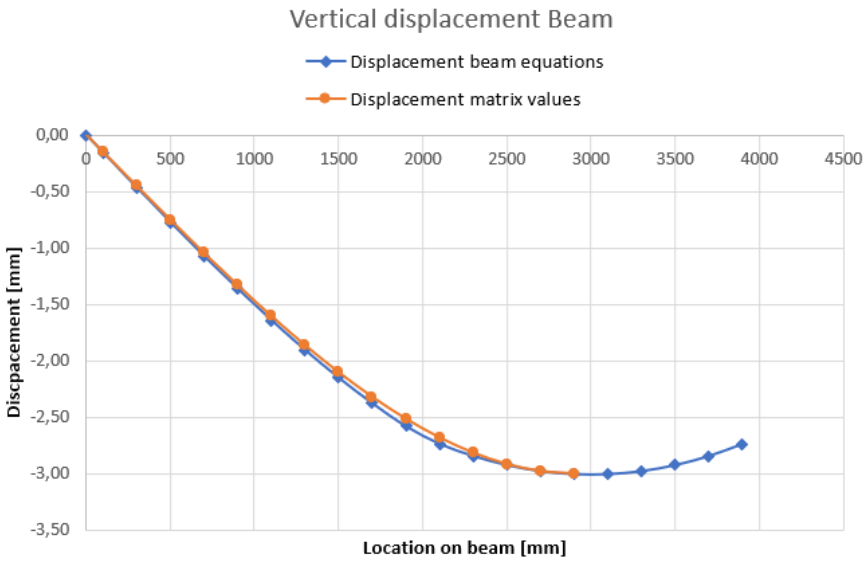

Figure 3.9: Deflection solved for $F_{r,v,i}$

Determining horizontal force transfer

A similar method is used for the horizontal force. Firstly, the horizontal displacement of the rivet locations of the beam in full cooperation is calculated. This displacement is calculated through the use of the rotation of the beam at certain points. To find this rotation, The first derivative of the deflection equation is determined, as shown in Equation 3.18 and Equation 3.19.

$$\frac{dw_1}{dx} = \frac{F \cdot x^2}{2 \cdot EI} + \frac{F \cdot L_a^2}{3 \cdot EI} - \frac{F \cdot L_a \cdot L}{2 \cdot EI} + \frac{F}{6 \cdot EI} \tag{3.26}$$

$$\frac{dw_2}{dx} = \frac{F \cdot L_a \cdot x}{EI} - \frac{F \cdot L_a \cdot L}{2EI} \tag{3.27}$$

With these equations the rotation at each point can be calculated. Using the rotation and the distance of the rivet location to the neutral axis of the beam, the displacement in horizontal direction for each rivet hole location is determined. After these displacements are known, the corresponding displacement for the flange elements are determined. The corresponding displacements for the flange profile are determined using the displacement matrix shown in Figure 3.12.

The used mechanical scheme for the flange profile is shown in Figure 3.10, where the fixed point on the right side of the beam is the symmetry point of the beam. On this beam several forces, equal to the number of rivets, act on the beam. In figure 3.11 a single force is shown as an example. For each rivet in the beam a force acts on this mechanical scheme.

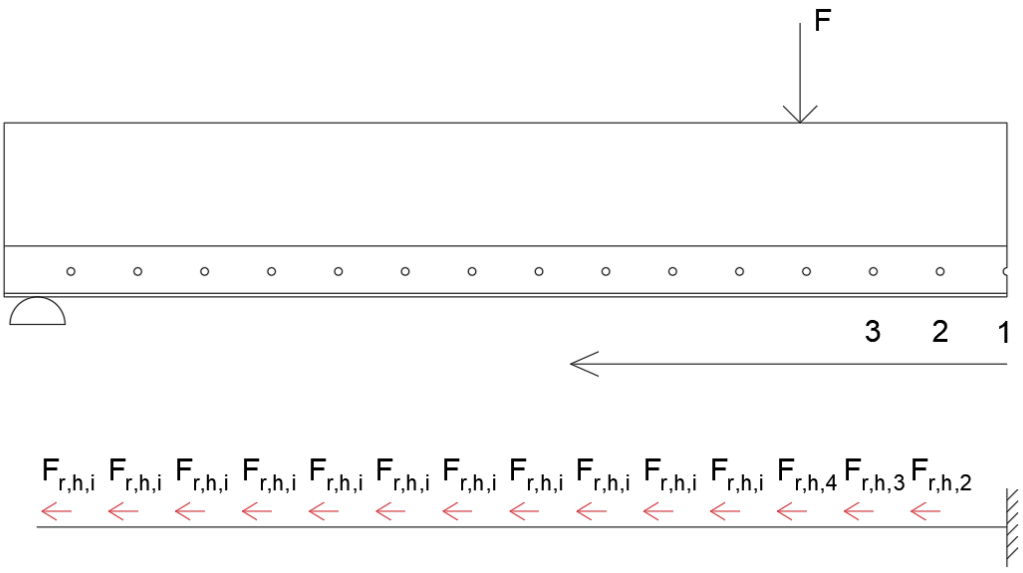

Figure 3.10: Mechanical scheme flange profile

A set of equations is made for determining the horizontal displacement for each point. Figure 3.11 shows an example of a force acting on the beam.
Every point on the right side of the force has a linear relation where the point of force application is at max displacement and at the fixed connection the displacement is zero. From these two points the displacement of a set point can be interpolated. For points on the left side of the force, the displacement is equal to the displacement at the point of force application. Likewise for the vertical displacement, a table is set up for the horizontal displacement calculating the effects of

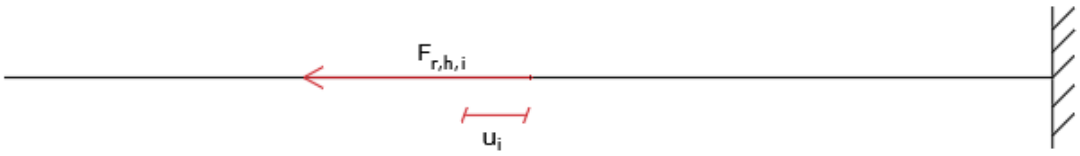

Figure 3.11: Variables for horizontal displacement

each force on each point. This gives a second table with a system of equations, shown in Figure 3.12.

		loc for gra	2700	2500	2300	2100	1900	1700	1500	1300	1100	900	700	500	300	100	0
		Loc.	100	300	500	700	900	1100	1300	1500	1700	1900	2100	2300	2500	2700	2900
F(h)	Loc.	Riv. Num	1	2	3	4	5	6	7	8	9	10	11	12	13	14	15
200,00	100	1	2,95E-05	2,95E-05	2,95E-05	2,95E-05	2,95E-05	2,95E-05	2,95E-05	2,95E-05	2,95E-05	2,95E-05	2,95E-05	2,95E-05	2,95E-05	2,95E-05	2,95E-05
200,00	300	2	2,95E-05	8,86E-05	8,86E-05	8,86E-05	8,86E-05	8,86E-05	8,86E-05	8,86E-05	8,86E-05	8,86E-05	8,86E-05	8,86E-05	8,86E-05	8,86E-05	8,86E-05
800,00	500	3	0,000118	0,000355	0,000591	0,000591	0,000591	0,000591	0,000591	0,000591	0,000591	0,000591	0,000591	0,000591	0,000591	0,000591	0,000591
2500,00	700	4	0,000369	0,001108	0,001847	0,002586	0,002586	0,002586	0,002586	0,002586	0,002586	0,002586	0,002586	0,002586	0,002586	0,002586	0,002586
5000,00	900	5	0,000739	0,002216	0,003694	0,005171	0,006649	0,006649	0,006649	0,006649	0,006649	0,006649	0,006649	0,006649	0,006649	0,006649	0,006649
8000,00	1100	6	0,001182	0,003546	0,00591	0,008274	0,010638	0,013002	0,013002	0,013002	0,013002	0,013002	0,013002	0,013002	0,013002	0,013002	0,013002
11000,00	1300	7	0,001625	0,004876	0,008126	0,011377	0,014627	0,017877	0,021128	0,021128	0,021128	0,021128	0,021128	0,021128	0,021128	0,021128	0,021128
14000,00	1500	8	0,002068	0,006205	0,010342	0,014479	0,018616	0,022753	0,02689	0,031027	0,031027	0,031027	0,031027	0,031027	0,031027	0,031027	0,031027
15000,00	1700	9	0,002216	0,006649	0,011081	0,015513	0,019946	0,024378	0,028811	0,033243	0,037676	0,037676	0,037676	0,037676	0,037676	0,037676	0,037676
15000,00	1900	10	0,002216	0,006649	0,011081	0,015513	0,019946	0,024378	0,028811	0,033243	0,037676	0,042108	0,042108	0,042108	0,042108	0,042108	0,042108
16000,00	2100	11	0,002364	0,007092	0,01182	0,016548	0,021276	0,026004	0,030731	0,035459	0,040187	0,044915	0,049643	0,049643	0,049643	0,049643	0,049643
15000,00	2300	12	0,002216	0,006649	0,011081	0,015513	0,019946	0,024378	0,028811	0,033243	0,037676	0,042108	0,04654	0,050973	0,050973	0,050973	0,050973
16000,00	2500	13	0,002364	0,007092	0,01182	0,016548	0,021276	0,026004	0,030731	0,035459	0,040187	0,044915	0,049643	0,054371	0,059099	0,059099	0,059099
18000,00	2700	14	0,002659	0,007978	0,013297	0,018616	0,023935	0,029254	0,034573	0,039892	0,045211	0,05053	0,055849	0,061168	0,066486	0,071805	0,071805
22000,00	2900	15	0,00325	0,009751	0,016252	0,022753	0,029254	0,035755	0,042256	0,048757	0,055258	0,061758	0,068259	0,07476	0,081261	0,087762	0,094263
		total	0,023448	0,070284	0,11706	0,163601	0,209403	0,253727	0,295687	0,334397	0,36897	0,399111	0,424819	0,445799	0,462347	0,474166	0,480667
		Residual	0,13	0,15	0,16	0,18	-0,01	0,01	0,02	0,04	0,06	0,07	0,08	0,10	0,11	0,11	0,12
		Res sqr.	0,02	0,02	0,03	0,03	0,00	0,00	0,00	0,00	0,00	0,00	0,01	0,01	0,01	0,01	0,01

Figure 3.12: System of equations for horizontal displacement

The green squares represent the displacement due to the force at the point at force application. This is calculated using Hook's law for continuous media Equation 3.28.

$$\epsilon = \frac{\sigma}{E} = \frac{F}{EA} \tag{3.28}$$

The displacement of the blue squares on the left side are equal to the displacement calculated with Equation 3.28. The values of blue squares on the right side are interpolated. On the bottom the summation of the displacements are shown. The forces are calculated by minimizing the residuals of the displacements of the fully cooperating beam and the displacement of this element.

The graph with the displacements is shown in Figure 3.13 and Figure 3.14 where the blue line represents the horizontal displacement of the fully cooperating beam, and the orange line represents the horizontal displacement of the element. The graph in Figure 3.13 represents the displacement under a load of 1kN. and the graph in Figure 3.14 represents the equations solved for F.

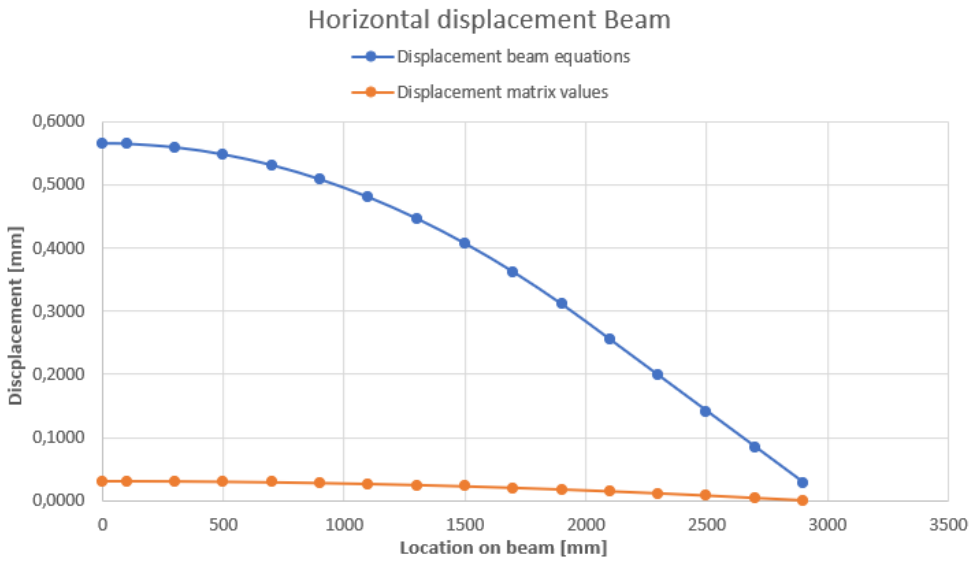

Figure 3.13: Horizontal displacements under 1kN

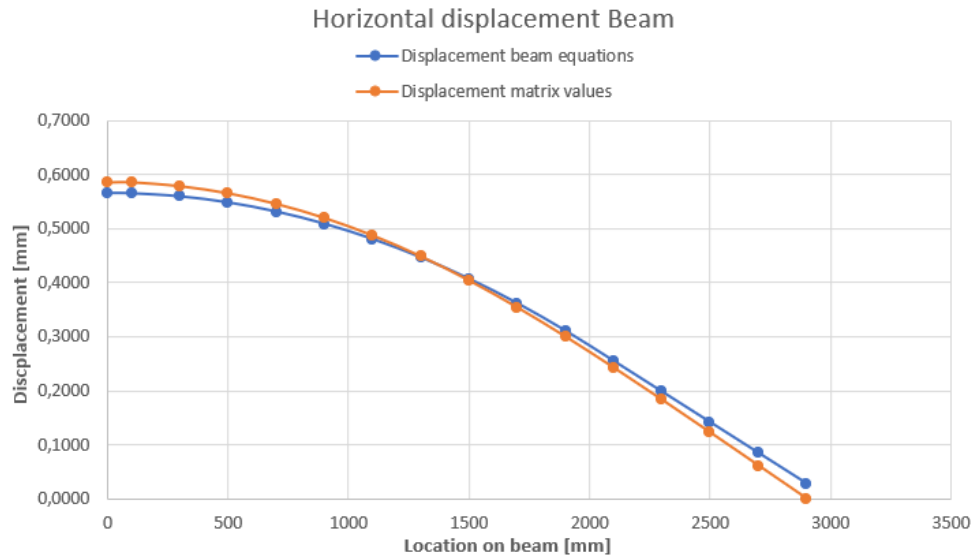

Figure 3.14: Horizontal displacement solved for $F_{r,h,i}$

The horizontal force and the vertical force for each location of a rivet is known, and thus the force distribution amongst the rivets.

3.3 Calculation in the model

Looking at above stated formula's in the previous section two main forces are needed to calculate the stress along the edge of the rivet hole. The force in the L-profile and the force transferred by a single rivet.

Stress in L profile

The stress in the L-profile is determined through the use of Bernouille's beam theory. Where M is the acting bending moment on the beam.

$$\sigma_z = \frac{M * z}{I_{yy}} \tag{3.29}$$

With the value z being the distance from the neutral axis to the top and bottom of the rivet hole. This gives a stress value at the top and bottom of the rivet hole in the gross section area of the beam.

Force transfer in rivet

The distribution of the transfer of forces from the web to the flanges is determined through the displacement matrices described in the known displacement method. The model uses two systems of equations to calculate the horizontal and vertical force of each of the rivets. It is chosen to neglect the effect of the vertical force transfer in the rivets. Due to these vertical forces in the being relative low to the horizontal forces, and the stress concentrations due to the horizontal component occurring at a different location than the other stress concentrations.

Stress concentration: Pin loading

Stress concentration in the section due to pin loading is related to the force transfer in the rivet. With the force transfer in the rivet calculated, this value is multiplied by the stress concentration factor for pin loading and this force is divided over the area around the rivet hole. The formula for the resulting stress due to the pin load is calculated using the following Formula.

$$\sigma_p = K_{tnd} * \frac{\Delta P}{dt} \tag{3.30}$$

Where d is the diameter of the rivet hole and t is the thickness of the plate.

Stress concentration: Bypass load

Stress concentrations due to bypass loading is based on the nominal stress state of the beam. With the stress in the net and gross section determined, the stress concentrations around the rivet hole are calculated . Where the Equation of the stress concentrations due to the bypass load is as follows.

$$\sigma_b = \frac{K_{tg} * P}{wt} \tag{3.31}$$

Where $\frac{P}{wt}$ is equal to the stress in the L-profile as determined in Equation **??**.

Friction of the rivet

Friction of the rivet is incorporated into the model by adjusting the force transfer from the rivet by pinload, and changing a certain percentage of this transfer into friction. In the analytical model, the solution with prying is used.

The solution with prying is based on the condition $K_{tg,friction} = 0,5 * Ktg, bypass$ for $\beta = 0$ and $K_{tg,friction} = Ktg, pin$ for $\beta = 1$

$$K_{tg}(\beta) = K_{tg,pin}(2\beta - \beta^2) + 0,5K_{tg,bypass}(0,5 - \beta + 0,5\beta^2) \tag{3.32}$$

Where the β factor determines the amount of stress decreasing the pin load stress concentration factor, and increasing the bypass loading stress concentration factor.

Total peak stress

The total stress concentration is calculated through Equation 3.33. This formula adds the two above stated stress concentrations. This value is multiplied by two factors α and β, of which the values are argued before.

$$K_t = \frac{\sigma_{max}}{\sigma_{ref}} = \frac{\alpha\beta}{\sigma_{ref}}(K_{tb}\frac{\Delta P}{dt} + K_{tg}\frac{P}{wt}) \tag{3.33}$$

This total peak stress is calculated for each rivet hole location. The rivets in the constant moment zone are subjected to a higher bypass load, where the rivets in the linear moment zone are subjected to a higher pin load concentration, due to the higher force transfer of the rivet. By calculating the peak stress for each of the rivets, the governing peak stress is found.

The example shown in Figure 3.15 is based on the geometry of the numerical model, which will be explained in Chapter 4. The calculation is made by calculating the pin load for each of the rivets, and the bypass load for each location of the rivet holes, after which the friction coefficient is used to reduce the pin load and increase the bypass load. An example of a plotted graph of the stresses of all these locations is shown in Figure 3.15. The stress values shown in the graph are peak values at the notches of each of the rivet locations. In this graph rivet number 1 is defined as the rivet in the midpoint of the beam.

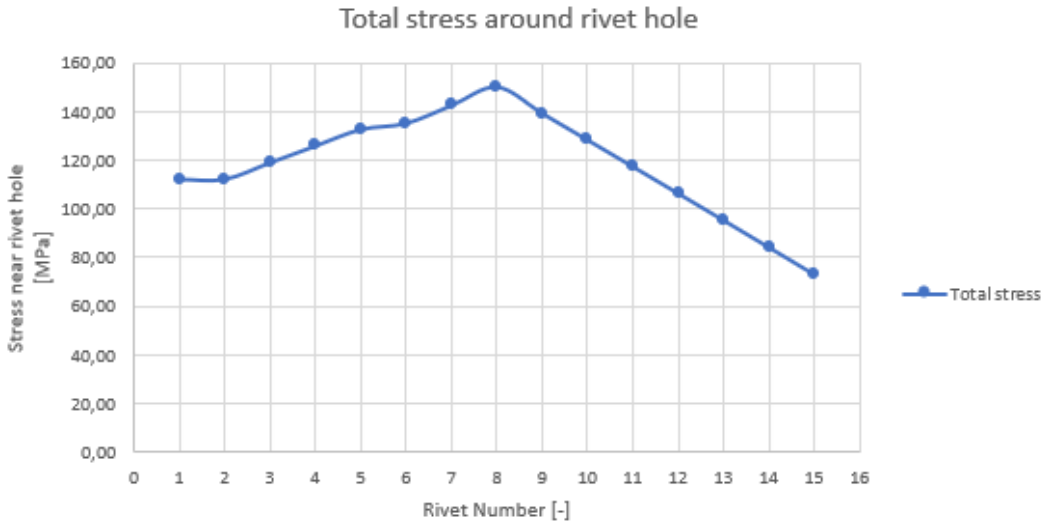

Figure 3.15: Maximum stress at the hole edge per rivet

Chapter 4

Numerical model

In the research a finite element model is made and sub-modelling strategy is used to check specific locations in more detail. The global model is a model of an entire riveted beam, with simplified modelling strategy applied for the riveted connections. The local sub-model aims at modelling in detail the actual geometry and force transfer of a row of six rivets with corresponding boundary conditions related to the model of an entire beam. The numerical analyses are conducted with the software package ANSYS analytical.

4.1 Global model

The global model of the beam serves two purposes, firstly the results of the model are used to validate the force transfer results of the analytical analysis conducted in Chapter 3. This will focus mainly on the force transfer for each rivet. Secondly this model will serve as a basis for the sub-model, where the boundary conditions will be taken from this model and imported to the sub-model.

4.1.1 Model composition

To reduce the model size and computing times two symmetry planes are introduced in the beam. The model consisting of solid elements made in the FEM software is shown in Figure 4.1.

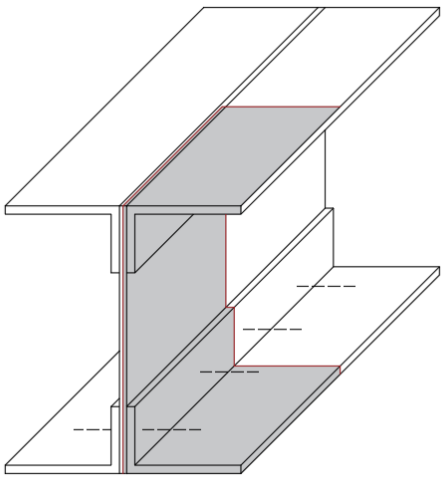

Figure 4.1: Section of the beam modelled in ANSYS

The symmetry planes are on the XZ-plane and the YZ-plane. The coordinate system used in ANSYS is shown in Figure 4.2. The whole height of the beam (thus no XY-plane symmetry) is modelled. There is no symmetry, or anti-symmetry in the beam in this plane. modelling the whole height of the beam also includes the effects of force going to the support through direct force transfer, instead of bending. This means the modelled beam is a quarter representation of the whole beam.

The main parts of the model are three parts, namely a single part for the plate, and two parts for both L-profiles. Each part is made of multiple bodies. Through the setting 'shared topology' in ANSYS, these bodies are connected. Shared topology will ensure a conformal mesh throughout the part.

4.1.2 Bodies

The parts used to model the L-profiles are shown in Figure 4.2.

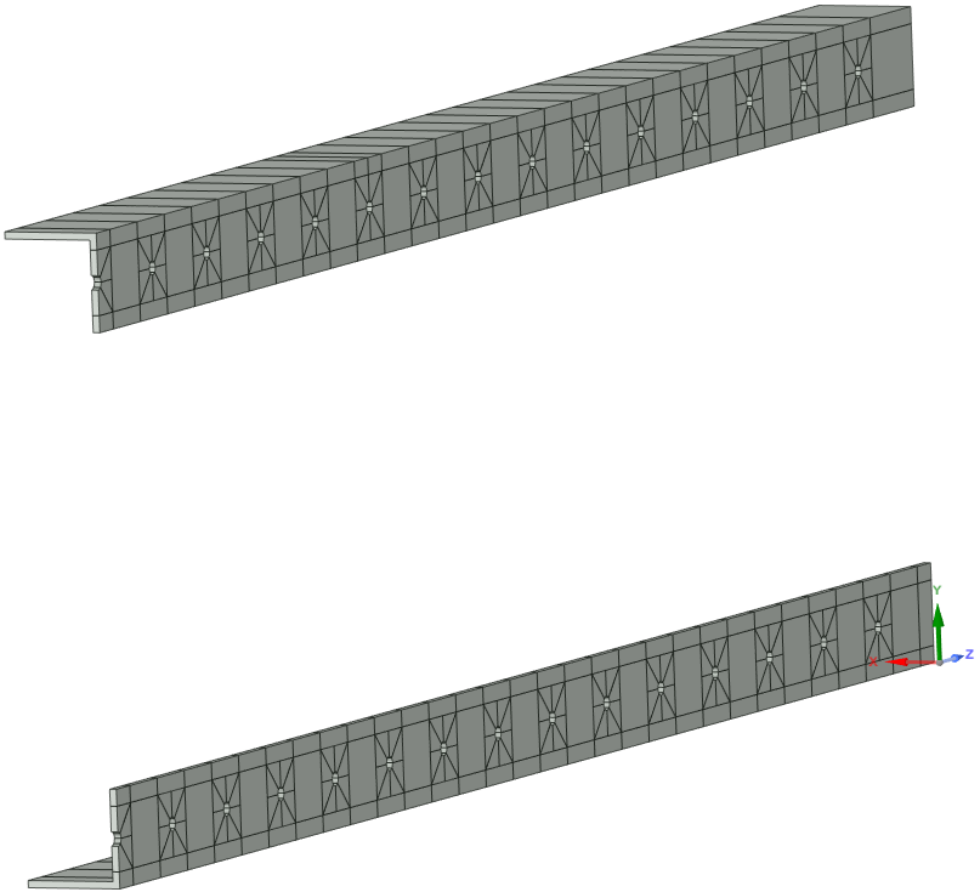

Figure 4.2: Bodies used for flange profile in the numerical analysis

The bodies are sliced up in smaller bodies to facilitate a better mesh for solving the model. While slicing up the solid the main goal is to be able to mesh using only hexahedron elements. This way, there is more control by the user on how the mesh and elements are defined and thus it enables to make a high quality and structured mesh.

The component used for the web of the profile is shown in Figure 4.3

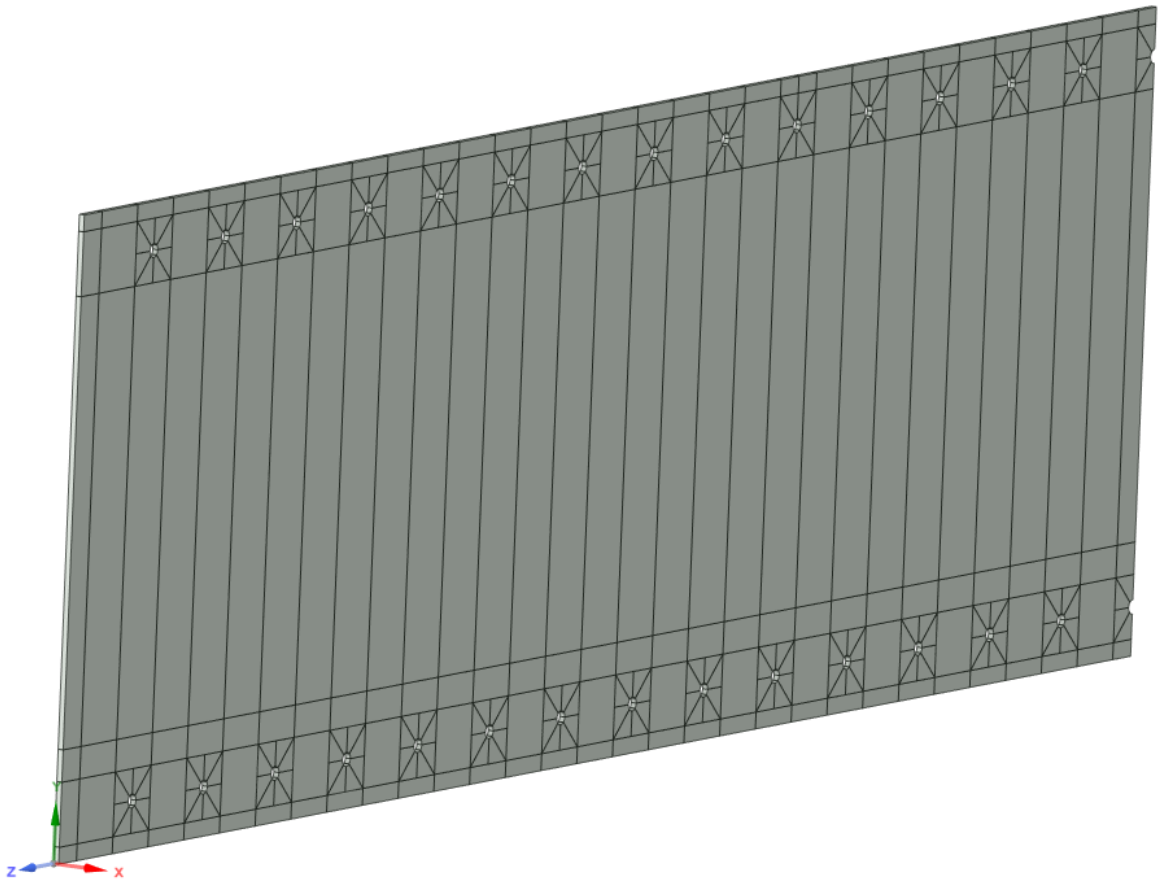

Figure 4.3: Bodies used for web profile in the numerical analysis

Likewise, the plate is sliced in sub-regions to facilitate the possibility to mesh using hexahedron elements and simultaneously facilitate the creation of the sub-model. Meshing of this element is conducted using a hex-dominant mesh setting in ANSYS. Most of the elements will be meshed using HEX20 elements, apart from some geometries where TET10 elements are used. Both of these are quadratic elements.

4.1.3 Supports

The support is modelled as a solid to reduce localized stress concentrations which were found when applying boundary conditions to the nodes directly. The modelled support in the mechanical scheme is a roller support which is only fixed in the Y-direction. In the ANSYS model it is modelled as a deformable solid body with a curved contact between the support and the beam as in Figure 4.4. The body is fixed in all rotational and translational directions at the surface on the bottom of the body. The girder beam can freely rotate over the curved face to model a roller support.

The width of the roller is the same as the width of the beam. The depth of the section is arbitrarily chosen, since the contact between the beam and the support is on the curved surface.

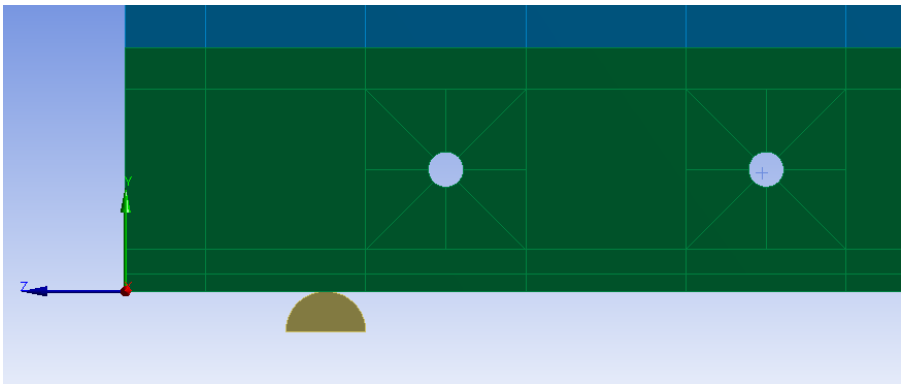

Figure 4.4: Solid element used as support

4.1.4 Load application

The point of Load application is modelled in the same manner as the support, as a deformable body with a curved face. The load application on the system is displacement based. Displacement based load application is used to ensure an easier convergence of forces and a better establishment of contacts.

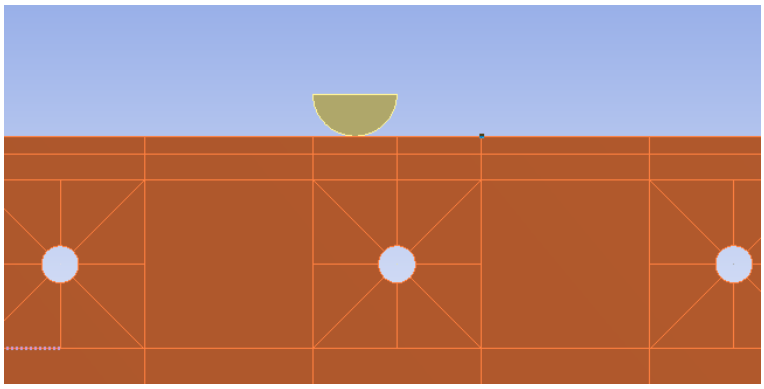

Figure 4.5: Solid used as force application

Displacement on the solid is introduced through the addition of a remote point on the face of the solid. A displacement of -2,5mm is assigned to this remote point. By introducing the load via the remote point corresponding with the face of the solid, the difference in stiffness of the web and flange profile does not interfere with the load introduction.

4.1.5 Contacts between bodies

There are two sets of contacts in the model.

- The contact between the web and the flange profile;
- The contact between the flange profile/web and the force introduction/support.

The contacts between the L-profile and the web will be no separation contact. This means no penetration and no separation of the two contacts surfaces, but the contacts can freely slide. It is chosen to use this contact because of the main purpose of this model, which is to find the distribution of forces among the rivets. This distribution is along the z-axis and y-axis of the model, separation of these two elements is along the x-axis. It is tested to see if the contact friction-less or

no separation makes a difference for the distribution of the forces by the rivets and it is concluded that these two contact types have very little differences on the distribution of the shear forces in the rivets. The no separation contact is a linear contact, opposed to the non-linear friction-less contact.

The contact between the support and the beam, and the force introduction and the beam differs from above stated contacts. When not carefully modelled, these contacts show large penetration of the elements. To reduce the penetration between these elements, several steps have been taken. Firstly the mesh around the contact area has been refined. The allowable penetration of these elements is reduced and the solving method is set to Normal Langrange, which allows the least penetration. Several tests have been conducted to check the penetration of the contacts, the results of these tests are shown in Table 4.1. The Penetration tolerance factor (PTF) has been modified until the percentage of penetration resulted below 0,5 percent.

Table 4.1: Tests penetration of contacts

	Force intro - plate			**Force intro - L-profile**		
	PTF	**Penetration**	**Percentage**	**PTF**	**Penetration**	**Percentage**
Test 1	0	0,018	0,72	0	0,11	4,4
Test 2	0,1	0,018	0,72	0,1	0,104	4,16
Test 3	0,01	0,0017	0,068	0,01	0,021	0,84
Test 4	0,01	0,0017	0,068	0,005	0,006	0,24

	Support - plate			**Support - L-profile**		
	PTF	**Penetration**	**Percentage**	**PTF**	**Penetration**	**Percentage**
Test 1	0	0,11	4,4	0	0,044	1,76
Test 2	0,1	0,11	4,4	0,1	0,058	2,32
Test 3	0,01	0,02	0,8	0,01	0,008	0,32
Test 4	0,005	0,011	0,44	0,01	0,0072	0,288

4.1.6 Rivets

The rivets are modelled using 1D beams, the elements are used are the BEAM118 elements, which is a linear element type. This beam element has a circular cross section with a diameter of 22mm. It is chosen to use a beam with the full diameter of the rivet hole to closely simulate the stiffness of the real rivet. The connections between the beam and the solids is deformable.

The edges of the rivet in this model are the midpoint at the flange, and the outer edge of the web profile. This simulates the midpoint of the rivet at both locations. the midpoint in the web is in the outer fibre of the element due to the symmetry axis in this plane. The rotation and translation of the nodes of the beam element are fixed, this simulates the symmetry plane of the rivet and the midpoint in the flange.

4.1.7 Connections

To connect the beam elements (rivet) and the solids (web and flange) a joint connection is used. The behaviour of the joint is set to deformable. Deformable behaviour will allow the contact area or target area to deform from it's original state, where rigid behaviour will lock the original state of the contact or target area. ANSYS calculates the deformability of the hole by defining constrain equations between the two or more coupled nodes.

A joint connection is made between the beam element and the inner face of the solid. The joint will connect the node of the beam element to the mesh nodes on the face of the rivet hole. The edges of the joint connections are fixed, to simulate the behaviour of the rivet. This means the beam element nodes can't rotate or translate. An example of the joint connection is shown in Figure 4.6, where the red lines are the connections between the beam node and the solid face. Per beam element there are two joints, one connecting the one side to the flange profile, and one connecting the other side to the web profile.

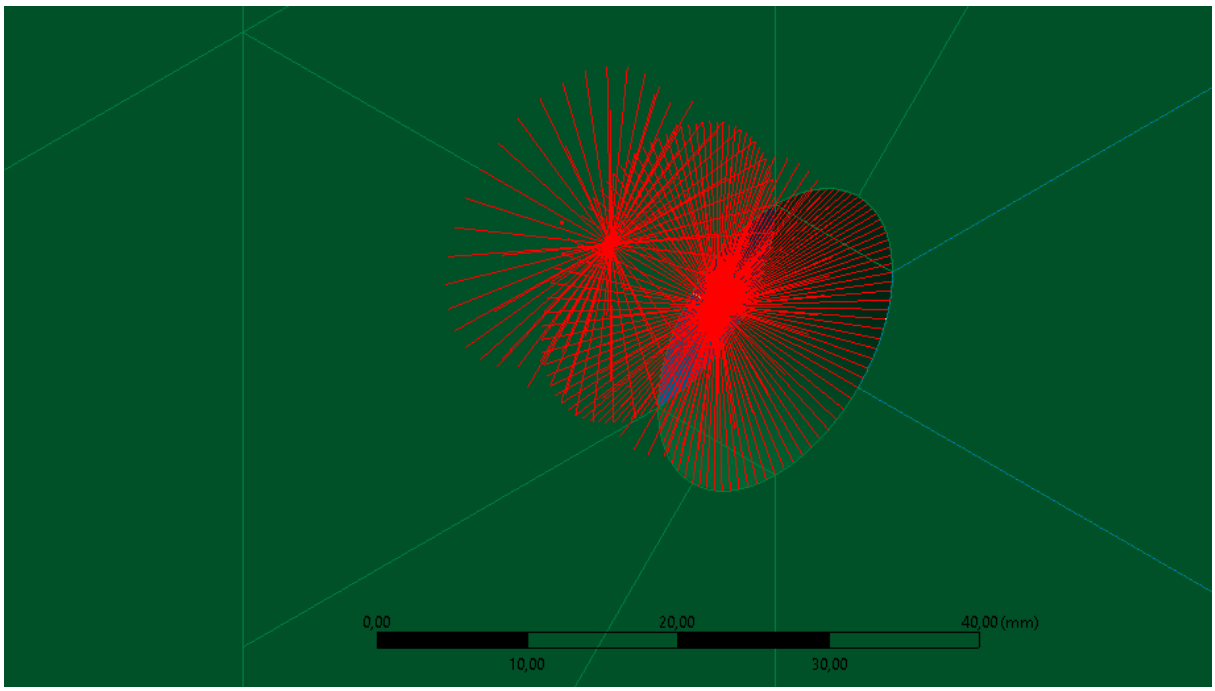

Figure 4.6: Connection between BEAM element and solid

4.1.8 Load steps

Multiple load steps are used in the model.

1. Thermal condition on rivets.
2. Loading of the beam
3. Unloading of the beam

The thermal constraint and displacements used in the model are shown in Figure 4.7.

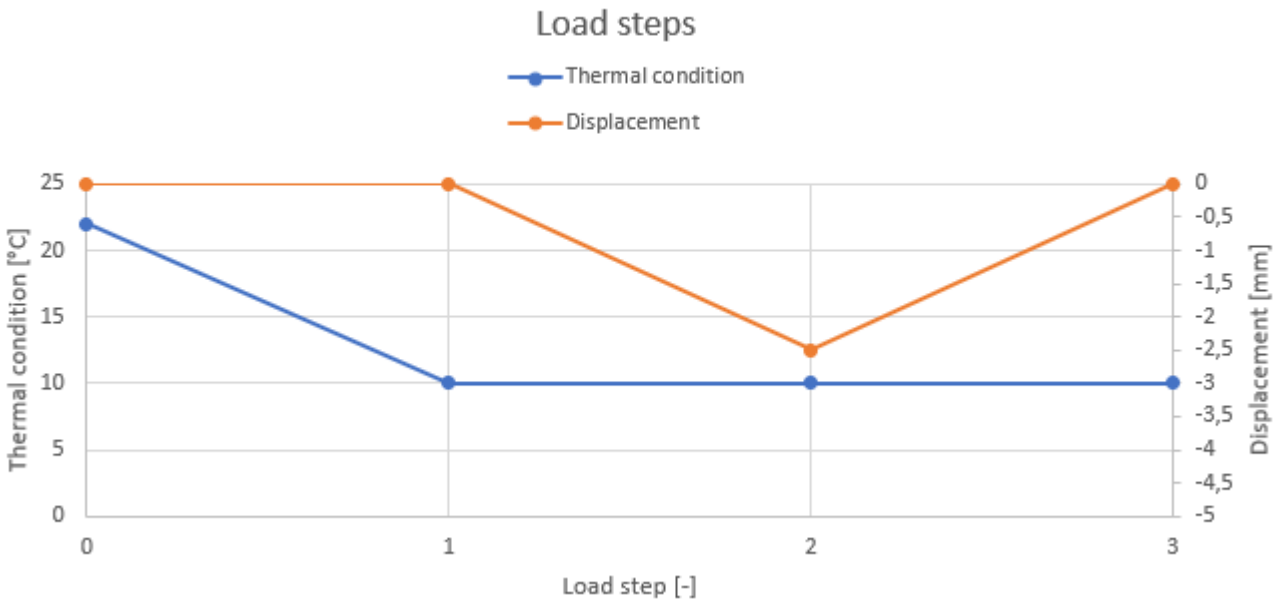

Figure 4.7: Load steps in model

In step 1 (0s - 1s) the thermal conditions on the rivets are applied. The thermal condition is used to create tension in the beam elements, simulating the clamping force present in hot rivets. In step 2 (1s - 2s) the beam is loaded by a displacement based boundary condition. In step 3 (2s - 3s) the beam is unloaded. Unloaded condition of the beam is modelled to check residual stresses in the beam after unloading. Residual stresses will not occur in the global model, for this model does not include the friction component. The sub-model does include the friction in the analysis and thus will provide the residual stresses, if any.

4.1.9 Geometrical properties

The geometrical properties of the beam are as follows

- Height = 1000mm
- Span = 3000mm
- Web thickness = 18mm
- Flange height = 152mm
- Flange width = 152mm
- Flange thickness = 11mm
- Rivet diameter = 22mm
- Rivet centre-to-centre distance = 200mm
- Vertical distance to rivet hole = 76mm

The value used as the Young's modulus is $210 \cdot 10^3$ MPa and a Poissons ratio of 0,3. The analytical model will fill in these geometrical properties to validate the results gained from both models

4.2 Validation global model

A discrepancy between the global model built in ANSYS and the behaviour of a full scale test is the connection between the rivets and the web/flange profile. One of the main differences is the possibility of a tensile force to arise in the connection used in the ANSYS model. The method used in the global model, i.e. coupling of the rivets and the plates/profiles using constraint equations, is a linear contact with an equal stiffness in compression and in tension, where in reality the connection between these two elements can't transfer any force via tension. The rivet only has a compression contact on a single side of the rivet. The effects of the extra force transfer via tension is checked by comparing the stiffness of the riveted girder with BEAM elements as rivets, and the stiffness of the riveted girder with full solid rivets.

For this check a second model is made using the BEAM elements (rivets) are replaced with the rivets modelled in solids, including the rivet heads. This model resembles reality more closely than the simplified model with the BEAM elements. The rivet shank transfers forces from the body to the flange. The connection between the rivet shank and the two elements are made with contact surfaces. In this case it is chosen to use a frictionless connection.

4.2.1 Force displacement graph

The first check is the force-displacement graph of the two models. The load used in both of the models is displacement based. If the force of the load is in the same order of magnitude for both of the models, the stiffness of both beams is in the same order of magnitude. This conclusion is based on the two models using the same material with the same Young's modulus, and a linear constitutive relation between the force and displacement.

Figure 4.8 shows the force due to the displacement to the time of the solution for the model with the solid rivet elements, where at t=1 the load increment starts from zero and at t=2 the displacement is 2,5mm. The green line represents the force in the Y-direction, which is the vertical component. At maximum displacement the value of this vector is 121,2 kN.

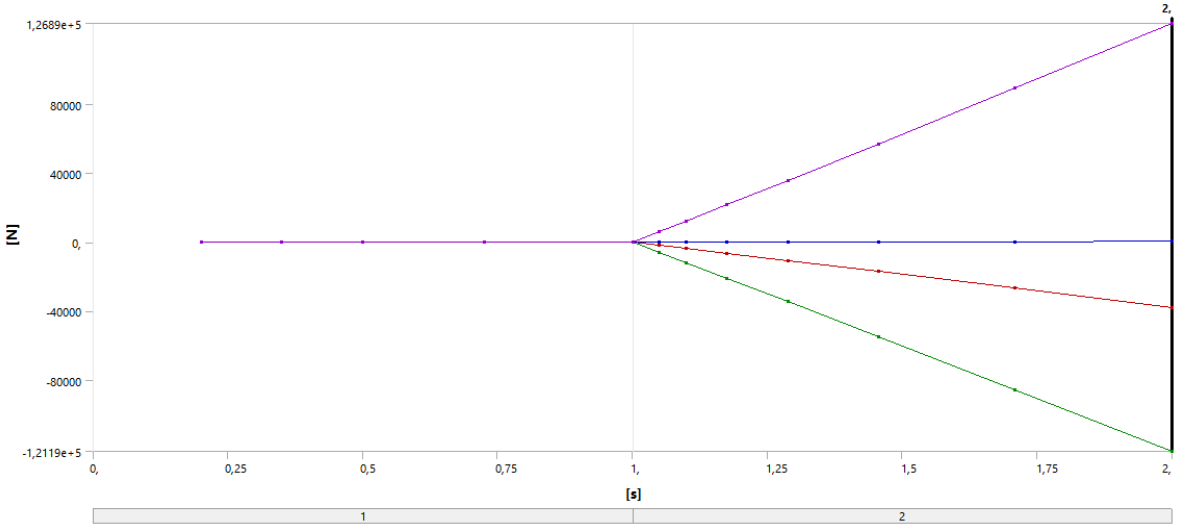

Figure 4.8: Force over time of the full rivet model

Figure 4.9 shows the force due to the displacement to the time of the solution for the model with the BEAM-elements used as rivets. where at t=1 the load increment starts from zero, and at t=2 the displacement is 2,5mm. The green line represents the force in the Y-direction, which is the vertical component. At maximum displacement the value of this vector is 125,0 kN.

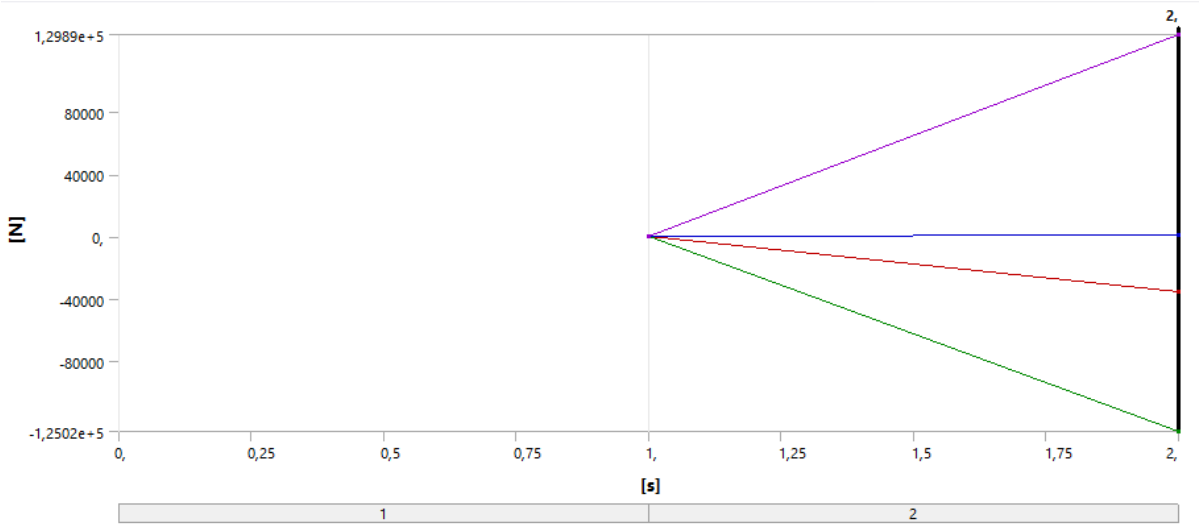

Figure 4.9: Force over time of the beam-element model

There is a marginal difference between the two forces. It is concluded that the stiffness increment due to the allowable tensile force in the DOF-coupling method can be neglected.

4.2.2 Check force transfer

A second check of the global model is done to determine validity of the force transfer in the rivets. In Figure 4.10 the horizontal force transfer of the two models is compared. Values in the graph are marginally different. Only the value at the first rivet is significantly different. This can be associated with the boundary condition applied to the first rivet to prevent this rivet being under-constraint. The difference in this value can be neglected, the governing peak stresses only occur at the locations near the load introduction.

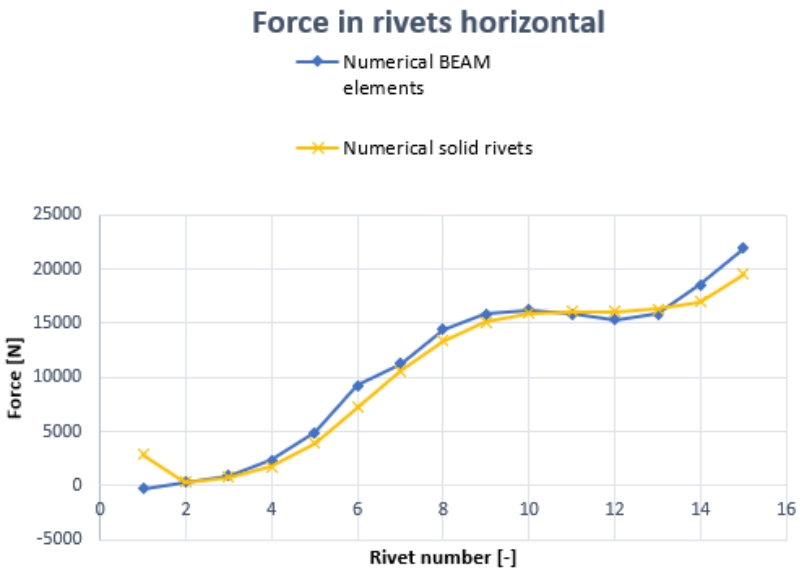

Figure 4.10: Horizontal force transfer rivets two models

4.3 Sub model

A section of the global model is taken out and modelled in a sub model. This model is a more detailed than the global model and it consist of a finer mesh, particular near the rivet hole. The second improvement is the modelling of the rivet. In the global model a beam element with DOF coupling between the vertex and the inner planes of the rivet is used to model the connection of the rivets. In the sub-model, all solid elements are used with contacts in between the bodies. The difference between the sub-model and the model to validate the beam element model is in the density of the mesh, where the sub-model has a significantly denser mesh all throughout the model.

The section that is taken out is the highest loaded section of the beam. This is the section around the rivet near the load introduction. A section of 6 rivets is included in the sub-model. The sub-model is shown in Figure 4.11.

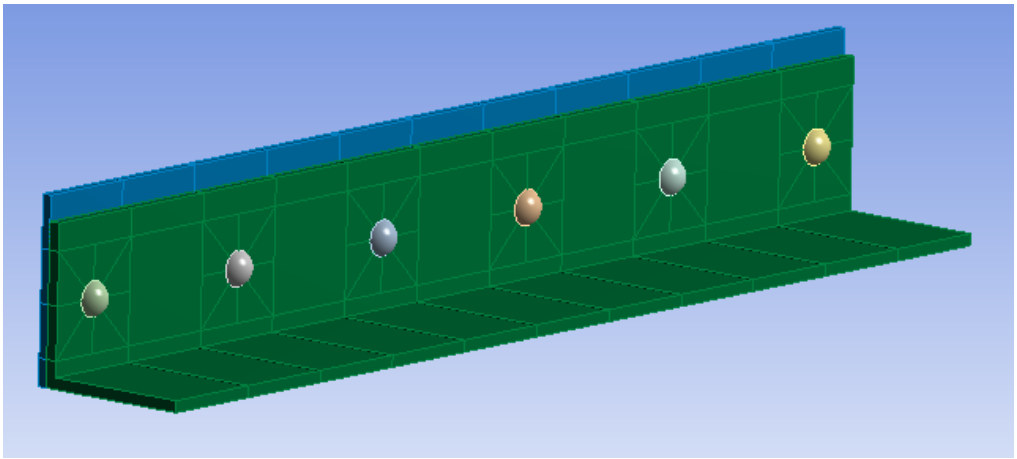

Figure 4.11: Overview submodel

4.3.1 Geometry

The submodel is split up into three main parts. The bodies taken from the flange of the model, the bodies taken from the web of the model, and the newly modelled bodies for the rivets. The flange profile is sliced in two locations, making a splice plane over the xy-plane. The web profile is sliced in two locations by cutting out two planes in the xy-plane and two over the zx-plane.

The rivets are modelled in accordance with "NEN N 667 Klinknagels met bollen kop" []. Which gives standardized geometrical properties of rivets as described in the literature review.

The sliced section of the web is shown in Figure 4.12. The section of the web profile is taken with a greater height than the height of the flange profile. In this manner, the full contact area of the flange profile is in contact with the web profile, to ensure correct frictional behaviour between the two bodies.

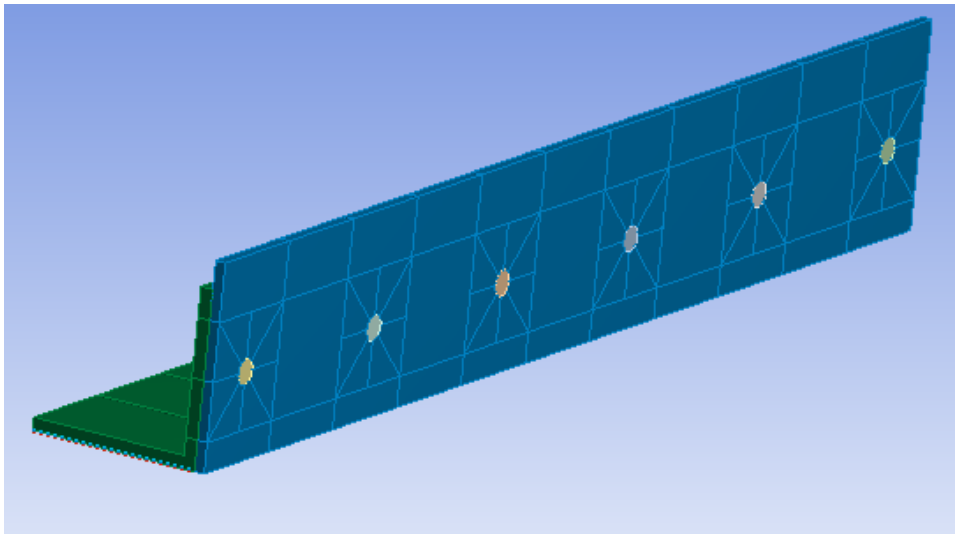

Figure 4.12: Overview web profile sub-model

Where the symmetry plane, as applied in the global model, still applies to the faces on the yz-plane of the web bodies. For this same symmetry plane, the outer faces of the rivet bodies are subjected to this symmetry condition.

4.3.2 Boundary constraints

To model the sub-model to the global model, boundary constraints are introduced. The boundary constrains are applied to each of the faces where a cut section is made. These imported boundary constraints take the displacement and forces of the nodes on the selected faces and apply these displacements on the sub-model.
For the flange profile boundary constraints are shown in Figure 4.13 with the same boundary conditions applied on the other side of the flange profile.

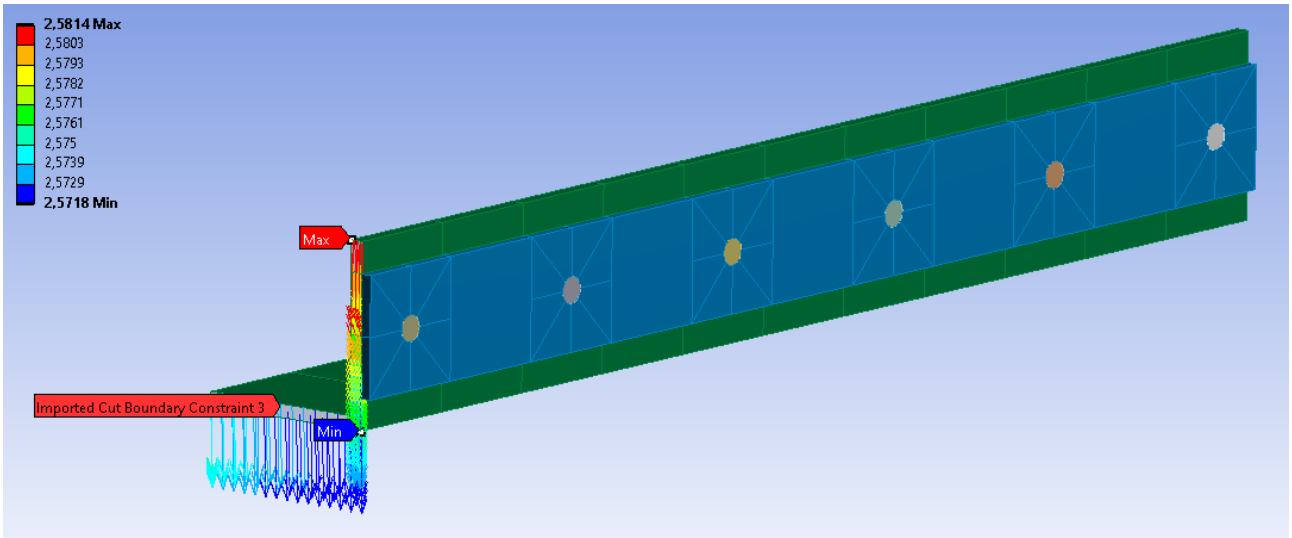

Figure 4.13: Boundary constraints flange

4.3.3 Contacts

There are two categories of contact in the sub-model, namely the contact between the flange profile and the web profile. and the contact between the rivets and the web/flange profile. For both of these instances a non-linear contact is defined. The contact used is a frictional contact with a programmed controlled contact formulation. A material friction coefficient of 0,3 is used.

4.3.4 Contact formulation

This contact is prone to penetration due to the large contact force between the rivet shank and the rivet hole. To ensure minimum penetration between these contacts, a normal Lagrange contact formulation is used.

4.3.5 Rivets in FEM model

The Rivets in the FEM model are modelled with a geometry according to the standard in NEN-N 667. The modelled rivet is shown in Figure 4.14. The rivet is created by modelling the shank with the desired width and length, in this case respectively 22mm and 20mm, where there is a symmetry plane at the end of the shank, after which a sphere is applied with a radius correspondent with the values in NEN-N 667. This sphere then is translated inwards of the rivet with a distance 'h' as defined in in NEN-N 667, and finally the excessive part of the sphere is cut of, creating a conformal rivet.

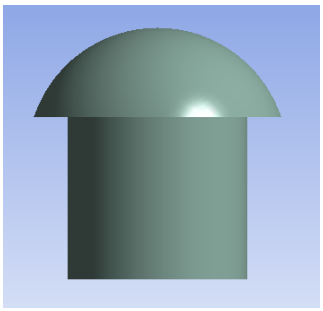

Figure 4.14: Rivet in the FEM model

4.3.6 Rivet mesh

The rivet is meshed using tetrahedron-elements. The non-standardized geometry makes the use of hexagon elements resulting in a higher number of low quality elements. Since there is a non-clean geometry a patch independent algorithm for meshing control is used. meaning that the volume mesh is generated first, and this is projected on the faces and edges of the solid. Using this method results in a higher quality mesh.

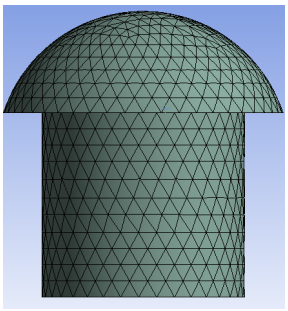

Figure 4.15: Mesh example rivet

Chapter 5

Comparison analytical and numerical models

The results from the numerical model are used as a verification for the analytical model. The distribution of the force transfer between rivet and web is compared to the global model. For the stress concentrations occurring at the notches of the rivet holes, the sub-model in combination with the global model is used. For this comparison, the dimensional parameters in the analytical model are set to the values used in the numerical model.

5.1 Force transfer in rivets

Horizontal force transfer

Looking at the force transfer in horizontal direction in the rivets in the numerical model, the values in Table 5.1 are found. These results are taken as the shear force in the beam elements in the global model

Table 5.1: Shear forces in horizontal direction rivets numerical model

Rivet number [-]	location [mm]	**Force [N]**
1	0	280
2	200	270
3	400	870
4	600	2330
5	800	4870
6	1000	9250
7	1200	11270
8	1400	14410
9	1600	15890
10	1800	16250
11	2000	15860
12	2200	15350
13	2400	15860
14	2600	18590
15	2800	21950
Support	2900	0

Where rivet number 1 is the rivet in the midpoint of the beam, and rivet number 15 the rivet closest to the support. A plotted graph of these values is shown in Figure 5.1.

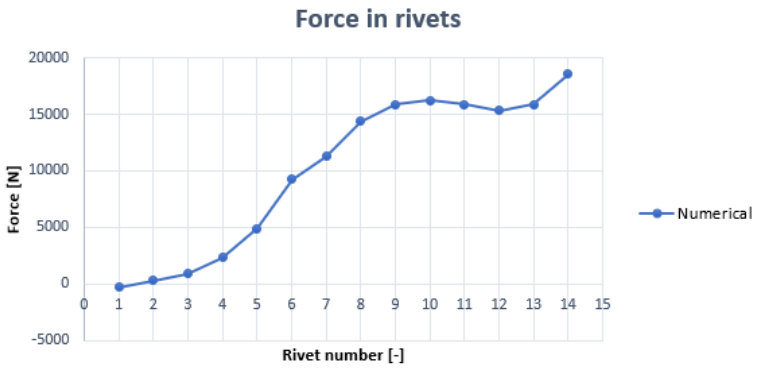

Figure 5.1: Shear force in rivets in vertical direction

Looking at the values gained from the analytical model compared to the numerical model, the two graphs are found as shown in Figure 5.2.

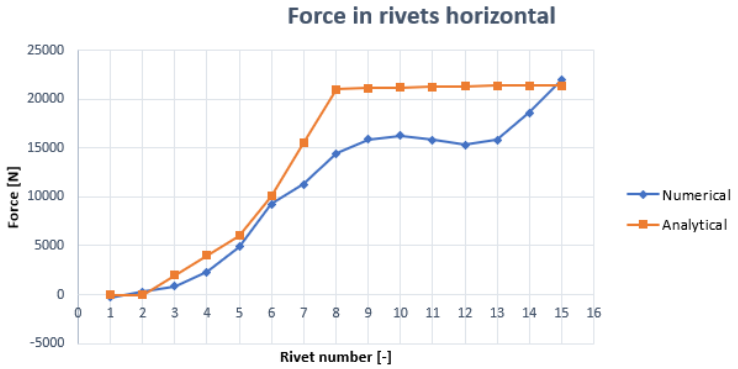

Figure 5.2: Comparison horizontal force transfer

This graph shows that the results gained from the analytical model are slightly higher than the results from the numerical model. This discrepancy in results increases in the linear moment zone, where in the constant moment zone, the results are more in accordance. In the collected data set the majority of failure occurred within or a few rivets next to the constant moment zone. Additionally, this is the region where the bypass loading is at maximum value, thus pin loading being a less significant part of the stress concentration around the rivet hole. For now it is assumed that the discrepancy in pin loading as described above does not significantly alter the maximum stress range found in the governing rivet holes. It should be noted that results giving a maximum stress range in the rivets in the linear moment zone could deviate from the real occurring stress range.

Vertical force transfer

Looking at the force transfer in vertical direction in the rivets the values in Table 5.2 are found in the global numerical model. These values are taken from the vertical shear force in the BEAM elements.

Table 5.2: Shear forces in vertical direction rivets numerical model

Rivet number [-]	location [mm]	**Force** [N]
1	0	-47
2	200	-2
3	400	147
4	600	441
5	800	805
6	1000	1010
7	1200	879
8	1400	508
9	1600	112
10	1800	289
11	2000	948
12	2200	2179
13	2400	3137
14	2600	3707
15	2800	34886
Support	2900	-

Where rivet number 1 is the rivet on mid-span of the beam, and rivet 15 is the rivet near the support. The values are plotted in a graph seen in Figure 5.3.

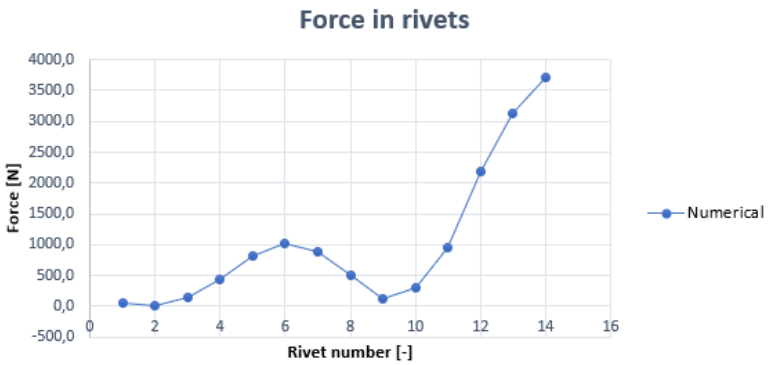

Figure 5.3: Shear force in rivet in vertical direction

Comparing these values to the graph of the values gained from the analytical model gives the graph as shown in Figure 5.4. As can be seen on the graph, the results gained from the analytical model are very much in accordance to the results gained from the numerical model.
Comparing the results from the horizontal load transfer to the results of the vertical force transfer in can clearly be seen that the horizontal load transfer is significantly higher. Transfer of load is larger with a factor of around 10 in horizontal direction. These load transfer also have the stress concentrations due to the pin load at the same locations as the stress concentrations due to the bypass loading.

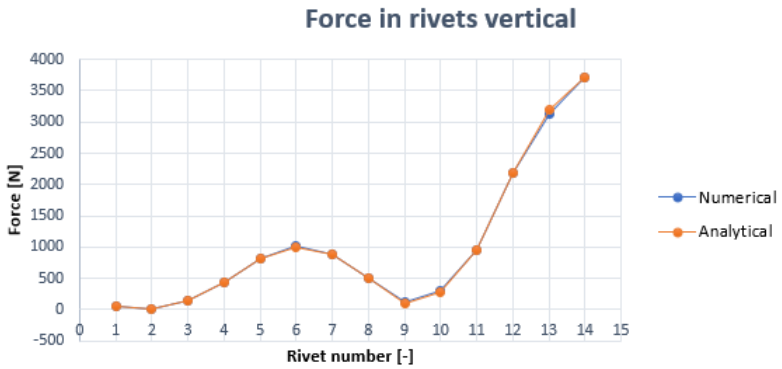

Figure 5.4: Comparison vertical force transfer

5.2 Results sub-model

To check the validity of the sub-model, the force transfer in the rivets of the two models are compared. The two graphs with the horizontal force transfer are plotted. This is shown in Figure 5.5. The sub-model is build up of six fully modelled solid rivets. The modelled rivets are number 3 through 6, which is the the rivets under the point of load application and the two adjacent rivets on one side, and three adjacent rivets on the other side.

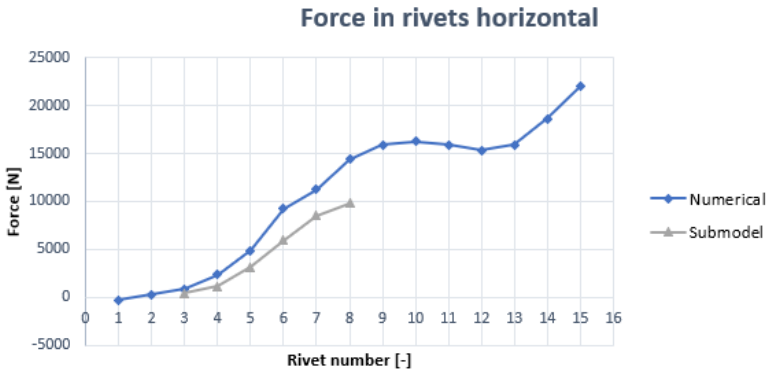

Figure 5.5: Comparison sub-model and global model

The values of the force transfer in the full solid rivets in the sub-model are lower than the force transfer in the global model. The values of the global numerical model using BEAM elements has been validated by comparing the results to a fully modelled build-up girder. For now it is unknown why the results in force transfer from the global model deviate from the values gained in the sub-model.

5.3 Results stress concentrations

The results from the stress concentration at each rivet location is shown in Figure 5.6. In this figure, the maximum stress state at each of the rivet holes is taken from the numerical model, and the calculated values for each of the locations of the numerical analysis.

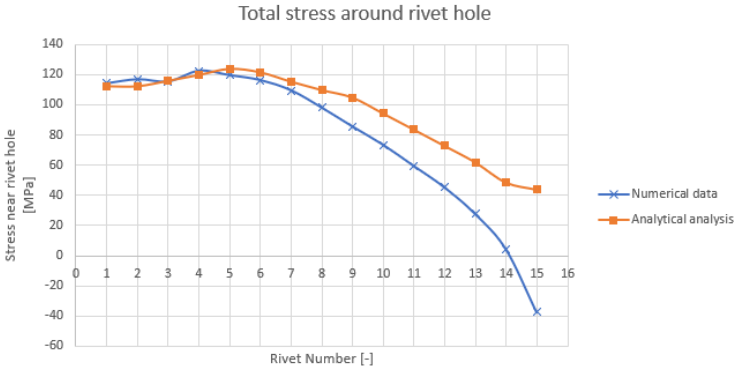

Figure 5.6: Results stress concentration

The maximum stress values at the governing locations, in this instance rivet number 1 through 7, are very similar. After this rivet the deviation in values becomes larger. This is to be expected, for the deviation of the values of the force transfer, and the share of the pin load become larger after this location. This results in the values after the load introduction to be inaccurate. Due to the lower stress state in these locations, these discrepancies in results are neglected.

Chapter 6

Processed data

In this chapter the data collected in the literature study will be processed. The parameters of the full scale tests found in literature are filled implemented in the analytical model. The results gained from the analytical model is the new stress range parameter including the effects of bypass loading, pin loading and friction between the web and flange profile.

Two different sets of data will be compared. The first set is the data collected in the literature study, this is the S-N data collected from papers which conducted full scale tests on bridge girders. The stress range as defined in these papers is generally the net-section stress range in the most outer fibre of the girder. There are various definitions among the papers for the value of cycles to failure. The only consistent definition among most of these papers is the numbers of cycles to crack initiation, this definition is used to check the influence of the newly defined stress parameter of the stress range.

The second set is the S-N data processed using the analytical model as described in Chapter 3. Each of the data-sets all known dimensional properties are filled in into the analytical model. The model then calculates the stress concentration at each of the rivet locations. The $\Delta\sigma$ in the processed data graphs is defined as the stress range at the notches of the rivet holes, with stress concentrations due to bypass loading, pin loading and friction.

Not all of the collected tests are suitable for processing using this method. Only the papers testing specimens in four point bending tests, with sufficient geometrical data are suitable. Table 6.1 shows a summary of the collected papers, and weather these are suitable for processing.

Table 6.1: Processed data set

Paper	**Type of test**	**Dimensions**	**Stress range**	**Processed**
Fisher [10]	4 point bending	Yes	Net section stress	Yes
Bruhwiller [4]	4 point bending	Yes	Unknown	Yes
Adamsson [12]	4 point bending	Yes	Strain gauges	Yes
Baker [3]	Tensile	Yes	Strain gauges	Yes
DiBattista [6] [7] [8]	Tensile	Yes	Strain gauges	Yes
Akesson [22]	4 point bending	Yes	Net section stress	Yes
Al-Emrani [2]	4 point bending	Yes	Net section stress	Yes
Out [19]	4 point bending	Yes	Unknown	Yes
Abe [13]	4 point bending	No	Unknown	No
Mang [13]	4 point bending	No	Unknown	No

6.1 Data Fisher

Table 6.2 shows the dimensions of the test set-up. In this test, test numer 1 - 2 and test number 5 - 8 are labeled as Fisher Type 1, where Test 3 - 4 are labeled as Fisher type 2.

Table 6.2: Dimensions test Fisher 1990

I.D	Length A [mm]	Length B [mm]	Length C [mm]
1 - 2	1524	3048	7620
3 - 4	1524	1908	5340
5 - 8	1524	3048	7620

The stress state in the section is built up of the elements as shown in Figure 6.1. The shares of the effect of the pin load, the effect of the bypass loading, and the effect of the friction are shown in the graph, these are effects contributing to the total stress in the notch of the rivet hole. This example is based on the Type 1 geometry of the Fisher data set.

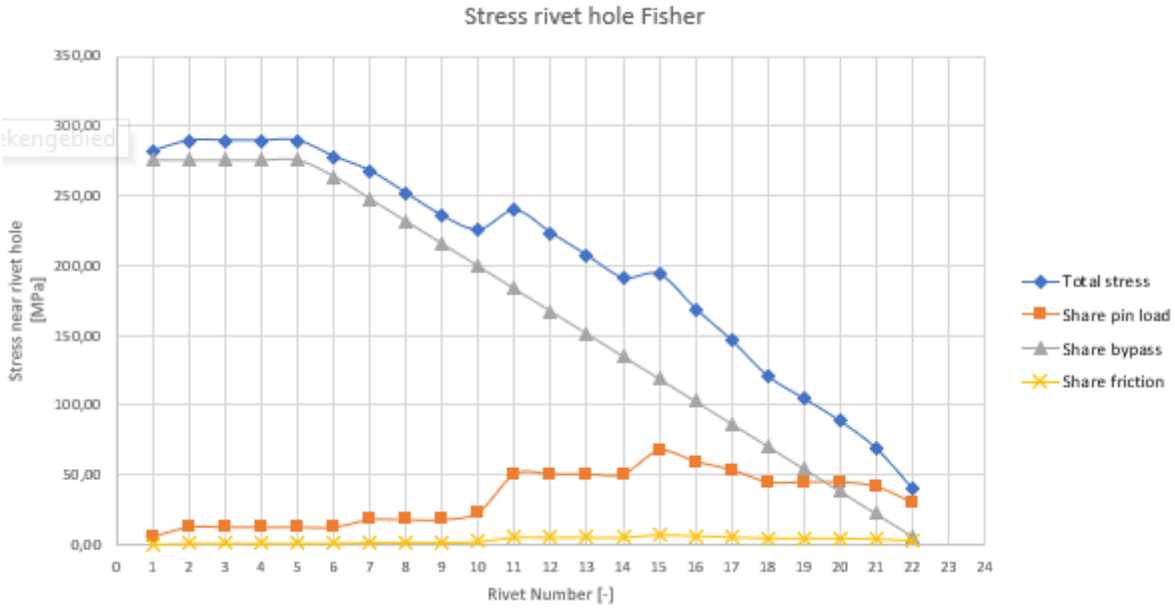

Figure 6.1: Stress state in beam Fisher

The graph shows the maximum stress occurring in rivet number 9. This is the location one rivet adjacent to the load introduction.

The unprocessed test data is shown in Figure 6.2. In this paper two different beam configurations are described, these are indicated with type 1 and type 2, due to the difference in geometry, the ratio between unprocessed data and processed data might differ for type 1 and type 2.

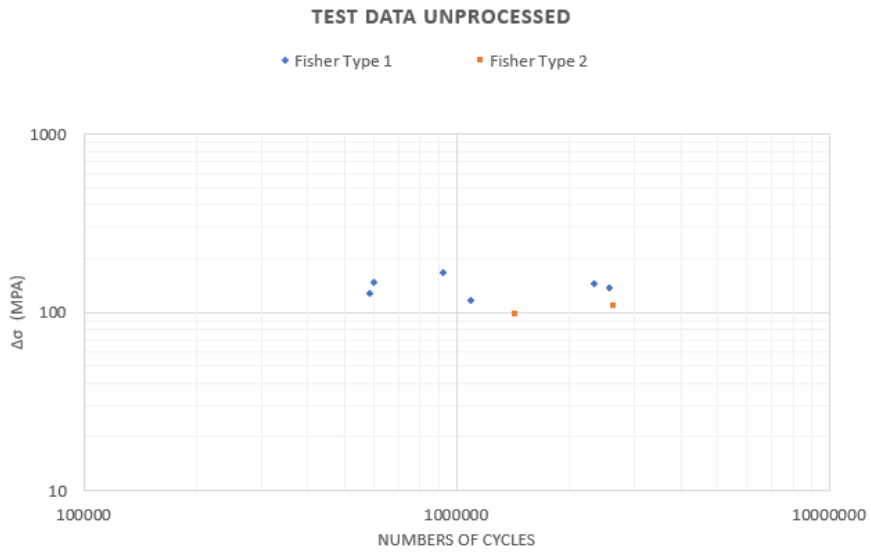

Figure 6.2: Test data Fisher unprocessed

The data with the new stress range parameter gives the values illustrated in Figure 6.3. The value presented in the plot of the new dataset is the maximum value taken from every rivet location according to Figure 6.1.

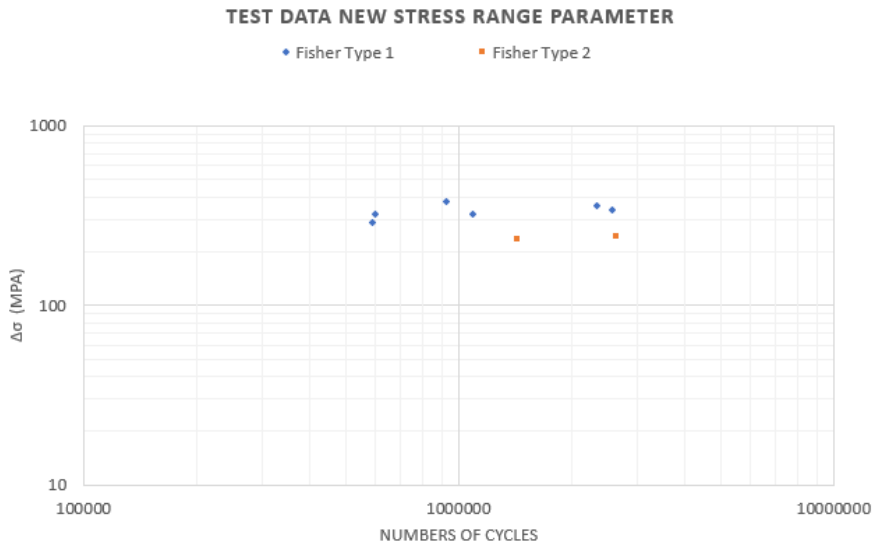

Figure 6.3: Test data Fisher with new stress range parameter

6.2 Data Adamson

Table 6.3 shows the relevant dimensions and test numbers of this paper. All of the tests have the same dimensional properties. Difference in tests consists of the different force range applied to the beam.

Table 6.3: Dimensions tests Adamson

I.D	Length A [mm]	Length B [mm]	Length C [mm]
All tests	2540	2540	7620

Figure 6.4 shows the shares of stress present in the beam at each of the rivet locations.

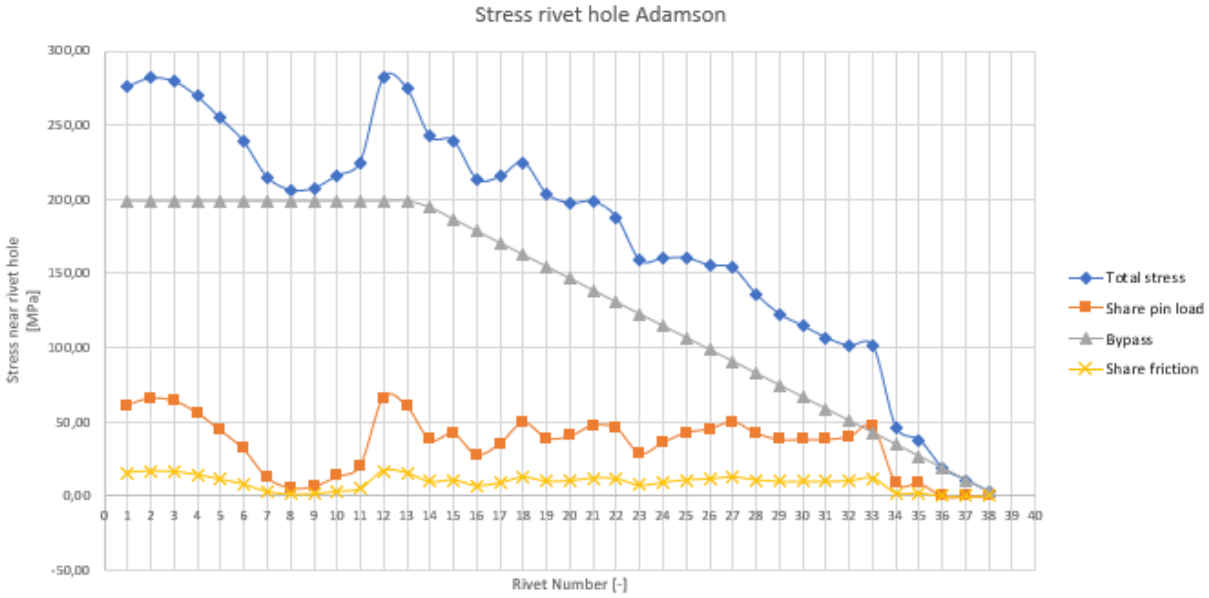

Figure 6.4: Stress state in beam Adamson

As can be seen the maximum stress is occurring at rivet number 12. This is the location 2 rivets adjacent to the load introduction. The maximum stress shown in the example is based on the test where the net section stress is 63 MPa. The share of pin load and friction(66 MPa and 17 MPa) is at the governing rivet significantly smaller than the share of the bypass loading (199 MPa).

The unprocessed data with the net section stress range is shown in figure 6.5.

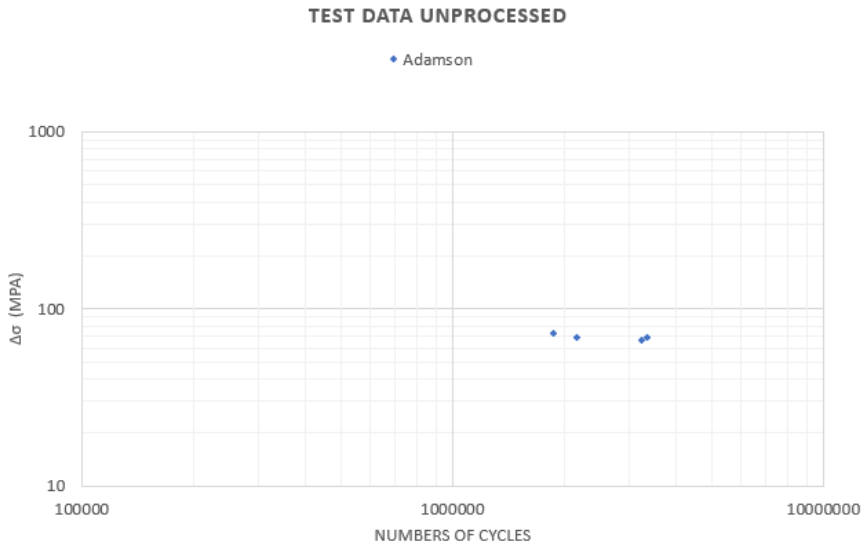

Figure 6.5: Test data Adamson unprocessed

The new data processed using the newly defined stress range parameter is shown in Figure 6.6.

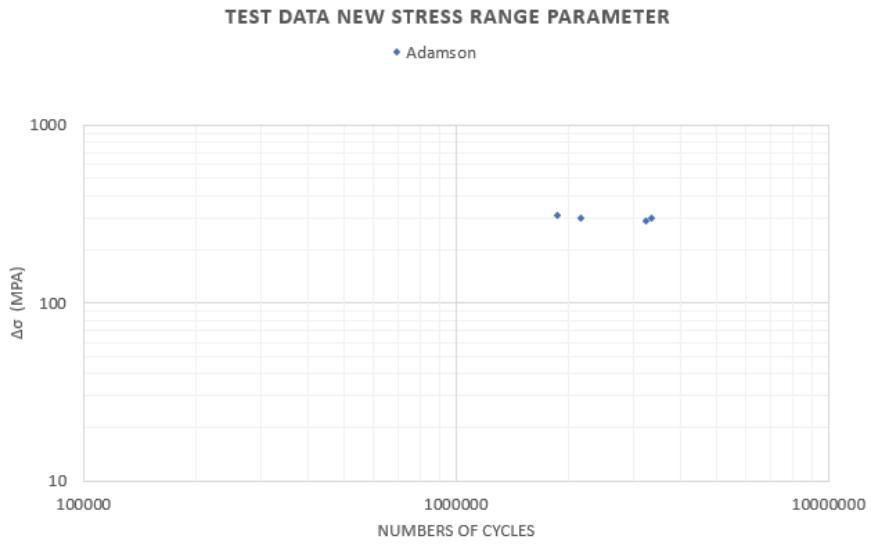

Figure 6.6: Test data Adamson new stress range paramater

6.3 Data Akkeson

Table 6.4 shows the relevant dimensions of tests from this paper.

Table 6.4: Dimensions tests Akesson

I.D	Length A [mm]	Length B [mm]	Length C [mm]
2A, 3B, 5B	1500	2000	5000
4B, 5A, 10B	1500	2000	5000

The stress occurring in the beam is build up at each of the rivet locations as shown in Figure 6.7.

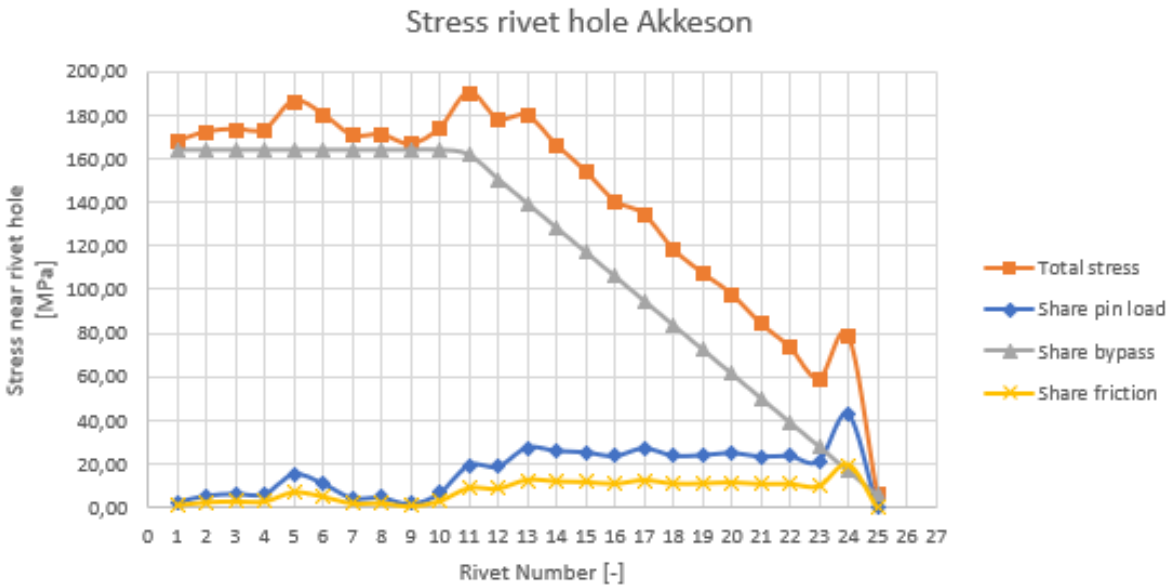

Figure 6.7: Stress state in beam Akkeson

The maximum stress is occurring at rivet number 11. This is the rivet directly adjacent to the load introduction. The share of bypass loading at this location is significantly higher than the share of pin loading and friction.

The test data from the paper is shown in Figure 6.8. This data is based on the net nominal stress. The numbers of cycles is defined as the number of cycles to crack initiation at the rivet hole.

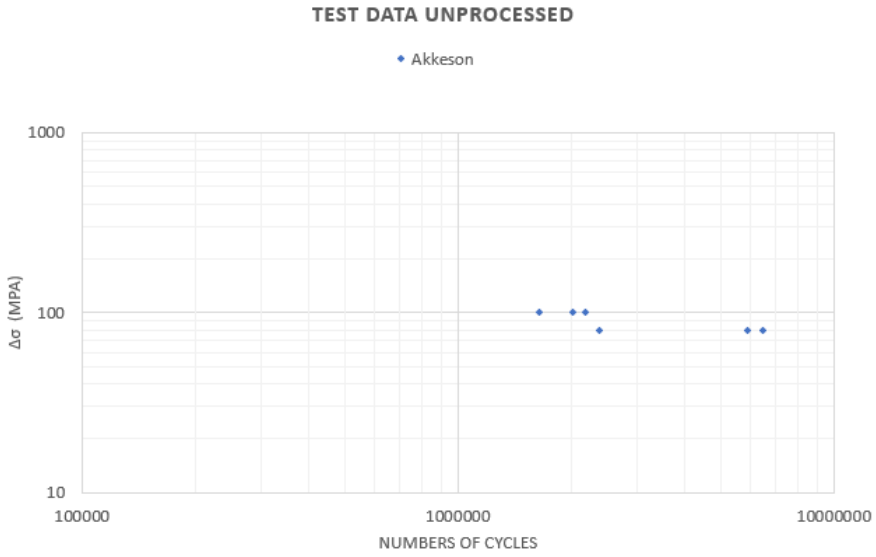

Figure 6.8: Test data Akkeson unprocessed

Figure 6.9 shows the data based on the new stress range parameter.

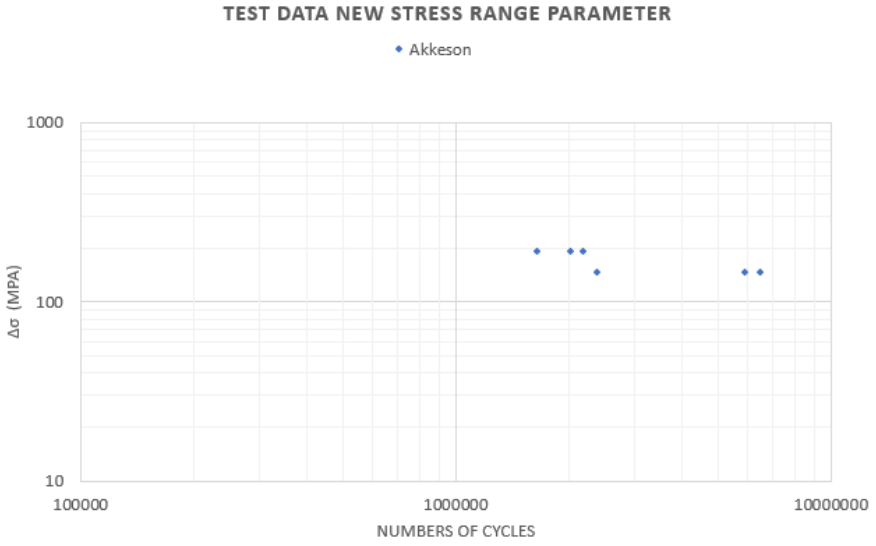

Figure 6.9: Test data Akkeson new stress range parameter

6.4 Data Al-Emrani

Table 6.5 shows the dimensions of the relevant tests from this paper.

Table 6.5: Dimensions tests Al-Emrani

I.D	Length A [mm]	Length B [mm]	Length C [mm]
All tests	2000	1250	4500

The stress state of the beam at each rivet location is shown in Figure 6.10.

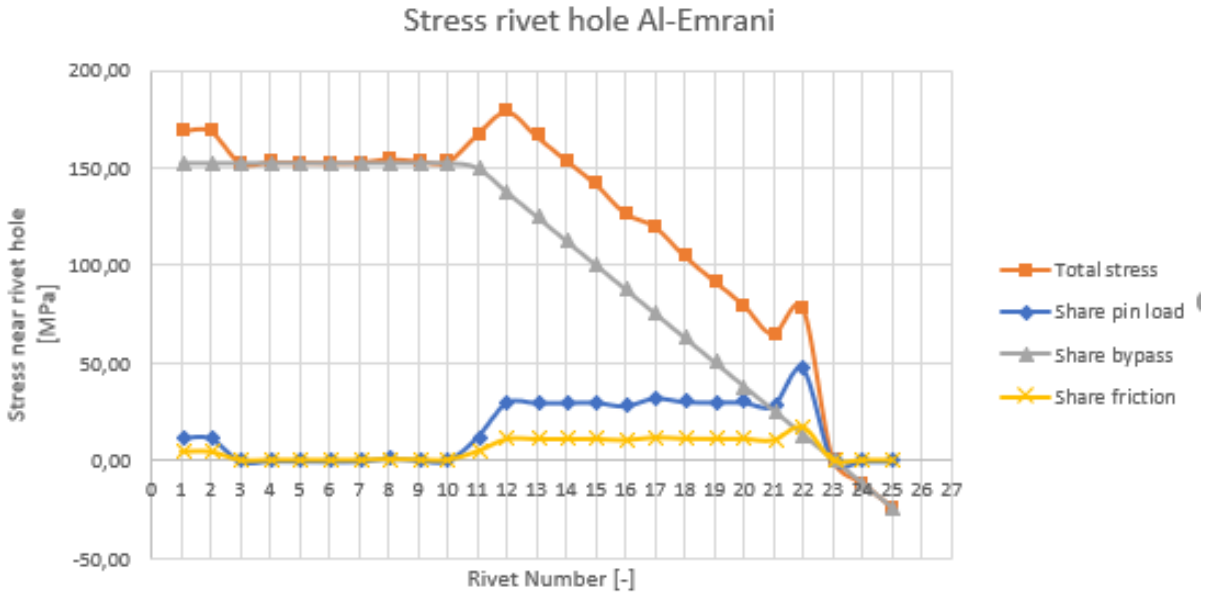

Figure 6.10: Stress state in beam Al-Emrani

The maximum stress is at rivet number 12, this is one rivet adjacent to the load introduction. The share of the bypass loading at this location (137 MPa) is significantly higher than the share of pin load and friction (30 MPa, 11 MPa).

Figure 6.11 shows the data collected from the paper. The stress range is defined as the net section stress at the most outer fiber of the beam. The number of cycles is defined as the number of cycles to crack initiation.

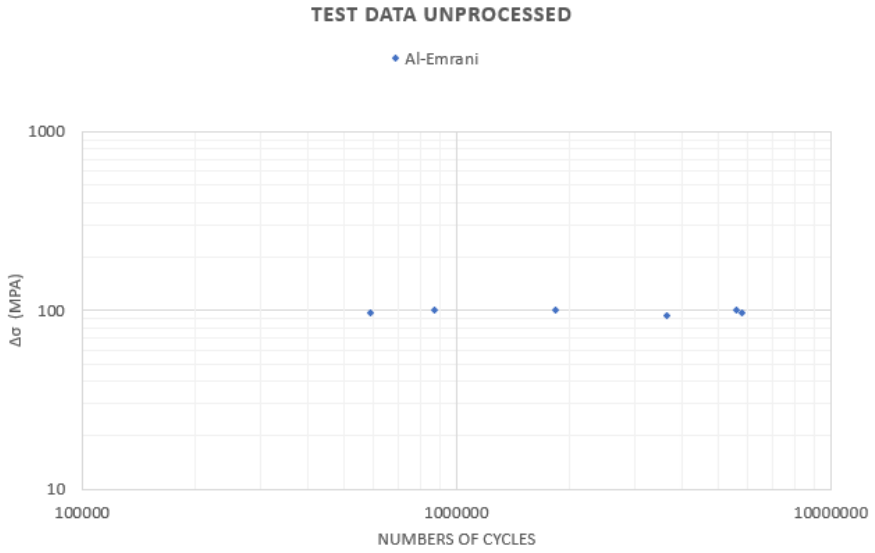

Figure 6.11: Test data Al-Emrani unprocessed

Figure 6.12 shows the processed data. The stress range is defined with the new stress range parameter.

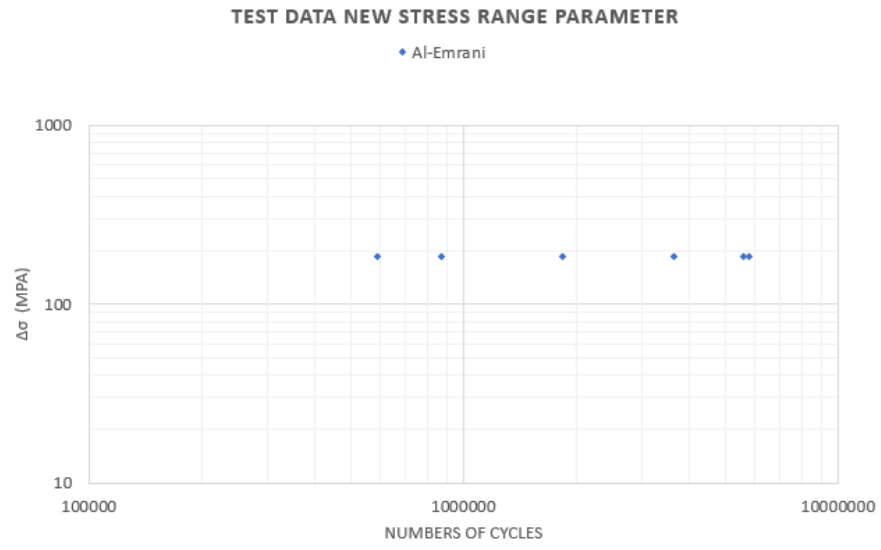

Figure 6.12: Test data Al-Emrani new stress range parameter

6.5 Data Out

Table 6.6 shows the dimensions of the relevant tests from this paper. In the paper five more beams are tested. These tests all failed in a location with a reduced area due to corrosion. This data is not suitable for processing using the analytical model.

Table 6.6: Dimensions tests Out

I.D	Length A [mm]	Length B [mm]	Length C [mm]
2A, 3B, 5B	1530	2285	6100

The stress state of the beam per rivet location is shown in Figure 6.13. The governing stress peaks occur at the rivets in the constant moment zone. There is no force transfer by the rivets in this part of the beam, and only bypass loading contributes to the stress of the beam. The absence of force transfer in the rivets in this specific beam could be explained by the large number of rivets in the linear moment zone. Due to the large number of rivets it is possible that the force transfer is evenly distributed along the beam, and approaches the theoretical shear flow. In this case there would be no shear, no shear flow, and thus no force transfer in rivets in the constant moment zone.

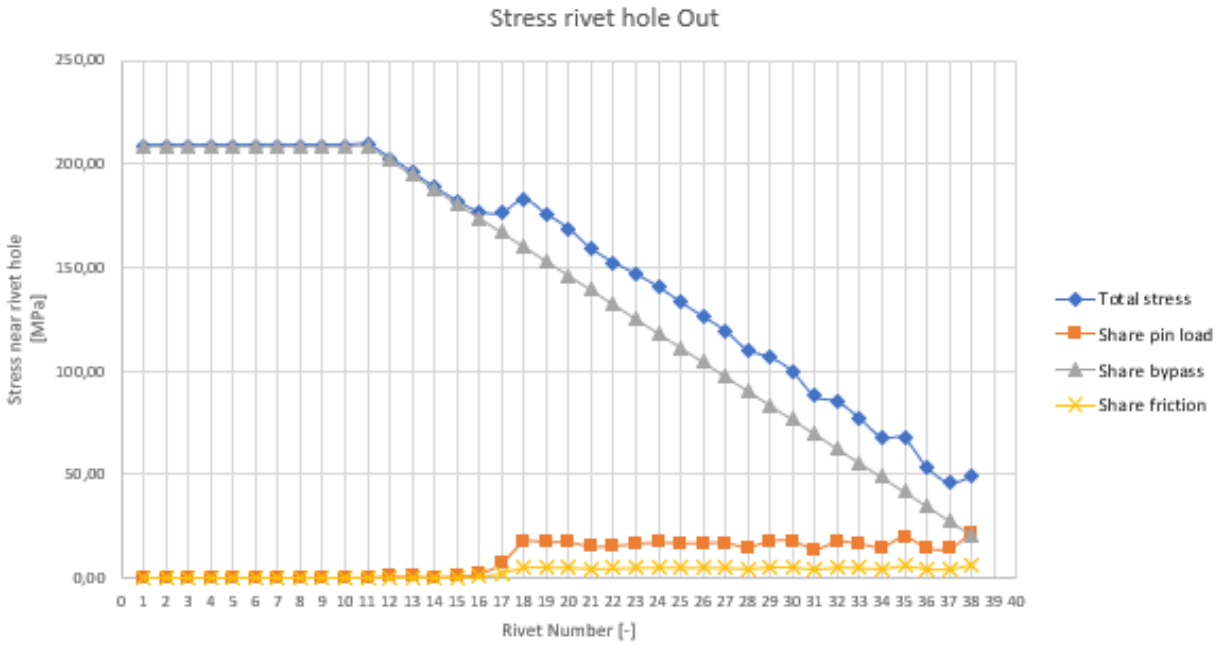

Figure 6.13: Stress state in beam Out

Figure 6.14 shows the data from the relevant tests from the paper. This stress range calculation is not described in the paper, it is assumed the stress range is based on the net section stress of the beam.

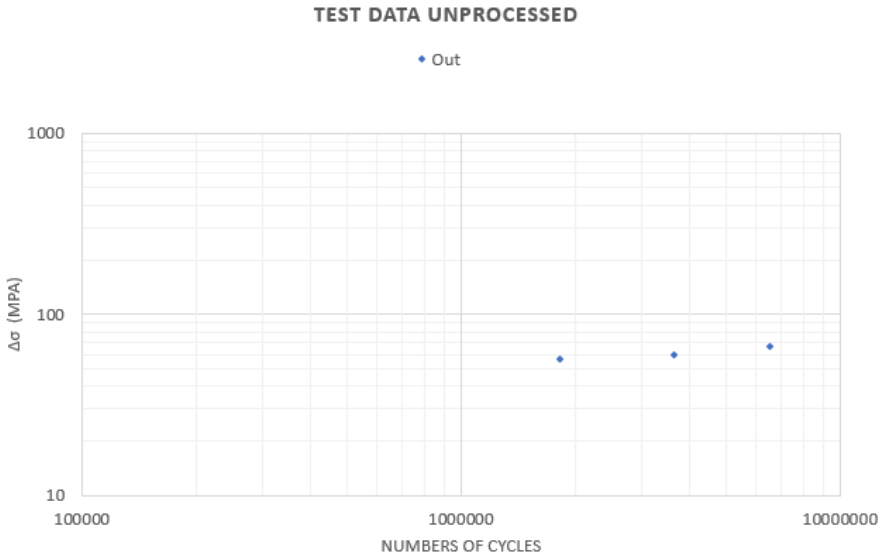

Figure 6.14: Test data Out unprocessed

Figure 6.15 shows the data with the newly defined stress range parameter.

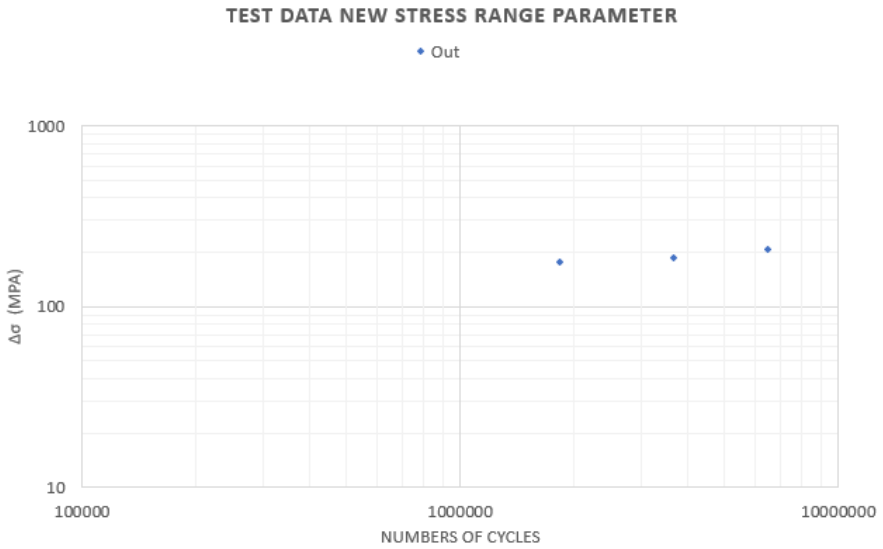

Figure 6.15: Test data Out processed

6.6 Tensile data

Two of the full scale tests were conducted as tensile tests. In this research, the peak stresses of build-up girders in four point bending are calculated with the numerical model. a simplified version of this calculation can be used to determine the peak stresses in elements loaded in tensile force. In this model, only the bypass loading will have an effect on the peak stresses occurring at the rivet holes. The following test data is processed using this simplified model.

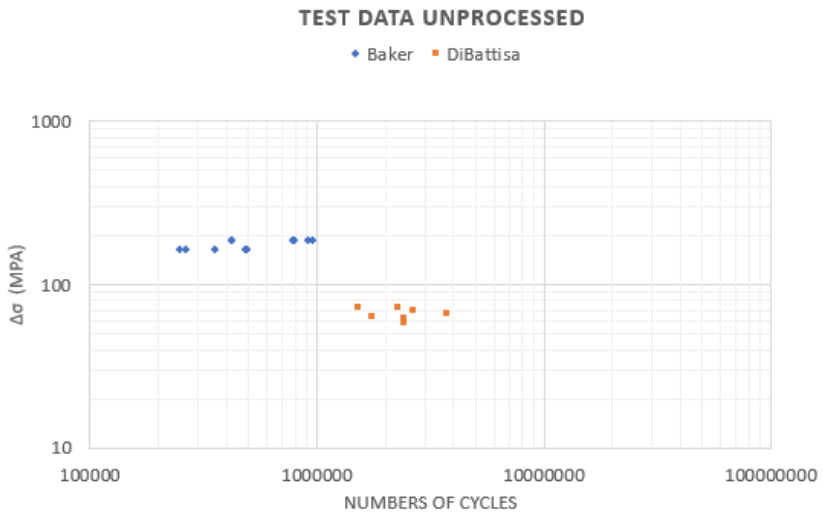

Figure 6.16: Data tensile tests unprocessed

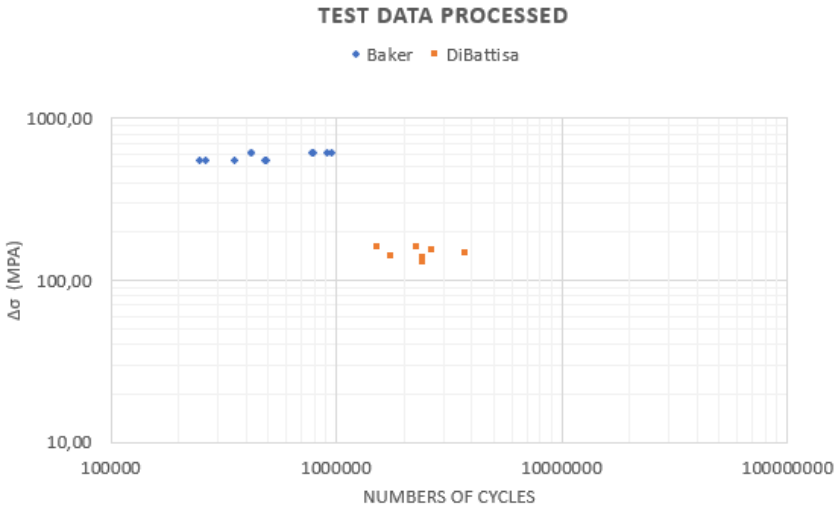

Figure 6.17: Data tensile tests processed

6.7 All data excluding tensile tests

All of the processed data is collected in Table 6.7. This summarises the number of cycles to crack initiation, the corresponding stress range based on the net section area, and the stress range as calculated using the analytical model from this research. The last column describes the ratio of the net section stress range compared to the new stress range parameter.

Table 6.7: Table with all processed data

Article	**Beam I.D.**	$\Delta\sigma_{net}$	$\Delta\sigma_{New}$	N_{ini}	**Ratio**
Fisher	**1**	128	289	588000	2,26
	2	117	320	1094000	2,74
	5	144	358	2344000	2,49
	6	138	341	2575000	2,47
	7	147	323	601000	2,20
	8	166	375	923000	2,26
	3	97	233	1435000	2,40
	4	108	243	2630000	2,25
Adamson	**ST9**	69	301	2486070	4,36
	ST3	73	311	1874730	4,26
	ST4	69	301	1521450	4,36
	ST7	66	290	2364230	4,39
Akesson	**A4**	80	145	5893400	1,81
	A5	80	145	2375500	1,81
	A6	80	145	6485300	1,81
	A7	100	190	1637900	1,90
	A8	100	190	2184900	1,90
	A9	100	190	2027300	1,90
Al-Ermani	**A1-1**	100	186	5571150	1,86
	A1-2	100	186	1840000	1,86
	A1-3	97	183	5799020	1,89
	A1-4	97	183	586700	1,89
	A1-5	100	186	872600	1,86
	A1-6	93	183	3639050	1,97
Out	**1**	65,9	184	6520000	2,79
	2	59,3	166	3650000	2,80
	3	56,2	157	1826000	2,79

Plotting all of the data with the stress range defined as the net section stress, the plot as seen in Figure 6.18 is obtained.

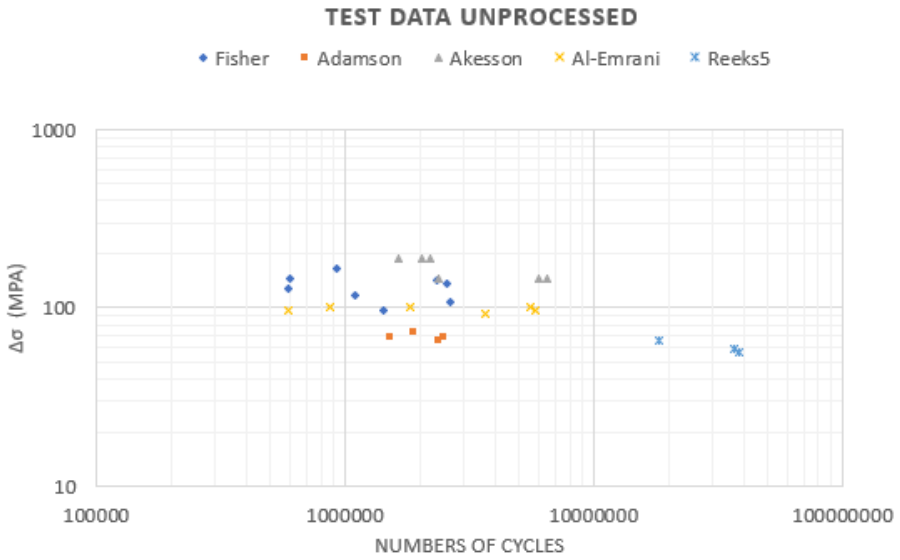

Figure 6.18: Total data set unprocessed

Plotting all the data with the newly defined stress range parameter, the plot as seen in Figure 6.19 is obtained.

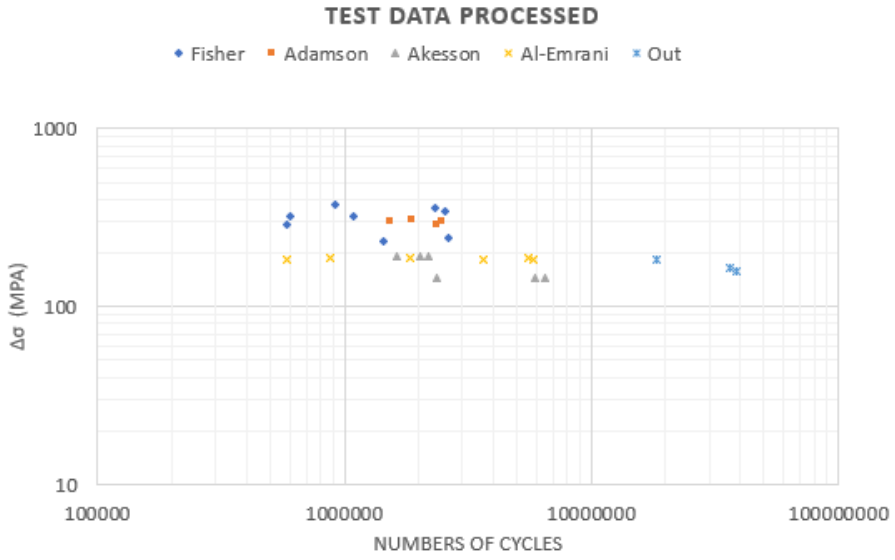

Figure 6.19: Total data set processed

6.7.1 Correlation of data

To obtain insight in the correlation of the data the correlation coefficient r of the two data sets are calculated. This coefficient describes the linear strength of the correlation of two data sets. The correlation between the two variables in this case is logarithmic. To describe the strength of the relationship the logarithmic values of the original tests results are calculated.

$\Delta\sigma_{net}[MPa]$	$\Delta\sigma_{New}[MPa]$	**N**	$Log(\sigma_{net})$	$Log(\Delta\sigma_{New})$	**Log (N)**
128	289	916000	2,11	2,46	6,0
117	320	1237000	2,07	2,51	6,1
144	358	2728000	2,16	2,55	6,4
138	341	3005000	2,14	2,53	6,5
147	323	773000	2,17	2,51	5,9
166	375	1315000	2,22	2,57	6,1
97	233	1623000	1,99	2,37	6,2
108	243	2836000	2,03	2,39	6,5
69	301	3336700	1,84	2,48	6,5
73	311	1874730	1,86	2,49	6,3
69	301	2168570	1,84	2,48	6,3
66	290	3240180	1,82	2,46	6,5
80	145	5995900	1,90	2,16	6,8
80	145	2375500	1,90	2,16	6,4
80	145	6485300	1,90	2,16	6,8
100	190	1637900	2,00	2,28	6,2
100	190	2184900	2,00	2,28	6,3
100	190	2027300	2,00	2,28	6,3
100	186	5571150	2,00	2,27	6,7
100	186	2002000	2,00	2,27	6,3
97	183	5959340	1,99	2,26	6,8
97	183	704090	1,99	2,26	5,8
100	186	1134280	2,00	2,27	6,1
93	183	3692050	1,97	2,26	6,6
65,9	184	18250000	1,82	2,26	7,3
59,3	166	36500000	1,77	2,22	7,6
56,2	157	38690000	1,75	2,20	7,6

The unprocessed logarithmic data, based on the net section stress, is plotted in Figure 6.20.

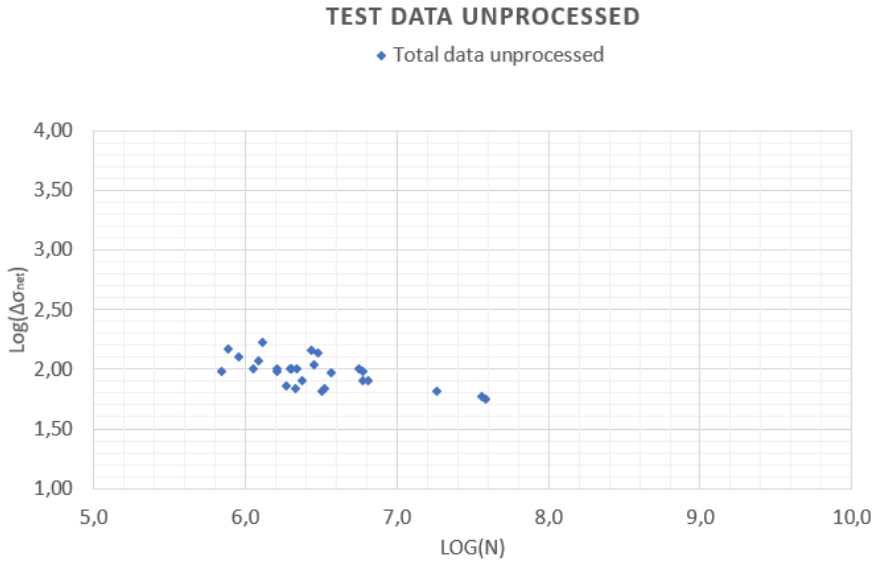

Figure 6.20: Total logarithmic data unprocessed

And the processed logarithmic data is plotted in Figure 6.21.

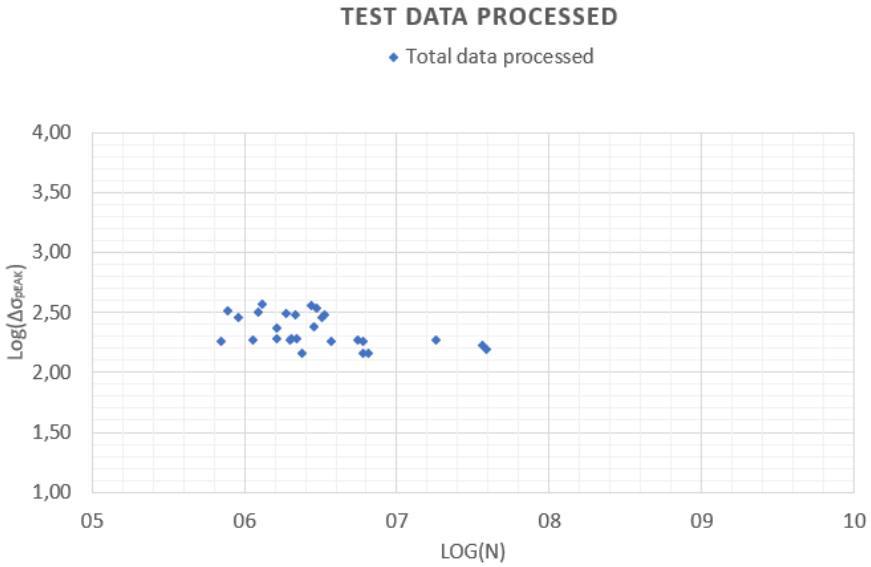

Figure 6.21: Total logarithmic data processed

The correlation coefficient between $Log(\Delta\sigma_{net})$ and Log(N) is -0,446. The correlation coefficient between $Log(\Delta\sigma_{New})$ and Log(N) is -0,468. This means that there is a very small increase in correlation strength with the new stress range parameter used in the processed data set.

6.7.2 Linear regression analysis

Table 6.8 calculates the standard deviation of C compared to a linear fit line of the logarithmic data. Variable C in the table represents the difference between the linear fit line and the real data. For the old data-set the standard deviation of C is 0,092 where the standard deviation of C for the new data set is 0,118. This means that there is no improvement in the correlation of the data-set calculated through a linear regression analysis.

Used linear formulas for the net section stress range is

$$M = -0,1776 \cdot Log(N) + 3,1225 \tag{6.1}$$

and the linear formula for the new stress range parameter fit for the data-set is.

$$M = -0,1441 \cdot Log(N) + 3,2808 \tag{6.2}$$

Table 6.8: Table calculating the standard deviation of C

			Linear fit formula		Linear fit formula	
			M =-0,1776 $\cdot Log(N) + 3,1225$		M = -0,1441 $\cdot Log(N) + 3,2808$	
log($\Delta\sigma_{net}$)	**log($\Delta\sigma_{new}$)**	**log(N)**	M_{net}	C_{New}	M_{new}	C_{new}
2,107	2,461	5,962	2,064	-0,044	2,422	-0,039
2,068	2,505	6,092	2,040	-0,028	2,403	-0,102
2,158	2,554	6,436	1,979	-0,179	2,353	-0,200
2,140	2,533	6,478	1,972	-0,168	2,347	-0,185
2,167	2,509	5,888	2,077	-0,091	2,432	-0,077
2,220	2,574	6,119	2,036	-0,184	2,399	-0,175
1,987	2,367	6,210	2,020	0,033	2,386	0,019
2,033	2,386	6,453	1,976	-0,057	2,351	-0,035
1,839	2,479	6,523	1,964	0,125	2,341	-0,138
1,863	2,493	6,273	2,008	0,145	2,377	-0,116
1,839	2,479	6,336	1,997	0,158	2,368	-0,111
1,820	2,462	6,511	1,966	0,147	2,343	-0,120
1,903	2,161	6,778	1,919	0,016	2,304	0,143
1,903	2,161	6,376	1,990	0,087	2,362	0,201
1,903	2,161	6,812	1,913	0,010	2,299	0,138
2,000	2,279	6,214	2,019	0,019	2,385	0,107
2,000	2,279	6,339	1,997	-0,003	2,367	0,089
2,000	2,279	6,307	2,002	0,002	2,372	0,093
2,000	2,270	6,746	1,924	-0,076	2,309	0,039
2,000	2,270	6,301	2,003	0,003	2,373	0,103
1,987	2,262	6,775	1,919	-0,068	2,304	0,042
1,987	2,262	5,848	2,084	0,097	2,438	0,176
2,000	2,270	6,055	2,047	0,047	2,408	0,139
1,968	2,262	6,567	1,956	-0,012	2,334	0,072
1,819	2,265	7,261	1,833	0,014	2,234	-0,030
1,773	2,220	7,562	1,779	0,006	2,191	-0,029
St. dev. of C			0,092664843		0,11803827	

6.8 All data including tensile tests

Table 6.9 shows the full data set including tensile tests and the logarithmic values of the test data. Plotting the data including the tensile tests gives the graph as seen in Figure 6.22. The correlation coefficient 'r' of the logarithmic values of this data-set is -0,693.

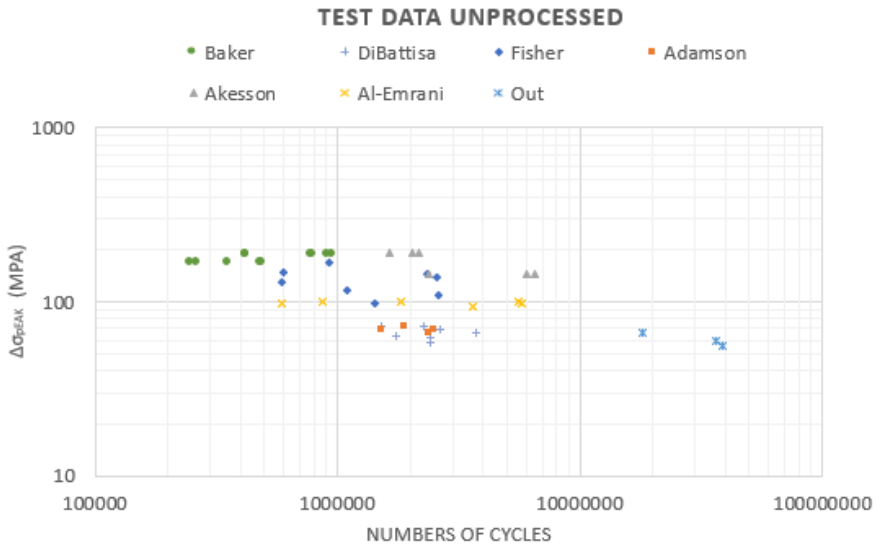

Figure 6.22: Total data set including tensile tests unprocessed

Plotting the data including the tensile tests using the newly defined stress range parameter gives the graph as seen in Figure 6.22. The correlation coefficient 'r' of the logarithmic values of this data set is -0,722.

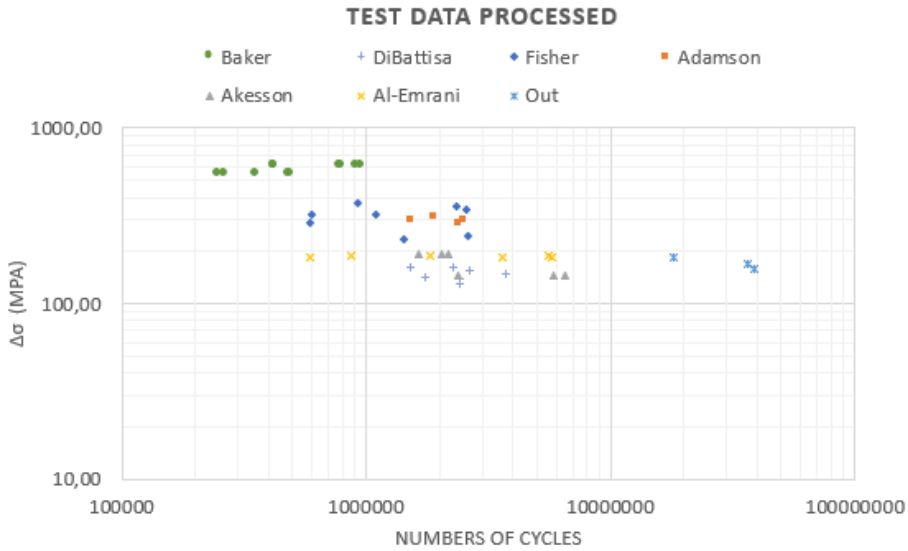

Figure 6.23: Total data set including tensile tests processed

The strength of the correlation coefficient of the data set with the newly defined peak stress range parameter is slightly higher than the correlation strength of the net section stress. The validity

of the tensile test data is not checked, since the only numerical model was a simulation of a four point bending test.

6.8.1 Linear regression analysis

Table 6.10 calculates the standard deviation of C compared to a linear fit line of the logarithmic data. Variable C in the table represents the difference between the linear fit line and the real data. For the old data-set the standard deviation of C is 0,117 where the standard deviation of C for the new data set is 0,358. This means that there is no improvement in the correlation of the data-set calculated through a linear regression analysis. Used linear formulas for the net section stress range is

$$M = -0,2755 \cdot Log(N) + 3,7406 \tag{6.3}$$

and the linear formula for the new stress range parameter fit for the data-set is.

$$M = -0,3599 \cdot Log(N) + 4,6718 \tag{6.4}$$

Table 6.9: Fatigue data including tensile tests

Article	**Girder no.**	$\Delta\sigma_{net}(Mpa)$	$\Delta\sigma_{New}(Mpa)$	**Cycles to failure**	**Ratio**
Fisher 1990	**1**	128	289	916000	2,26
	2	117	320	1237000	2,74
	5	144	358	2728000	2,49
	6	138	341	3005000	2,47
	7	147	323	773000	2,20
	8	166	375	1315000	2,26
	3	97	233	1623000	2,40
	4	108	243	2836000	2,25
Adamson	**ST9**	69	301	3336700	4,36
	ST3	73	311	1874730	4,26
	ST4	69	301	2168570	4,36
	ST7	66	290	3240180	4,39
Akesson	**A4**	80	145	5995900	1,81
	A5	80	145	2375500	1,81
	A6	80	145	6485300	1,81
	A7	100	190	1637900	1,90
	A8	100	190	2184900	1,90
	A9	100	190	2027300	1,90
Al-Ermani	**A1-1**	100	186	5571150	1,86
	A1-2	100	186	2002000	1,86
	A1-3	97	183	5959340	1,89
	A1-4	97	183	704090	1,89
	A1-5	100	186	1134280	1,86
	A1-6	93	183	3692050	1,97
Out	**1**	65,9	184	18250000	2,79
	2	59,3	166	36500000	2,80
Baker	**BkC-1s**	188	615,74	418500	3,28
axial tension	**BkC-1b**	188	615,74	418500	3,28
	BkC-1c	188	615,74	958300	3,28
	BkC-2a	188	615,74	782300	3,28
	BkC-2b	188	615,74	793600	3,28
	BkC-2c	188	615,74	911800	3,28
	Bkd-3a	166	543,69	263100	3,28
	Bkd-3b	166	543,69	493300	3,28
	BkD-4a	166	543,69	249100	3,28
DiBattisa	**BD1**	73	161,81	1509710	2,22
axial tension	**BD2**	69	152,94	2655330	2,22
	BD3	73	161,81	2273500	2,22
	BD4	66	146,29	3722300	2,22
	TD1	64	141,86	1735140	2,22
	TD2	62	137,43	2415840	2,22
	TD3	58	128,56	2415140	2,22

Table 6.10: Linear regression calculation with tensile data

			Linear fit formula M = -0,2755 $\cdot Log(N) + 3,7406$		Linear fit formula M = -0,3599 $\cdot Log(N) + 4,6718$	
$log(\Delta\sigma_{net})$	$log(\Delta\sigma_{new})$	$log(N)$	M_{net}	C_{Net}	M_{new}	C_{new}
2,107	2,461	5,962	2,097	-0,010	2,526	0,065
2,068	2,505	6,092	2,062	-0,007	3,927	1,422
2,158	2,554	6,436	1,967	-0,191	3,895	1,341
2,140	2,533	6,478	1,955	-0,185	3,902	1,369
2,167	2,509	5,888	2,118	-0,050	3,892	1,383
2,220	2,574	6,119	2,054	-0,166	3,873	1,299
1,987	2,367	6,210	2,029	0,042	3,957	1,589
2,033	2,386	6,453	1,962	-0,071	3,940	1,554
1,839	2,479	6,523	1,943	0,104	4,010	1,531
1,863	2,493	6,273	2,012	0,148	4,001	1,508
1,839	2,479	6,336	1,994	0,156	4,010	1,531
1,820	2,462	6,511	1,946	0,127	4,017	1,555
1,903	2,161	6,778	1,873	-0,030	3,987	1,826
1,903	2,161	6,376	1,983	0,080	3,987	1,826
1,903	2,161	6,812	1,863	-0,040	3,987	1,826
2,000	2,279	6,214	2,028	0,028	3,952	1,673
2,000	2,279	6,339	1,993	-0,007	3,952	1,673
2,000	2,279	6,307	2,002	0,002	3,952	1,673
2,000	2,270	6,746	1,881	-0,119	3,952	1,682
2,000	2,270	6,301	2,004	0,004	3,952	1,682
1,987	2,262	6,775	1,873	-0,113	3,957	1,694
1,987	2,262	5,848	2,129	0,142	3,957	1,694
2,000	2,270	6,055	2,072	0,072	3,952	1,682
1,968	2,262	6,567	1,931	-0,038	3,963	1,701
1,819	2,265	7,261	1,740	-0,079	4,017	1,752
1,773	2,220	7,562	1,657	-0,116	4,034	1,814
2,274	2,789	5,622	2,191	-0,083	3,853	1,064
2,274	2,789	5,622	2,191	-0,083	3,853	1,064
2,274	2,789	5,982	2,092	-0,182	3,853	1,064
2,274	2,789	5,893	2,116	-0,158	3,853	1,064
2,274	2,789	5,900	2,115	-0,159	3,853	1,064
2,274	2,789	5,960	2,098	-0,176	3,853	1,064
2,220	2,735	5,420	2,247	0,027	3,873	1,137
2,220	2,735	5,693	2,172	-0,049	3,873	1,137
2,220	2,735	5,396	2,253	0,033	3,873	1,137
2,220	2,735	5,548	2,212	-0,008	3,873	1,137
2,220	2,735	5,686	2,174	-0,047	3,873	1,137
1,863	2,209	6,179	2,038	0,174	4,001	1,792
1,839	2,185	6,424	1,970	0,131	4,010	1,825
1,863	2,209	6,357	1,989	0,125	4,001	1,792
1,820	2,165	6,571	1,930	0,110	4,017	1,852
1,806	2,152	6,239	2,021	0,215	4,022	1,870
1,792	2,138	6,383	1,981	0,189	4,027	1,889
1,763	2,109	6,383	1,981	0,218	4,037	1,928
	St. Dev C			0,117		0,358

Chapter 7

Conclusions

The research is based on the question whether a new stress range parameter can be defined to more accurately describe the fatigue life of riveted girders. In excising full scale tests the stress range is mostly calculated using the net section stress in the most outer fibre of the beam. The new stress range parameter includes the effect of the stress concentration around the rivet holes, and accounting for different geometries around the rivet hole. The check whether the new parameter is more accurate is based on the correlation in the S-N curve of the test data.

The new stress range parameter is generally higher than the stress range defined by the net section stress. This result is to be expected for the new parameter is based on the peak stresses occurring near the rivet hole. Looking at the complete set of unprocessed and processed data it can be concluded that the correlation between the separate tests is slightly higher for the new stress range parameter compared to the net section stress. The correlation of the net section stress range (-0,446) is lower compared to the correlation of the new stress range parameter (-0,468). The new stress range parameter has an neglectable increase in correlation strength. The standard deviation after a linear regression analysis increased from 0,093 to 0,188, meaning that the data is more scattered for the new stress range parameter than for the net section stress range.

The new stress range parameter is mainly built up of three components. The stress due to bypass loading, due to the pin loading, and due to friction. The bypass loading, based on the stress in the section at each location, is fairly accurately described in the analytical model. The corresponding stress concentration at the notches of these locations are equally accurate. However, the analytical model lacks the accuracy of calculating the force transfer in the rivets in a precise manner. The three proposed methods used to calculate these force transfer each have a deviation from the force transfer in the numerical model. The force transfer in the rivets near the force introduction and in the constant moment zone have less deviation than the locations outside of that zone.

Given that the governing stress concentration, and thus the new stress range definition, occurs near the point of force application, it can be explained that the correlation of the data is slightly improved, since the majority of stress occurring at these locations is caused by the bypass loading, which could be accurately calculated. However, there is still a large percentage of stress occurring due to the inaccurate pin loading.

7.1 Discussion

As mentioned in the conclusion, the results of the force transfer in the rivets did not have the accuracy needed to correctly describe the real situation. Compared to the numerical model the results, especially in the linear moment zone, deviate from the results gained from the analytical model.

Once the analytical model was used to process the data from the papers, it became clear that the data solver could not find one single unique solution for the force transfer in the rivet. The theoretical method was to solve the residual between the two displacements to zero, however the solver could not find a single solution with a precise value of zero residual. Only solutions with a residual approaching zero could be found, however these solutions were not unique. Theoretically speaking, the solver should be able to find a unique solution since the number of equations and the number of unknowns are equal. This suggests that the problem for solving the system of equations is not in the method used but in the limitations of the excel data solver.

A second cause of the inaccuracy of the distribution of forces could be in the initial conditions used in the analytical model. While calculating the horizontal force transfer, an assumption is made that the horizontal force on the flange profile causes pure tension in the section. In reality the rivets are outside of the neutral axis of the flange profile, which will cause a additional bending moment for every force. These bending moments could have a effect on the distribution of forces among the rivets.

7.2 Recommendations

Recommendation for follow-up research is to improve the analytical model of the force transfer in the rivets. The currently used method, calculating the forces in the rivets by following the known displacements, seems to be a good fit to calculate these forces. However, the method used to solve the forces using the excel data solver lacks the ability to find a single unique solution where the residual between the results is zero. An additional improvement can be made by incorporating the bending moment caused by each of the horizontal forces on the flange profile. This could be checked separately to examine whether these bending moments have an effect on the distribution of forces.

After improvement of the force transfer, an additional check can be made to see whether the improvement of the correlation is higher or remains the same. After this it can be concluded if this newly defined stress range parameter could describe the life expectancy of riveted bridge girders in a more precise manner than the net section stress.

Bibliography

[1] *Eurocode 3: design of steel structures : part 1-5 : plated structural elements*. BSI, London, 2010. Incorporating corrigendum April 2009. 12

[2] M. Al-Emrani. Fatigue performance of stringer-to-floor-beam connections in riveted railway bridges. *Journal of Bridge Engineering*, 10(2):179–185, 2005. 6, 50

[3] K.A. Baker and G.L. Kulak. *Fatigue Strength of Two Steel Details*. Structural engineering report. Department of Civil Engineering, University of Alberta, 1982. 6, 50

[4] E. Bruhwiller, I.F.C. Smith, and M.A. Hirt. Fatigue and fracture of riveted bridge members. *Journal of Structural Engineering*, 116, january 1990. 6, 50

[5] B. Cornell and L Darby. Correlation of anaylysis and test data to the effect of fastener load transfer on fatigue. In *6th Aircraft Design, Flight Test and Operations Meeting*, page 983, 1974. 11

[6] J.D. DiBattista. Fatigue of riveted tension members. 1995. 6, 50

[7] J.D. DiBattista, D.E.J Adamson, and G.L. Kulak. Evaluation of remaining fatigue life for riveted truss bridges. *Canadian journal of civil engineering*, 25(4):678–691, 1998. 50

[8] J.D. DiBattista, D.E.J. Adamson, and G.L. Kulak. Fatigue strength of riveted connections. *Journal of structural engineering*, 124(7):792–797, 1998. 50

[9] S. Dosman. Use and abuse of the stress severity factor. 2019. IX, 11, 17

[10] John W. Fisher, B.T. Yen, D.A. Wang, and J.E. Mann. *Fatigue and fracture evaluation for rating riveted bridges*. Number 302. 1987. 1, 6, 50

[11] T.R. Gurney. *Fatigue of welded structures*. CUP Archive, 1979. 5

[12] G. Kulak and D.E.J. Adamson. Fatigue tests of riveted bridge girders. 1995. 6, 50

[13] T. Larsson. *Fatigue assessment of riveted bridges*. PhD thesis, Luleå tekniska universitet, 2009. 6, 50

[14] D. Leonetti, J. Maljaars, G. Pasquarelli, and G. Brando. Rivet clamping force of as-built hot-riveted connections in steel bridges. *Journal of Constructional Steel Research*, 167:105955, 2020. 12

[15] C. Maas. Stress intensity factors of cracked riveted joints. 2018. 12

[16] L.G. Mayorga, S. Sire, J.A.F.O. Correia, A.M.P. D Jesus, C. Rebelo, M. Fernández-Canteli, A.and Ragueneau, and B. Plu. Statistical evaluation of fatigue strength of double shear riveted connections and crack growth rates of materials from old bridges. *Engineering Fracture Mechanics*, 185:241–257, 2017. 1

[17] P.L. Moore and G. Booth. *The welding engineer's guide to fracture and fatigue*. Elsevier, 2014. 5

[18] C. Niu. *Airframe structural design: practical design information and data on aircraft structures*. Conmilit Press, 1988. 9, 11

[19] J.M. Out. The fatigue strength of weathered and deteriorated riveted members. 1984. 6, 50

[20] W.D. Pilkey and D.F. Pilkey. *Peterson's stress concentration factors*. John Wiley & Sons, 2008. V, 7, 8, 9, 10

[21] K.N. Shivakumar. *Stress concentrations for straight-shank and countersunk holes in plates subjected to tension, bending, and pin loading*, volume 3192. National Aeronautics and Space Administration, Office of Management ..., 1992. 9

[22] B. Åkesson. *Fatigue life of riveted steel bridges*. 01 2010. 6, 50

Appendix A

Literature study

Appendix B

Unprocessed test data

Department of Built Environment
Architecture, Building and Planning

Literature Study

Literature Study for the thesis: Stress Concentrations in Riveted Plate Girders due to Fatigue Loading

Ing. T.A.W. Gremmen

Supervisors:

Prof. Dr. Ir. J. Maljaars
Dr. Ir. D. Leonetti

Concept version 1.0

Eindhoven, April 2021

Colophon

Subject: Fatigue in Rivet Connected Plate Girders
Document: Literature Study University: TU/e
Author: Ing. T.A.W. Gremmen
Student number: 1244270
Graduation Committee:

First chair:
Prof. Dr. Ir. J. (Johan) Maljaars
Eindhoven University of Technology
Full Professor
Chair of Aluminum Structures

Second chair:
Dr. Ir. D. Leonetti
Eindhoven University of Technology
Assistant professor

Third chair:
Ing. R. van der Zwan
ProRail

Version 3.0

Contents

List of Figures

List of Tables

Chapter 1

Fatigue

1.1 fatigue loading

The nature of loading that causes fatigue failure is cyclic loading. This means that the structure is loaded and unloaded over time. Actual occurring cyclic loading on structures is random and inconsistent. The only way to obtain a quantitative measure of fatigue strength is to carry out fatigue test under controlled conditions [16]. Within these controlled conditions there are three basic types of cyclic loading illustrated in Figure 1.1.

- (a) Reversing (smin = negative, Smax = positive)
- (b) Pulsating (smin = 0, Smax = positive)
- (c) Fluctuating (smin = postivie, Smax = positive)

This loading cycle is characterized by the variable R. This is the stress ratio (S_{min}/S_{max}). R=0 corresponds to a pulsating load. A negative R with reversing and a positive R with a fluctuating cyclic load. This variable is the dominant stress variable causing crack growth [16].
these cyclic loads are shown on Figure 1.1 [23]. The important variables regarding the fatigue loading are as follows.

Cyclic stress range: $\Delta\sigma = \sigma_{max}{-}\sigma_{min}$
Cyclic stress Amplitude: $a = \sigma_{max}{-}\sigma_{min}/2$
Mean stress: $\sigma_m = \sigma_{max} + \sigma_{min}/2$
Stress Ratio: $R = \sigma_{min}/\sigma_{max}$

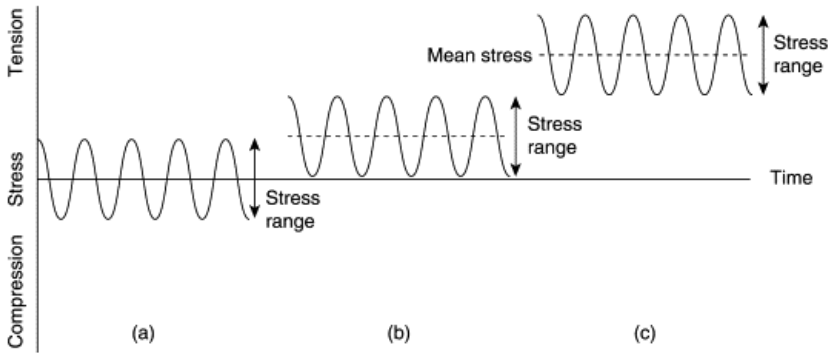

Figure 1.1: Basic stress range conditions

In the fatigue loading, two types of loading are distinguished, high-cycle fatigue, and low-cycle fatigue. High-cycle fatigue is where the number of cycles is large, at about N >105 cycles. The stress applied for the high-cycle fatigue loading is low enough to stay in the elastic stress range of the material. low-Cycle fatigue, with number of cycles to failure at about N <104, will have plastic and elastic deformation components each cycle [8]. The fatigue working on Riveted build-up beams from bridges concerns High-cycle fatigue.

1.2 Eurocode analysis on fatigue strength

In Eurocode EN 1993-1-9 the calculations of fatigue strength are illustrated. This method describes a relationship between cycle stress range ($\Delta\sigma$) and the number of cycles to failure (N). The relationship between these two variables is logarithmic.

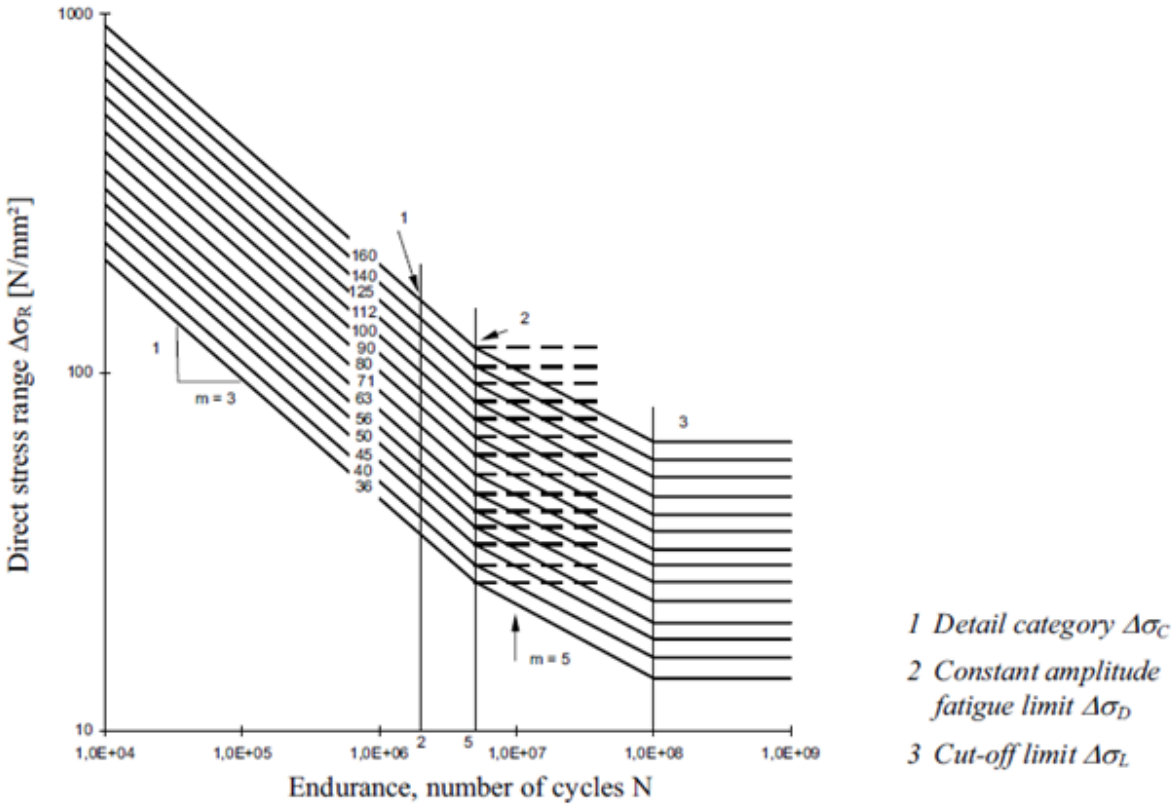

Figure 1.2: S-N curve normal stress

Figure 1.2 shows a plotted S-N curve describing steel fatigue strength as found in the Eurocode. This S-N curve describes multiple variables. $\Delta\sigma_s$ (detail category) describes the stress range to failure at 2 million cycles, the number corresponding with the curve represents the stress range in $\Delta\sigma$ to failure at 2 million cycles. These numbers are given in tables in the Eurocode. $\Delta\sigma_d$ (the constant amplitude fatigue limit) which describes the limit where the component would last forever given a single stress range. $\Delta\sigma_d$ (cut off limit) describes the stress level below which the stress range makes no contribution to the cumulative damage [1]. In this method, the effective stress range is calculated by adding the tensile range and 60 percent of the compressive range together as shown in Equation 1.1:

$$\Delta\sigma_{max} = |\sigma_{max}| + 0,6|\sigma_{min}| \tag{1.1}$$

Two different methods are used to verify the fatigue strength. The cumulative damage method and the geometric (hot spot) stress method. In the cumulative damage method, the loading sequence and stress history is transformed into a stress range spectrum using cycle counting (e.g. reservoir method). Using the stress range spectrum, the damage per cycle can be determined and accumulated using the damage summation (Palmgren-Miner rule).

1.3 Fatigue Failure

Structural members subjected to repeated cyclic loading may eventually fail due to fatigue or stable crack growth. This failure occurs even if the maximum applied stress is less than the yield stress of the material [16]. The fatigue failure occurs due to a progressive and localized structural damage and the growth of cracks. After initiation of a crack, each cycle will increase the damage within the crack.

The fatigue process is generally agreed on that there are four distinct phases [18].

- Crack nucleation (crack initiation)
- Structurally dependent crack propagation (short crack growth)
- Crack propagation characterized by (long crack growth)
  - Elastic plastic fracture mechanics
  - Elastic fracture mechanics
  - Fully plastic fracture mechanics
- Final instability and failure.

The crack nucleation, or fatigue crack initiation, are consequences of cyclic clip. The crack nucleation occurs at a low stress level. In this state plastic deformation occurs in some of the grains of the material. This plastic deformation has a higher chance of occurring on localized shear plane at or near high stress concentrations such as inclusions, porosity or discontinuities [21] and has a higher chance of occurring at the outer grain of the material since the free surface gives less constraint [27]. After initiation of this slip, a slip step is created in the material surface. This implies a new material is exposed to the surface and is covered with an oxide layer. Upon unloading a larger shear stress acts on the same plane in opposite direction. This process is non-reversible due to the oxide mono-layer occurring in the slip step [27].
Fatigue failure can be classified in two categories. Ductile and brittle failure. Ductile fracture occurs from an application of a force which exceeds the force needed to deform the material permanently prior to fracture. These fractures have the following characteristics [8].

- Considerable plastic deformation in the region of the fracture
- The micro mechanism of the fracture is in the shear direction
- Appearance of surface is dull and fibrous
- Fractures only proceed as song as the material is being strained.

Brittle fracture takes place at stresses below the net section yield strength, with very little observable plastic deformation and a minimal absorption of energy. Such fracture occurs very abruptly with little or no warning and can take place in all classes of materials [8]. These fractures have the following characteristics.

- No plastic deformation of metal in the region of the failure
- Fracture is perpendicular to the principle tensile stress

1.4 Steel Fracture

The failure occurring during the fatigue loading of the material is part of fracture mechanics. This describes the propagation of cracks in materials. The failure can be described by three modes [20]. These are the three modes a stress can be applied to increase the size of a crack. within these three modes, superposition of the modes can be used to describe general cases of crack opening [19].

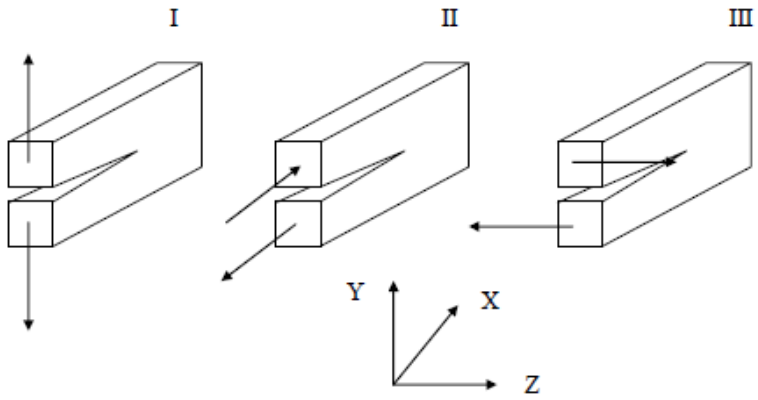

Figure 1.3: Fracture modes

Where the most common mode is failure mode I. The stress at the crack tips in failure mode I are given in Equation 1.2 and 1.3. In the vicinity of the crack tip, the occurring stresses tend towards infinity. looking at mode I, the elastic stress in the x axis is defined by Equation 1.2 [19].

$$\sigma_x = \frac{K_I}{\sqrt{2 * \pi * r}} \cos\frac{\theta}{2} * (1 - \sin\frac{\theta}{2} \sin\frac{3 * \theta}{2}) \tag{1.2}$$

And the elastic stress in the y axis is defined by Equation 1.3 [19].

$$\sigma_y = \frac{K_I}{\sqrt{2 * \pi * r}} \cos\frac{\theta}{2} * (1 + \sin\frac{\theta}{2} \sin\frac{3 * \theta}{2}) \tag{1.3}$$

Variables used in Equation 1.2 and 1.3 are shown in Figure 1.4 [19]. in the case where θ is zero, the shear stress τ_{xy} equals zero and the principle stresses are equal to the x and y stresses.

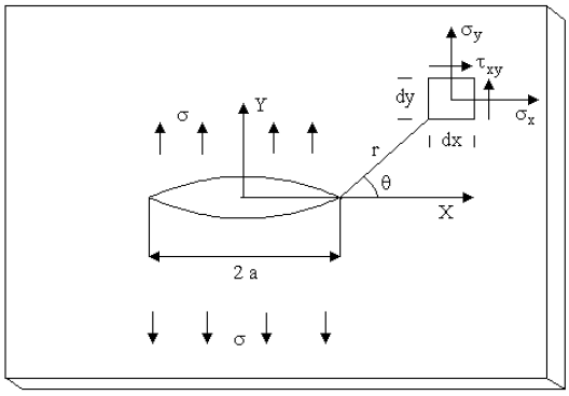

Figure 1.4: Variables fracture

In the equations K_I is the stress intensity factor for the crack. for a plate of infinite width equation 1.4. The indication I states that the stress concentrations are derived from failure mode I as described in figure 1.3. stress intensity factor describes effect of the load and the geometry of the plate on the intensity of the stress near the crack [19].

$$K_I = \sigma\sqrt{\pi a} \tag{1.4}$$

and for a plate with a finite width Equation 1.5

$$K_I = \sigma\alpha\sqrt{\pi a} \tag{1.5}$$

In equation 1.5 where α is a function of the dimensions of the geometry and the loading conditions on the plate. where the stress intensity factor K_I is a single parameter describing the effect of the stress acting and the effect of the crack of undefined dimensions. Two configurations of crack initiation related to riveted connections are shown. in Figure 1.5 [8] the variables for a crack initiation at the center and edge are shown.

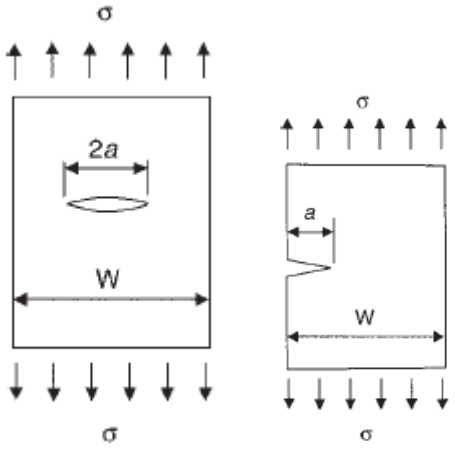

Figure 1.5: Variables dimensions stress intensity factor

in the case of a crack in the center of a section Equation 1.6 gives the value for α [8].

$$\alpha = \frac{1}{\sqrt{1 - (\frac{2a}{W})^2}} \tag{1.6}$$

In the case of a single crack at the edge of the section equation gives the value for α. In case of a small crack the value α can be taken as 1,12 [8].

$$\alpha = 1,12 - 0,213(\frac{a}{W}) + 10,55(\frac{a}{W})^2 - 21,72(\frac{a}{W})^3 + 30,39(\frac{a}{W})^4 \tag{1.7}$$

1.5 Load distribution among rivets

Shear flow method

The first method determining load transfer in the rivets is through the shear flow in the beam. The shear flow in this case describes the longitudinal shear in bending. The shear flow is calculated through the use of Formula 1.8.

$$q = \frac{V_y * Q_x}{I_x} \tag{1.8}$$

where the first moment of area is taken as the area of the L-profile. Using the L-profile area as the shearing plane, the shear flow can be determined between these two elements. The shear flow is a unit given in force divided by length, multiplying the shear flow with the spacing between the rivets. The force transfer per rivet can then be determined.

As shown in Formula 1.8 the shear flow has a linear relation with the shear force. Considering the static system of a fully cooperating built-up beam, there is no shear force in the constant moment region. When all of the fasteners are 100 percent stiff, this would mean that the fasteners in the constant moment region transfer no force from the plate to the L-profile. However, the riveted connections in the built-up girders are not fully stiff, causing a different force distribution over the rivets. From the observations in the full scale tests it can be seen that the majority of the girders fail at a rivet hole in the constant moment zone, near the point of force application. This observation does not concur with these rivets not transferring force. When all of the rivets in the constant moment zone transfer no force, the crack initiation could happen at any arbitrary rivets in the constant moment zone, since there is no difference in stress state in between these locations.

Known displacement method

The second method to determine the force transfer in the rivet is by using the known displacements of the web profile to determine the unknown forces in the rivets. The force transfer in the rivets is due to the flange profile following the displacement of the web profile. For this method the displacements for the rivet locations of the complete beam are determined. After the displacement of the full beam is known, the forces needed for the flange profile corresponding with the same displacement can be determined using the constitutive relation between the displacement and the applied force. Using this relation, a set of forces among the rivets is determined which will result into the same deflection or displacement on the flange profile as calculated on the whole beam.

For the force transfer in the vertical direction the displacement of the locations of the rivets are determined by deriving the deflection formula. Using this formula, the deflection on each coordinate of the beam can be determined. Equation **??** describes the derivation of the deflection formula of the four point bending beam. The beam is divided into three parts. Segment 1: from support to first force, Segment 2: in between the two forces, and Segment 3: from second force to second support. The variables used in the derivation are shown in Figure **??**.

1.6 Stress concentration factors

Stress concentration occurs when in a local area the stress is significantly higher than the mean section stress. This phenomenon usually takes place around irregularities in cross sections or irregularities in material which causes disturbance in the flow of forces. Stress concentrations within a section regarding plate girders can be divided into three separate occurrences. The clamping force of the rivet causing force transfer via friction. Bypass loading, caused by adjacent connections, and pin load case, caused by the transfer of the bolt. To determine the stress concentration, the ratio of the discontinuity is defined as Kt (theoretical stress concentration factor). This factor is the ratio between the highest stress and the nominal section stress. Two different theoretical stress concentration factors are defined for this. The factor K_{tg} based on the gross section of the element, and K_{tn} based on the net section near the discontinuity of the element.

$$K_{tg} = \frac{\text{Highest value of stress at a discontinuity}}{\text{Nominal stress at the gross cross-section}} \tag{1.9}$$

$$K_{tn} = \frac{\text{Highest value of stress at a discontinuity}}{\text{Nominal stress at the minimum cross-section}} \tag{1.10}$$

These stress concentrations are visualized in Figure 1.6 [14]

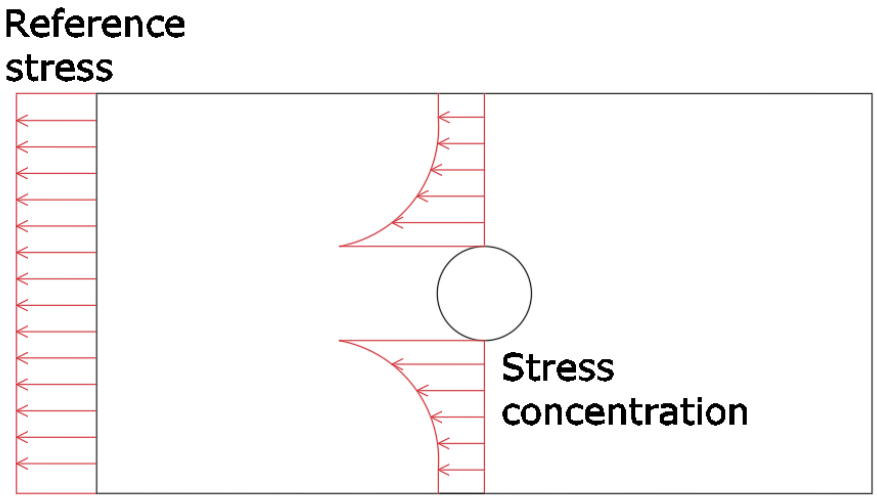

Figure 1.6: Visualisation stress concentrations

1.6.1 Bypass Loading

Stress concentration due to bypass loading occur due to the hole in the plate disturbing the normal flow of forces. This means that the stress concentrations of bypass loading are based on the reference stress flowing through the section. To determine the effect of bypass loading, the Tables 1.1 and 1.2 can be used to determine the concentrations within the disturbed zones. Looking at a plate with a hole at the center of the width as seen on Figure 1.7 [9] with undefined dimensions.

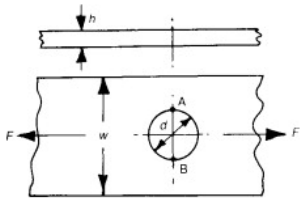

Figure 1.7: Dimensions finite plate

The nominal section stress at an undisturbed section is defined in the Formula 1.11:

$$\sigma = \frac{F}{w * h} \tag{1.11}$$

From this nominal stress and the stress concentration factor the maximum stress can be determined. This maximum stress occurs at points A and B as shown on Figure 1.7 [9]. The stress concentration factor is dependent on various parameters. This includes the location of the hole, the geometry of the section and the location of the forces. For plates with a hole at the center of the section, as the example shown above, the following K values correspond with the geometry of the plate [9].

Table 1.1: Stress concentration factors finite plate

d/w	0,00	0,10	0,20	0,30	0,40	0,50	0,55
Kt	3,00	3,03	3,14	3,36	3,74	4,32	4,70

In case of a semi-infinite plate, as shown in Figure 1.8 [9], where the point a is located on the finite side of the opening, and point b located on the semi-infinite side of the opening.

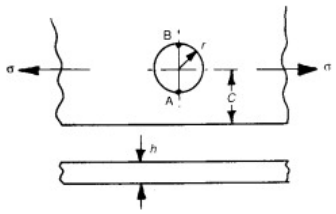

Figure 1.8: Parameters semi-finite plate

In this case, σ_b equals the stress at point B and σ_a equals the stress at point A, with Equation 1.11 for the stress at the undisturbed region. The stress concentration factors in this example are

$$K_a = \frac{\sigma_a}{\sigma} \tag{1.12}$$

$$K_b = \frac{\sigma_b}{\sigma} \tag{1.13}$$

Table 1.2: Stress concentration factors semi-infinite plate

r/c	0,00	0,10	0,20	0,30	0,40	0,50	0,60	0,70	0,80
Kt(a)	3,00	3,05	3,15	3,25	3,40	3,70	4,12	4,85	6,12
Kt(b)	3,00	3,03	3,07	3,10	3,15	3,18	3,25	3,32	3,42

In the situation where there is a semi-infinite section, the stress concentration at the limited side will see a higher increase in stress as follows from the higher stress concentration factors [9]. This shows that the ratio between the gross section and the net section has a high influence of the stress concentration of bypass loading.

The top graph in Figure 1.9 describes two variables over the d/H ratio. The Stress concentration factor of the gross section (K_{tg}) and the stress concentration factor of the net section (K_{tn}). This graph describes the case of a finite element with symmetrical dimensions of the disturbance. The values given in this graph are in good agreement with analytical results [26].

The graph does not cover the whole d/H range, it describes from 0 to 0,5. An empirical formula is proposed to describe the stress concentration factors over the whole d/H range (Heywood, 1952). The formula described is in good agreement with the graph for d/H <0,3 and 1,5% lower at d/H = 0,5 [26] which is not of significance in design applications. The formula for the stress concentration factor of the net section.

$$K_{tn} = 2 + (1 - \frac{d}{H})^3 \tag{1.14}$$

This formula, expressed in the form of the stress concentration factor of the gross section is.

$$K_{tg} = (2 + \frac{1 - \frac{d}{H})^3}{(1 - \frac{d}{H})} \tag{1.15}$$

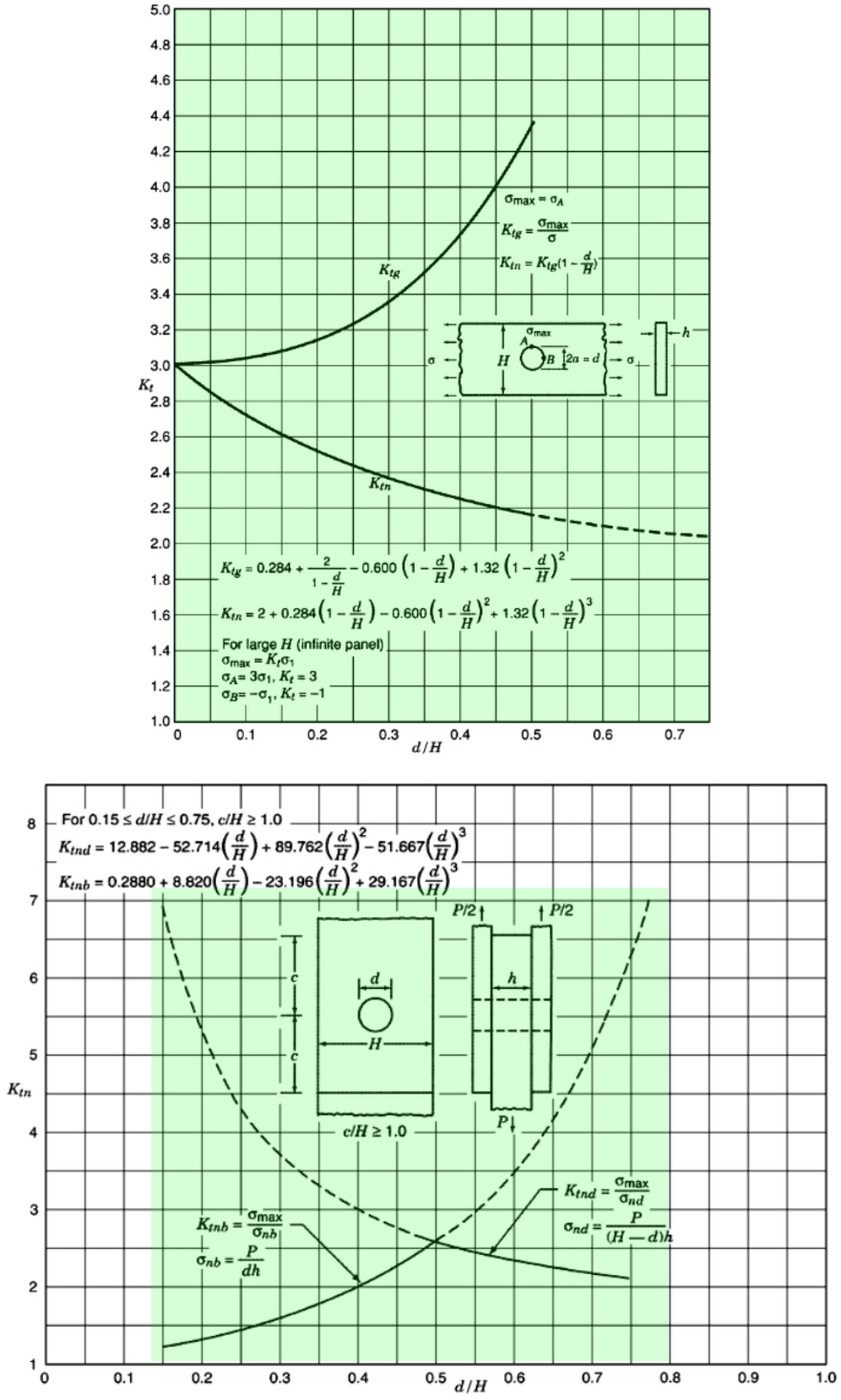

Figure 1.9: Graph stress concentration factors bypass (top) pin loading (bottom)

1.6.2 Pin loading

Stress concentrations due to pin loading occur due to the pin loading the plate. This means that the stress concentrations in the plate are based on the force transfer in the rivet. Stress concentration factors regarding pin loading can be determined using two different approaches. Nominal stress based on the net section, and nominal stress based on the bearing area [28]. The formula for the stress based on the net section is shown in Equation 1.16 and Equation 1.17. The formula for the stress based on the bearing area is shown in Equation 1.18 and Equation 1.19 [26].

Equations based on the net section area

$$\sigma_{nd} = \frac{P}{(H-d)h} \tag{1.16}$$

$$K_{tnd} = \frac{\sigma_{max}}{\sigma_{nd}} = \sigma \frac{(H-d)h}{P} \tag{1.17}$$

With these formula written in the form of the nominal stress based on the bearing area of the section.

$$\sigma_{nb} = \frac{P}{dh} \tag{1.18}$$

$$K_{tnb} = \frac{\sigma_{max}}{\sigma_{nb}} = \frac{\sigma_{max} dh}{P} \tag{1.19}$$

Within the range of $0,15 \leq d/H \leq 0,75, c/H \geq 1,0$ the following equations are used to calculate the stress concentration factors for the net section in Equation 1.20. The parameters given in these formulas are defined in the bottom graph on Figure 1.9.

$$K_{tnd} = 12,882 - 52,741(\frac{d}{H}) + 89,762(\frac{d}{H})^2 - 51,667(\frac{d}{H})^3 \tag{1.20}$$

And the bearing stress concentration factor section in Equation 1.21 [26].

$$K_{tnb} = 0,2880 - 8,820(\frac{d}{H}) - 23,169(\frac{d}{H})^2 + 29,167(\frac{d}{H})^3 \tag{1.21}$$

This same approach of calculation of the bearing stress is stated by Niu in 1998 [24]. The stress bearing factor in this paper is determined with a curve following the same formula as in Equation 1.21. This formula determines the stress concentrations on the locations shown in Figure 1.10.

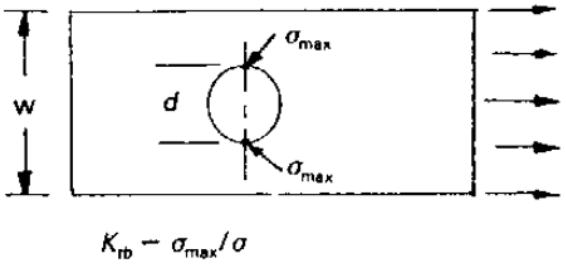

Figure 1.10: Location of the stress concentrations due to bearing

Both of the methods for determining the stress concentrations in the plate use the force transfer of the fastener as a basis to calculate the concentrations. In contrary to the bypass loading, which uses the reference stress in the profile.

1.6.3 Friction

The friction of the plate elements has an influence on the force transfer in the rivet, for a percentage of the force transfer will be directly from the web plate to the L-profile. The force transfer in the beam is dependent on two factors. The clamping force of the rivet, and the friction coefficient of the material. The maximum clamping stress of a rivet ($\sigma_{c,0}$) according to Eurocode 1-8 [1] is 0,70 of the yield strength of the rivet [22].

$$\sigma_{c,0} = 0,7 * f_{yr} = 165MPa \tag{1.22}$$

In the paper "Rivet clamping force of as-built hot-riveted connections in steel bridges" [**?**], the clamping force from hot-riveted connections are analysed. In the paper the clamping stress in the riveted connection are set out against a function of the ratio between the grip length (g) over the rivet diameter (d). The collected data gives the graph as seen in Figure 1.11 [**?**].

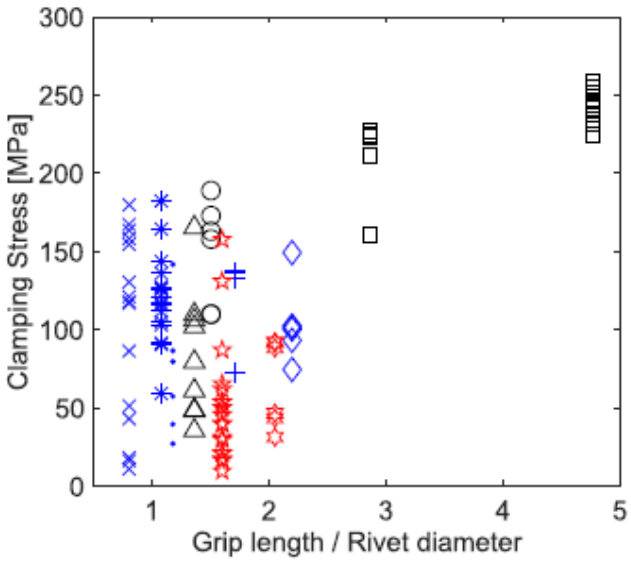

Figure 1.11: Clamping stress as a function of g/d

As can be seen from the graph, the theoretical maximum value of 165 MPa is around the same value as the maximum value's seen in the graph. Since it is not possible to know the real value of the clamping stress, and thus the friction in the build-up beams, a theoretical value must be chosen. For this research it is chosen to use this theoretical maximum value as described in the eurocode.

Two options for an analytical approach to Stress concentrations due to friction are presented in *Stress Intensity Factors of cracked riveted joints* [22] These methods are based on the theoretical bearing ratio β. Given in Equation 1.23. With μ is the friction coefficient and n is the number of rivets.

$$\beta = \frac{F - F_{c,0} * n * \mu}{F} \tag{1.23}$$

For $\beta = 0$, there is no bearing transfer, and $\beta = 1$ there is a full transfer via bearing.

$$\begin{aligned} K_{tb} &= K_{tb,friction} \qquad for \beta = 0 \\ K_{tb} &= K_{tb,pin} \qquad for \beta = 1 \end{aligned} \tag{1.24}$$

In this situation, a linear relation between β and the distribution is assumed. Combining these equations into Equation 1.25.

$$K_{tb}(\beta) = \beta * K_{tb,pin} + (1 - \beta) K_{tb,friction} \tag{1.25}$$

From this point, two different approaches are given [**?**]. Firstly, a solution where the distribution transferred by friction is equally distributed over the plate. Secondly a solution where prying occurs. For the solution with a equally distributed stress over the plate in contact with the rivet head, the following conditions are in place. $K_{t,g,friction} = 0,5 K_{t,n,bypass}$.

$$K_{tb}(\beta) = K_{tb,pin}(\beta) + 0,5 K_{tb,bypass}(1 - \beta) \tag{1.26}$$

The solution with prying is based on the condition $K_{tg,friction} = 0,5 * Ktn, bypass$ for $\beta = 0$ and $K_{tg,friction} = Ktg, pin$ for $\beta = 1$

$$K_{tb}(\beta) = K_{tb,pin}(2\beta - \beta^2) + 0,5 K_{tb,bypass}(0,5 - \beta + 0,5\beta^2) \tag{1.27}$$

When the β factor determines the amount of stress decreasing the pin load stress concentration factor, and increasing the bypass loading stress concentration factor.

1.6.4 Combined effects on a plate

The following section describes a situation where two plates with a fastener are loaded. the load situation is shown in figure 1.12 [14].

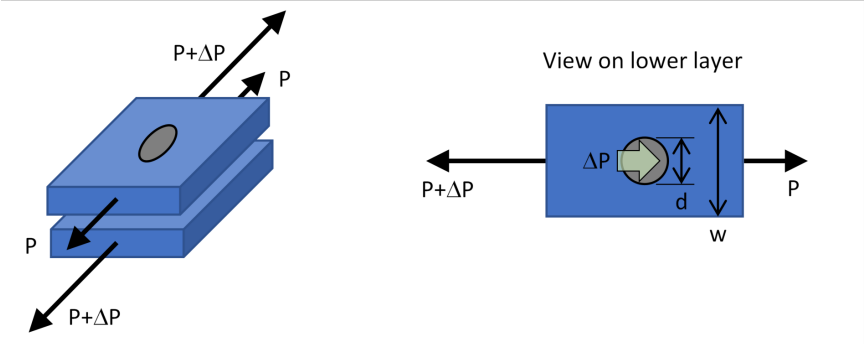

Figure 1.12: Load situation combined effects

As is shown in the figure, the plate is loaded in a load 'P'. due to the fastener loading the plate there is an increased load on each side of 'ΔP. The formula stated for the stress concentrations in this situation is formulated in Equation 1.28 [14].

$$Stressconcentration = \frac{\sigma_{max}}{\sigma_{ref}} = \frac{\alpha\beta}{\sigma_{ref}}(K_{tb}\Theta\frac{\Delta P}{dt} + K_{tg}\frac{P}{wt}) \tag{1.28}$$

Where α is a hole condition factor and β is a hole filling factor. These two factors are empirically tested. K_{tb} is the bearing stress concentration factor (pin load on the plate) and K_{tg} is the bypass stress concentration factor and can be analytically determined. in the Figure 1.12 and Equation 1.28 P represents the bypass load and ΔP is the load from the fastener (pin loading). Looking at the empirical factors α and β the following parameters are suggested by Dosman [14]. α, The hole condition factor, addresses the quality of the hole during production, as well as residual stresses in the material. it is suggested to use a value of 1,0 for connections where specific test data is not known in regards to the quality of the rivet hole. β, the hole filling factor, take the effect of the constraint of the rivet in the hole in account. Test data from Tom Swift's FAA report [30] some parameters are suggested for rivets and (zero interference) bolts.

Table 1.3: Suggested β factors

mean life	effective β, Rivets	Effective β, bolt
$5 * 10^4$ cycles	0,78	0,83
$1 * 10^5$ cycles	0,67	0,73
$1 * 10^6$ cycles	0,67	0,77

looking at Table ?? it can be seen that the suggested β factor for riveted connections with high cycle fatigue is 0,67. The values however are dependent on how well the rivets are bucked. poorly bucked rivets can achieve values closer to bolts or open holes.
in Formula 1.28 the factor theta represents the bearing distribution factor. This means the effects of local bending on the bearing stress distribution. This factor is mentioned in the AIAA paper[12] where a detailed method for generating this factor is derived from test data. An other method for obtaining a value for theta is the, more conservative, single shear curve used by NIU [24]. This curve is shown in Figure 1.13

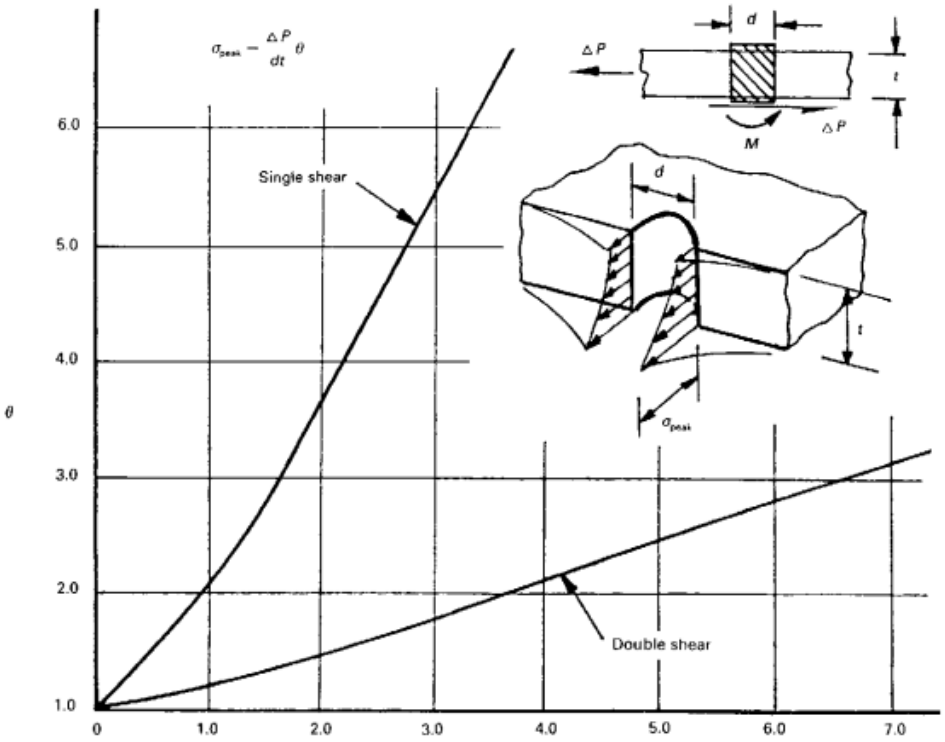

Figure 1.13: Factor θ in single and double shear

Where the x-axis of the curve represents the $\frac{t}{d}$ ratio, and the y-axis the θ factor. This means, a higher thickness of the plate compared to the diameter of the hole gives a higher θ factor. Formula 1.29 describes the stress concentration occurring near the hole compared to the bearing force from the fastener.

$$\sigma_{max} = \frac{\Delta P}{dt}\theta \tag{1.29}$$

Where the factor θ is only used as a factor on the pin load from the fastener in Equation 1.28.

Chapter 2

FEM Literature

In the research, two distinguished models are made. One global model, with simplified models of the riveted connections. And a local model, which will specifically model a single rivet with corresponding boundary conditions simulating a specific location within the global model. The detailed model of the single connection will be made using sub-modelling within ANSYS workbench. using the boundary conditions gained from the global model and apply these conditions on the outer edges of the sub-model.

2.1 FEM modelling

The global model is made using simple solid elements for the web plate and the L-profiles. The general area of these solids will be meshed using the Hex-dominant setting within the mesher. Using this setting for the general area's will improve the menageability of the density of the mesh by the user. An cubic area around the rivet holes will be spliced out of the general area of the web and the L-profile, with dimensions of about 5 times the diameter of the rivet hole. This area will be meshed with a higher density of elements.

2.1.1 Modelling of riveted joints

To limit calculation times of the FEM model, a global model with simplified rivet connections is made. Different possibilities for simplifying connections can be used. Idealization of riveted joints [2] states the use of beam elements using RBE3 elements. The nodes of the beam element (beam element) are connected with the nodes of the shell elements.

In the paper 'Finite element analysis and modeling of structure with bolted joints' [17] different types of approximations for fasteners are tested. This includes (a) a solid element, which approximates the real situation as much as possible, (b) degree of freedom coupling, where the rivet is represented with a beam element connected to the nodes of the solid (c) a beam element representing the rivet, with the connection of the beam element to the solid with other beam elements, and (d) a preload by out-of-plane loading on the plates. These situations are shown in Figure 2.1.

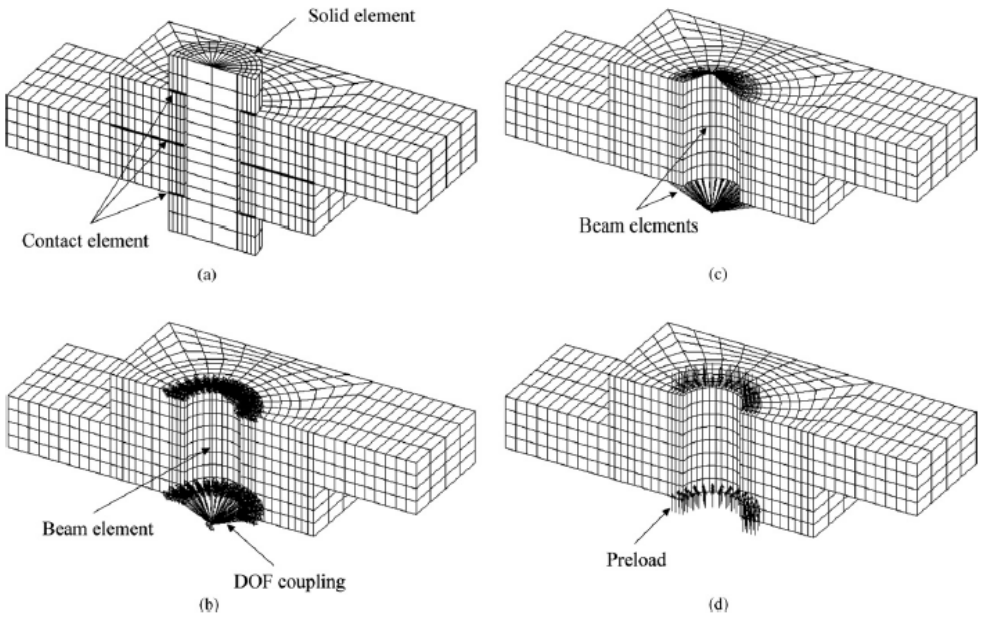

Figure 2.1: Types of tested connections

These elements are tested where the solid element represents the real situation the most. as the deflection of the other models approaches the deflection of the solid, the approximation of connections represent the real situation better.

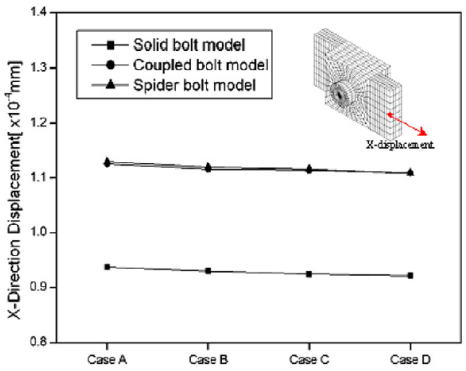

Figure 2.2: Deflection of multiple connection types

As can be seen in Figure 2.2 both the DoF-Coupled model and the spider bolt model (beam element with connected nodes) have a slightly higher deflection than the solid model. however, computational times are significantly reduced [17].

2.2 FEM elements and DoF

Here the different elements for fem modelling are described. This can be divided in elements used for solids (3D elements), elements used for plates (2D elements), and elements used for beam elements (1D elements).

2.2.1 3D elements

The two main 3D elements found in FEM are the tetrahedron elements and hexahedron elements. both of these elements can be separated in elements using only vertex nodes, and elements with intermediate nodes. Each of these nodes have the degrees of freedom U_x, U_y, and U_z. When using 3D elements FEM solvers only need the directional degrees of freedom. Deformation of a solid is solely determined from the displacement vectors [11]. This means that each node of the 3D element has 3 DoF.

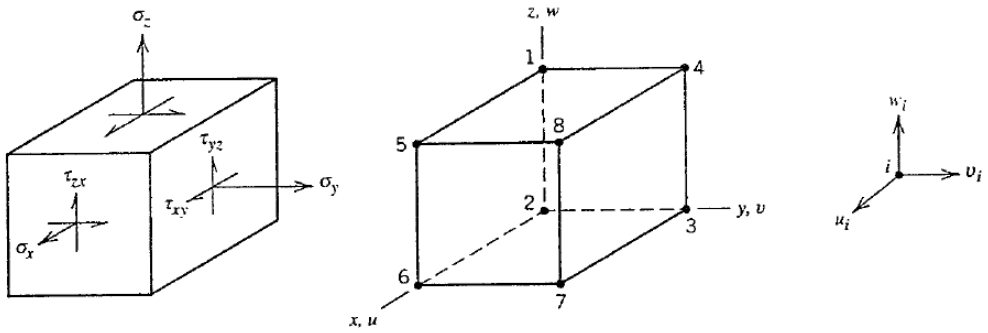

Figure 2.3: Degrees of freedom solids [11]

The elements can be categorized in the following items, as shown in Figure 2.4, from left to right.

- 3-D tetrahedron (4-node element) - Constant Strain Tetrahedron
- 3-D Tetrahedron (10-node element) - Linear Strain Tetrahedron
- 3-D hexahedron (8-nodes element) - Trilinear Hexahedron
- 3-D hexahedron (20-nodes element) Quadratic Hexahedron

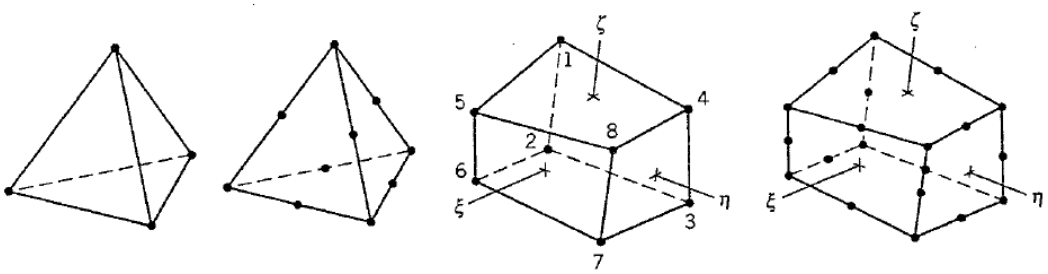

Figure 2.4: Types of 3D elements [11]

The Linear strain Tetrahedron is a 10-node element, each of these nodes have three degrees of freedom. This gives a total of 30 degrees of freedom for this element. The ten node tetrahedron has a strain field that is linear in the coordinates, thus can represent fields of pure bending exactly [11].
The trilinear hexahedron, also called a eight node brick, has a displacement field consisting of tree linear expressions. An hexahedron element can be of arbitrary shape if the elements are formulated as an isoparametric element. An trilinear hexahedron element is not well suited to model beam action. The sides of the element remain straight when deformation is happening. if elongated in bending, it suffers from shear locking [11]. The quadratic hexahedron is a extension on the trilinear hexahedron. This element can model linear strain fields exactly if the element is rectangular. The edges of non-deformed elements can either be straight or curved. This element is a 20 node element, with three degrees of freedom in each node, thus making this a 60 DoF element. [11]

2.2.2 2D elements

The 2D elements found in finite element modelling are triangles and quadrilaterals. like the 3d elements these elements can be separated in elements using only vertex nodes, and elements with intermediate nodes. When using 2D elements, to solve the model, each node can have 3 directional degrees of freedom (U_x, U_y, and U_z) and 3 rotational degrees of freedom (θ_x, θ_y, and θ_z). Meaning that each node can have has 6 degrees of freedom when a 2d element is taken in a 3D space. However, if a 2D element is only modelled in a 2D space, only two transnational degrees of freedom apply on the elements (U_x, U_y in the xy-plane), and possibly one rotational degree of freedom.

- 2-D Constant strain triangle (3-node element)
- 2-D Linear strain triangle (6-node element)
- 2-D Bilinear quadrilateral (4-node element)
- 2-D Quadratic quadrilateral (8-node element)

In Figure 2.5 the degrees of freedom of the triangle elements is shown.

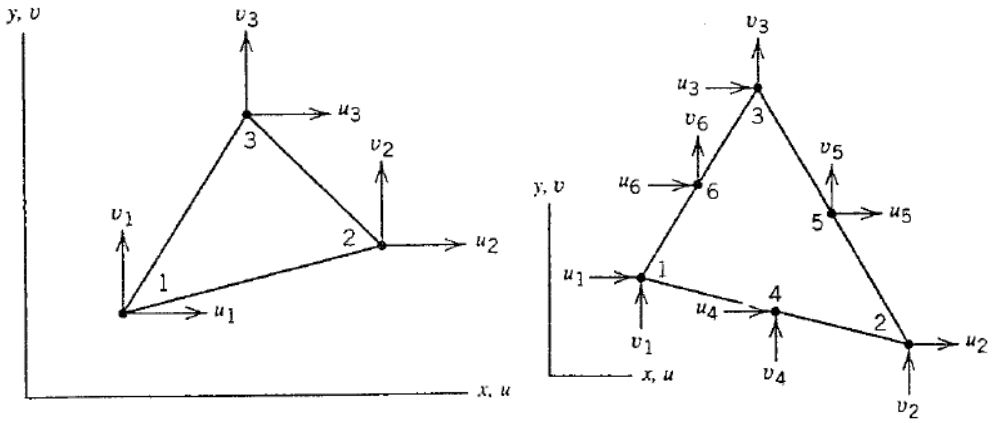

Figure 2.5: DoF constant strain triangle (left) linear strain triangle (right) [11]

In the constant strain triangle, the strains do not vary. In a 2D space this element has 3 nodes with each 2 degrees of (translational) freedom. Thus having 6 degrees of freedom.
The linear strain triangle has intermediate nodes additional to the vertex nodes. in this element

the strain can vary linearly. if the element is used in pure bending, exact results for deflection and stress can be assumed[11]. This element having 6 nodes with each 2 degrees of freedom, thus having 12 degrees of freedom for an element.
In figure 2.6 the degrees of freedom of the quadrilateral elements is shown.

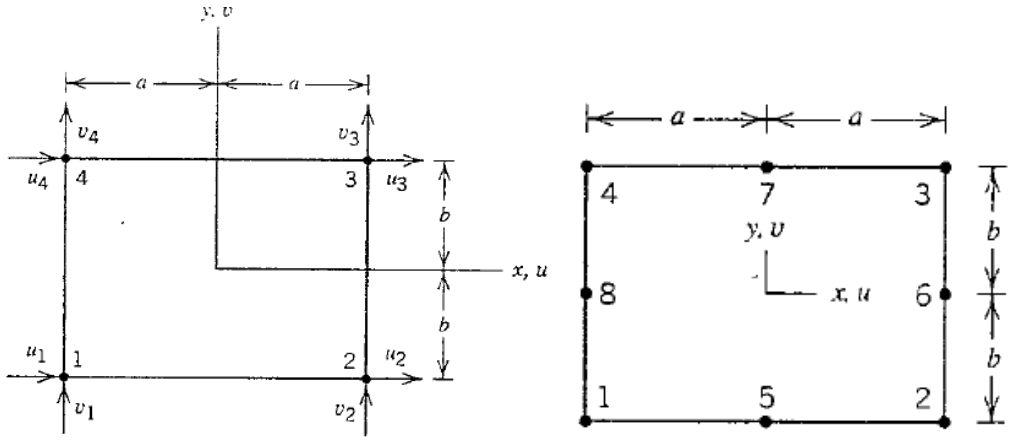

Figure 2.6: DoF bilinear quadrilateral (left) quadratic quadrilateral (right) [11]

The bilinear quadrilateral element is shown in Figure 2.6 on the left side. There are two linear expressions describing the displacement field. These expressions are shown in Equation 2.1

$$\begin{aligned} u &= \beta_1 + \beta_2 x + \beta_3 y + \beta_4 xy \\ v &= \beta_5 + \beta_6 x + \beta_7 y + \beta_8 xy \end{aligned} \tag{2.1}$$

This element cannot model for example a cantilever beam with a non axial force, where the axial strain has a linear relation with the x coordinate. The elements is also unable to model pure bending [11]. The element has 4 nodes with each 2 degrees of freedom. The bilinear quadrilateral has 8 degrees of freedom.
The quadratic quadrilateral element is shown in Figure 2.6 on the right side. There are two quadratic equations describing the displacement field of this element. These expressions are shown in Equation 2.2.

$$\begin{aligned} u &= \beta_1 + \beta_2 x + \beta_3 y + \beta_4 x^2 + \beta_5 xy + \beta_6 y^2 + \beta_7 x^2 y + \beta_8 xy^2 \\ v &= \beta_9 + \beta_1 0 x + \beta_1 1 y + \beta_1 2 x^2 + \beta_1 3 xy + \beta_1 4 y^2 + \beta_1 5 x^2 y + \beta_1 6 xy^2 \end{aligned} \tag{2.2}$$

from these displacement equations, the strain of the element can be derived. The strain equation in the x-direction is shown in Equation 2.3.

$$\epsilon_x = \beta_2 + 2\beta_4 * x + \beta_5 y + 2\beta_7 xy + \beta_y^2 \tag{2.3}$$

The strain formula for the quadratic quadrilateral contains the linear terms and quadratic terms. This element can describe the example given above, a cantilever beam with non axial force. This element can also describe the stress and strain state of a element in pure bending.

2.3 Contacts

2.3.1 Contact types

Within ANSYS analytical multiple kinds of contact types between faces can be used. These contacts define the behaviour of the nodes of a face in relation to connecting or nearby nodes of different element faces. The following contacts can be used as shown in Table 2.1.

Table 2.1: Contact types Ansys [29]

Contact type	Penetration	Separation	Sliding	Linear contact type
Bonded	No	No	No	Yes
No Seperation	No	No	Free	Yes
Frictionless	No	Yes	Free	No
Rough	No	Yes	No	No
Frictional	No	Yes	If $F_{sliding} > F_{friction}$	No

The three non linear contact types (Frictionless, Rough and Frictional) can model the contact between elements more accurately, for lateral displacements are allowed. Using these modes of contact, gaps within the area of contact are taken into account during solving. However, using these non-linear contact types the solution times of the model are increased.
The fictional contact uses the frictional coefficient to calculate the behaviour of the contact. This is accounted for using Coulomb's Law 2.4.

$$F_{tangential} < \mu * F_{normal} \tag{2.4}$$

Where μ is the coefficient of static friction. The contact will allow sliding if $F_{sliding} > F_{friction}$

2.3.2 Contact formulation

Ansys analytical offers four kinds of contact formulations. The formulation defines the relations between the contact faces or edges.

- Augmented Lagrange
- Pure Penalty
- Multi-Point Constraint
- Normal Lagrange

Where every contact formulation uses a different method for describing the contact, and every formulation has its strengths and weaknesses [10].

Augmented Lagrange This is the default contact formulation used by Ansys, and is suitable for most situations. The method minimizes penetration compared to the Pure Penalty method [4].

Pure Penalty This contact is occurring only on edges or corner elements, and offers easy convergence compared to the other formulations. This formulation is use full when contact convergence is a challenge, and some penetration is acceptable [4].

Multi-Point constraint This contact formulation can be used for all Bonded and No Separation contact types where there is no over constraint. This method is recommended for large bonded contact models to enhance run time. This method can produce over-constraints in the model [4].

Normal Lagrange method This method is most suitable for elements where penetration is critical, for contact with shells or thin layers, and large sliding problems. The Normal Lagrange method offers near-zero penetration of the contacts. This method might require more iterations and thus more computing time [4].

In Table 2.2 the compatibility of contacts, the possible types, and formulations is shown.

Table 2.2: Compatibility contacts of elements [5]

Contact Geometry	**Solid body face (contact)**	**Solid body edge (contact)**
Solid body face (target)	All types All formulations Symmetry respected	Bonded, No Seperation All formulations Symetry not respected
Solid body edge (target)	Not supported	Bonded, No seperation All formulations Symmetry not respected
Surface body face (target)	All types All formulations Symmetry respected	All types All formulations Symmetry not respected
Surface body edge (target)	Not supported	Bonded MPC formulation Symmetry not respected
	Surface body face (contact)	**Surface body edge (contact)**
Solid body face (target)	All types All formulations Symmetry respected	Bonded MPC formulation Symmetry not respected
Solid body edge (target)	Not supported	Bonded MPC Formulation Symmetry not respected
Surface body face (target)	All types All formulations Symmetry respected	Bonded Augmented Lagrange, Pure Penalty, and MPC formulation Symmetry not respected
Surface body edge (target)	Not supported	Bonded Augmented Lagrange, Pure Penalty, and MPC formulation Symmetry not respected

In the model of the riveted girder only solid elements are used for the main geometry. looking at the compatibility, it can be seen that the solid-body-face to solid-body-face contacts supports all types, all formulations and respect symmetry. When a contact between a solid-body-face and solid-body-edge is made in the model the target geometry should be the face, and the contact geometry the contact. Defining the contacts the other way around is not supported in the software. When the contact between the solid-body face and solid-body-edge is formulated in the right way, the possible contact types are Bonded, and No Separation, all formulations can be used, and symmetry is not respected. An other general rule of thumb is to use the flat face as the target and a face with a (slight) convex curvature the contact for better results.

Chapter 3

General information rivets

The rivets used in the research are based on the NEN N 667. This file describes a standardization of dimensions used in rivets. The parameters used in these dimensions are shown in Figure 3.1. Of these shown rivets, type 'A' is used for bridges and general structural purposes. This configuration is used in the research.

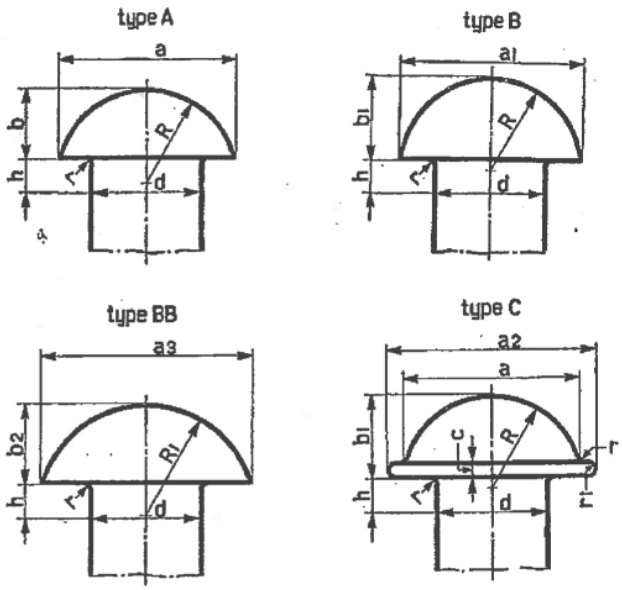

Figure 3.1: Parameters rivets

The following dimensional properties are generally used for the rivets. As shown in Figure 3.2.

Maten in mm

d	d_1	d_2	d_3	h	r	Type A				Type B				Type BB				Type C						
						a	b	R	G	a_1	b_1	R	G	a_3	b_2	R	G	a	a_2	b_1	c	R	r_1	$G^{2)}$
6	6,3	5,8		5	0,4	11	4,5	5,6	0,2															
8	8,3	7,8		5	0,4	14	5,5	7,2	0,4															
10	10,3	9,8		5	0,4	17	6,5	8,8	0,7	17,5	8	8,8	1,0											
13	13,3	12,8	12,2	5	0,6	21	8	10,9	1,3	21,5	9,5	10,9	1,7	25	9,5	13,0	2,9							
16	16,3	15,8	15,2	5	0,8	25	9,5	13,0	2,9	26,0	11,5	13,0	3,0	30	11	15,7	3,6	25	29,5	11,5	2	13,0	1	3,0
19	19,4	18,8	18,1	5	0,8	30	11	15,7	3,6	31	13,5	15,7	5,0	35	13	18,5	5,8	30	35	13,5	2,5	15,7	1	5,0
22	22,4	21,8	21,1	5	1	35	13	18,5	5,8	36	15,5	18,5	7,9	40	15	20,8	8,9	35	40	15,5	2,5	18,5	1	7,9
25	25,5	24,8	24,0	5	1	40	15	20,8	8,9	41	17,5	20,8	11,3	45	17	23,4	12,6	40	45	17,5	2,5	20,8	1	11,3
28	28,5	27,7	26,7	5	1	45	17	23,4	12,6	46	19,5	23,4	16,1	50	19	25,9	17,9	45	50	19,5	2,5	23,4	1	16,1
31	31,5	30,7	29,7	5	1,6	50	19	25,9	17,0	51	21,5	25,9	21,5	55	21	28,5	23,4	50	56	21,5	2,5	25,9	1	21,5

1) Bij de berekening is voor het soortelijk gewicht van staal 7,85 aangenomen.
2) Na verwijdering van den kookrand.

Figure 3.2: Dimensions rivets

The table describes the dimensional properties of the rivet head in comparison with the radius of the rivet shank. In the table, the dimensions d_1 and d_2 can be found. These two parameters respectively describe the maximum and minimum diameter directly under the rivet head, thus describing the bandwidth of the radius after riveting.

3.1 Rivets in FEM model

The Rivets in the FEM model are modelled to these standards. The modelled rivet is shown in Figure 3.3. The rivet is created by modelling the shank with the desired width and length, in this case respectively 22mm and 20mm, where there is a symmetry plane at the end of the shank. After which a sphere with a radius correspondent with the values of table 3.2 is used. This sphere then is translated inwards of the rivet with the distance 'h' in the table, and finally the excessive part of the sphere is cut of. Creating a conformal rivet.

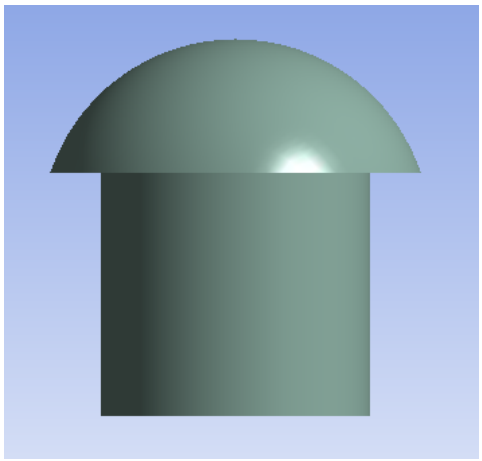

Figure 3.3: Rivet in the FEM model

Chapter 4

Fatigue data

The collected data from full scale fatigue tests can be found in the excel sheet. The following sets of data are collected from below stated sources. The stress range with the corresponding cycles to failure. This stress range concerns two variables, the net section stress and the gross section stress of the section. The dimensions of the test setup, and the dimensions of the tested girder are collected, through the dimensions of the whole test set up, the methods used to determine the gross and net section area stress can be found. The failure data of the girder is collected, meaning which failure mode occurred for each girder, at which position on the beam did the failure occur, only fatigue failure at the rivet holes is applicable for this research.

For each of the research paper, the dimensions of each individual test or group of tests is given. The parameters given in each tests are defined as shown in figure 4.1. Where 'A' is the distance between the two points of force introduction, 'B' the distance between the force introduction and support, 'C' the total span of the test.

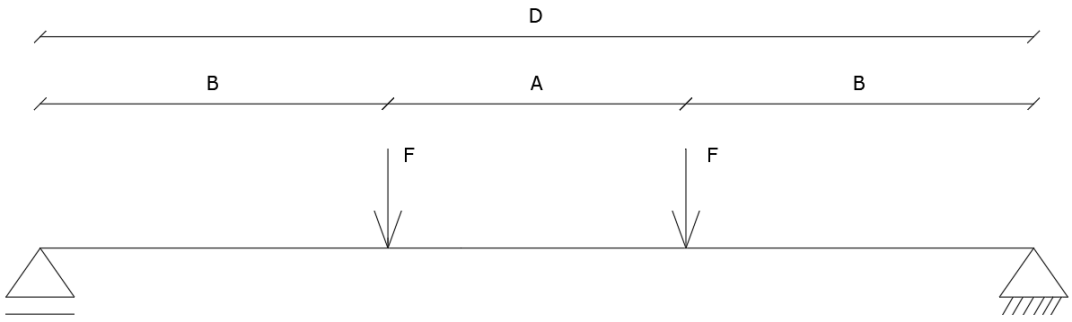

Figure 4.1: Parameters dimensions test

The four point bending tests used in most of the tests gives a constant and pure bending moment in between the two applied forces. The magnitude of the bending moment in all cases of four point bending is.

$$M = F * B \tag{4.1}$$

For every beam there is a given net section stress. In several cases, the method to calculate this stress is given in the article. When the method is unknown, the acting bending moment and the given net section stress can be used to determine the method used to calculate the net section stress.

4.1 Test data Fisher

The data collected in this chapter is found in the paper Fatigue Strength of Riveted Bridge members by Fisher written in 1990 [15].

Test setup The test in this paper describes the testing of three different types of specimens.The tests conducted are all four point bending tests, with variable spans and stress ranges among the tests. The dimensions of the parameters stated in Figure 4.1 are given in Table 4.1.

Table 4.1: Dimensions test Fisher 1990

I.D	Length A [mm]	Length B [mm]	Length C [mm]
1 - 2	1524	3048	7620
3 - 4	1524	1908	5340
5 - 7	1524	3048	7620
8 - 14	1524	3198	7920

Tested section Three types of sections were tested in the study conducted by Fisher [15]. The first section tested in this articles has the dimensions as shown on figure 4.2(a) this section concerns the tests with Identification number 1 through 8. The rivets are placed in an alternating pattern, the exact locations of the rivets are not specified in the article. The location of the rivets on the beams are extracted from the pictures taken during the experiments Both the L-profile connection with the web and flange has the alternating pattern of two rows of rivets. A figure of the rivet configuration is shown in Figure 4.3.

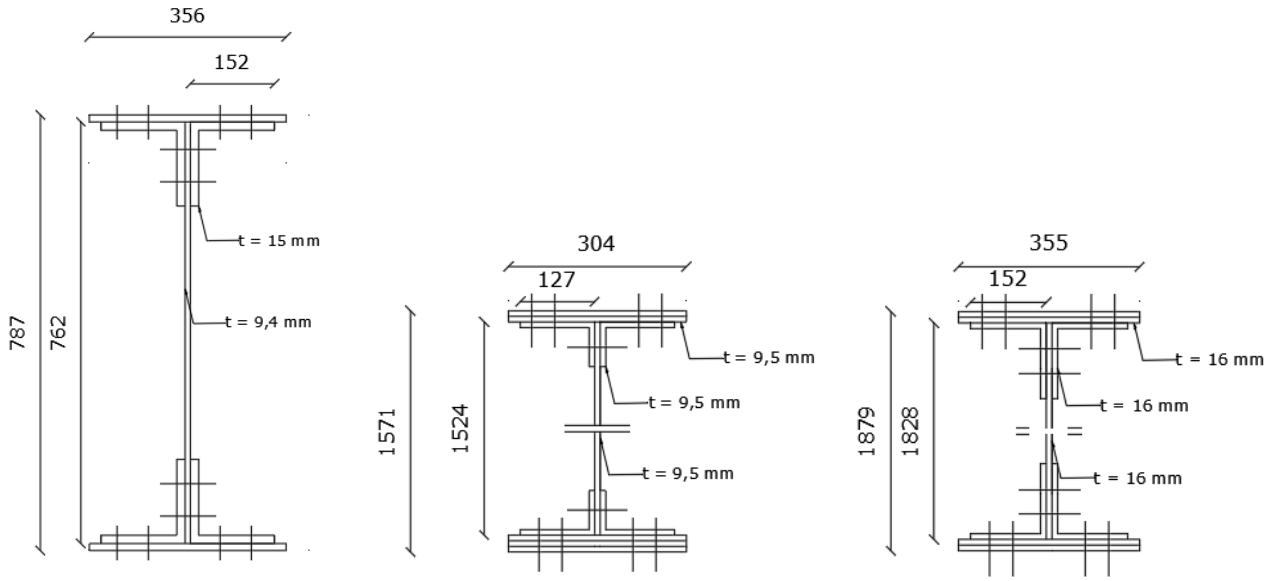

(a) Section 1-8 (b) Section 9-12 (c) Section 13-14

Figure 4.2: Sections Fisher

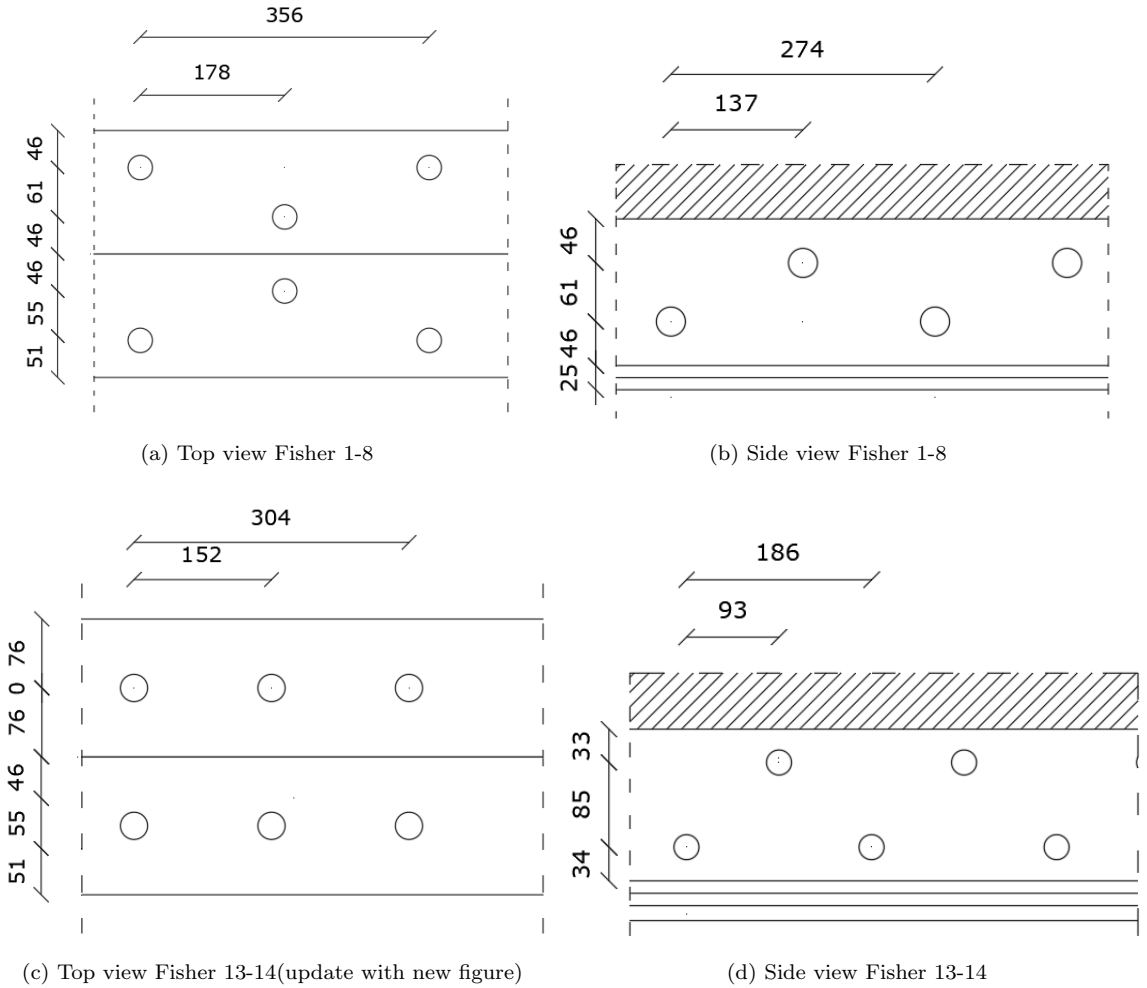

(a) Top view Fisher 1-8

(b) Side view Fisher 1-8

(c) Top view Fisher 13-14(update with new figure)

(d) Side view Fisher 13-14

Figure 4.3: Top and side views members Fisher

Section The section on figure 4.2(b) shows the section of the second set of tests. This concerns tests 12 - 14. the section has two cover-plates on the topside of the section and three-cover plates on the bottom side of the section. The connection between the L-profile and the cover-plates has an alternating pattern of two rows of rivets. The connection between the L-profile and the web has one single row of rivets. Exact dimensions of these beams is not extracted from the data, since the failure modes of these beams are not related.

The last section of the paper is shown in figure 4.2(c). This is the section of the tests with ID 13 and 14. These members have one row of rivets in the flange, and an alternating pattern of rivets in the web. The top view of the member is shown in Figure 4.3(c), and the side view of the members is shown in figure 4.3(d).

Failure criteria In the fatigue failure data, two types of measurements are collected, at first when the crack initiation starts, this number of cycles is taken at the first observed crack. Secondly, the number of cycles to complete failure of the beam where there is no resistance left.

Stress section calculation The net section stress is calculated through the use of the moment range and the net section modulus of the section. this means the net section stress shown in the figure is the stress at the most outer fiber. Using the formula $\Delta\sigma_{net} = M_r/W_{net}$. The paper states no further use of stress concentrations within the calculation of the net section stress.

Fatigue loading The forces applied on the beams are listed in Table 4.2. Along with the minimal section stress, maximal section stress and the net section stress range.

Table 4.2: Force range per test

I.D.	ΔF [Kn]	σ_{min} [MPa]	σ_{max} [MPa]	$\Delta\sigma$ [MPa]	**I.D.**	ΔF [Kn]	σ_{min} [MPa]	σ_{max} [MPa]	$\Delta\sigma$ [MPa]
1	356	14	142	128	**8**	467	55	221	166
2	396	14	131	117	**9**	187	14	200	186
3	467	14	111	97	**10**	400	55	309	254
4	489	14	122	108	**11**	400	97	318	221
5	445	55	199	144	**12**	254	14	268	254
6	423	55	193	138	**13**	463	55	208	153
7	400	14	161	147	**14**	414	55	217	162

Test data Table 4.3 shows the data collected from the article. The values marked in red indicate that there is no failure related to this research. The beam did not fail or initiated cracks at rivet holes in these tests.

Table 4.3: Test data Fisher, 1990

I.D.	$\Delta\sigma_{net}$ [MPa]	N_{ini}	N_{fail}	Failure mode	Failure zone	rivet no.
1	128	588000	916000	Rivet hole flange	Linear moment zone	
2	117	1094000	1237000	Rivet hole flange	Constant moment region	3rd rivet
3	97	1435000	1623000	Rivet hole flange	Constant moment region	1st rivet
4	108	2630000	2836000	Rivet hole flange	Constant moment region	3rd rivet
5	144	2344000	2728000	Rivet hole flange	Constant moment region	5th rivet
6	138	2575000	3005000	Rivet hole flange	Constant moment region	5th rivet
7	147	601000	773000	Rivet hole flange	Constant moment region	6th rivet
8	166	923000	1315000	Rivet hole flange	Constant moment region	6th rivet
9	186	0	415000	Static test	N/a	
10	254	471000	512000	Corroded section	Coverplate termination	
11	221	522000	657000	Corroded section	N/a	
12	254	0	827000	Corroded section	N/a	
13	153	3568000	3613000	Rivet hole flange	Constant moment region	
14	162	1446000	1563000	Rivet hole flange	Constant moment region	

The data of this table is visualized in the scatter-plot as seen in Figure 4.4.

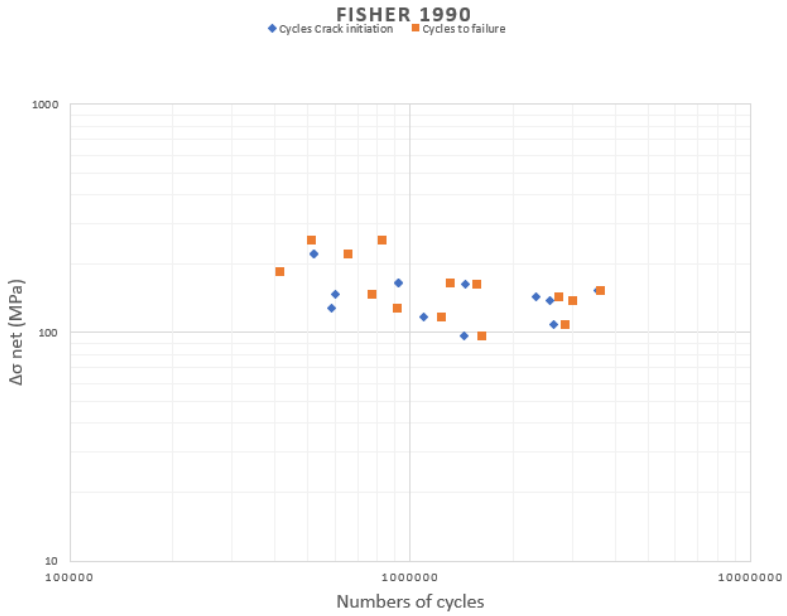

Figure 4.4: Fatigue data Fisher-1990

4.2 Test data Bruhwiller

The data collected in this chapter is found in the paper Fatigue and fracture of riveted bridge members by Bruhwiller in 1990 [7].

Test setup In this paper, three types of beams are tested. For this research, two of those are relevant. The first test (a) is conducted on a rolled girder (HEB1000) with a rivet connected bottom cover plate, the second test (b) consists of a built-up girder connected with rivets. The dimensions of the tests are given in Table 4.4.

Table 4.4: Dimensions tests Bruhwiller

I.D	Length A [mm]	Length B [mm]	Length C [mm]
A.i	3100	3340	9780
B.i	1500	650	2800

Tested sections Tested specimens marked with 'A' are four point bending test with a span of 9780mm. The height of the section is a HEB1000 beam with a cover plate of 450x18 connected with rivets to the bottom flange. The section is on Figure 4.5(a). The rivets are placed at a center to center distance of 220mm, with a rivet hole diameter of 21mm.

Tested beams marked with 'B' are four point bending test with a span of 2800mm. the height of the section is a 600mm web with four 70x8 L-profiles connected with rivets. The cross section is shown on Figure 4.5(b). the spacing of the rivets in longitudinal direction is 130mm, with a rivet hole diameter of 19mm. It is assumed for this paper that the placement of the rivets is halfway on the L-profile at 35mm.

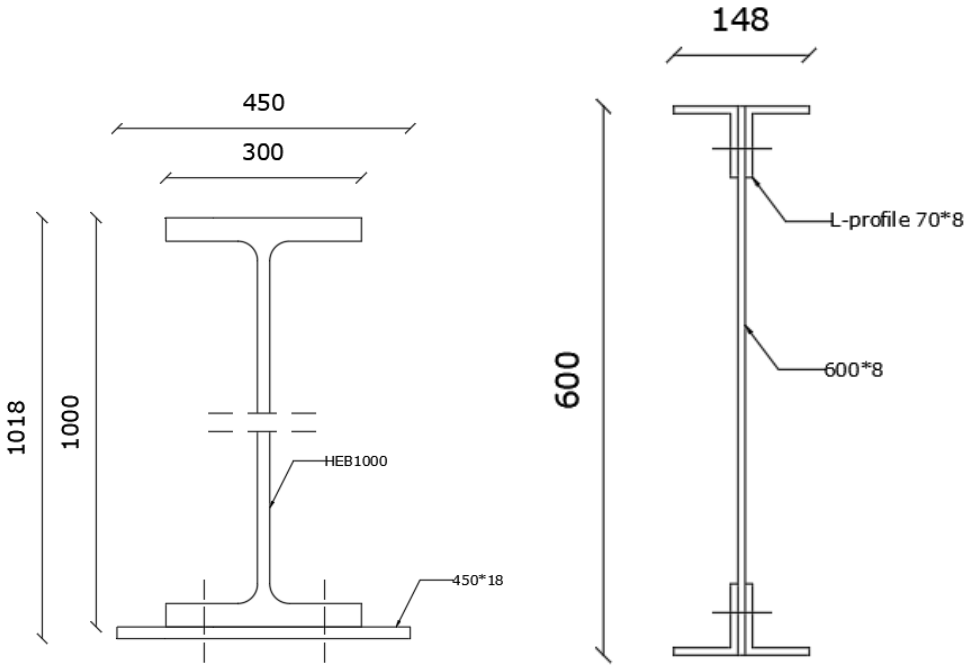

(a) Section "A" tests (b) Section "B" tests

Figure 4.5: Section A and B Bruhwiller

Failure criteria In the research, one type of data is described: the number of cycles to failure of the beam. The failure of the beam is assumed when the increase of the deflection of the girder reaches 0,2mm due to the cyclic loading. at this stage, cracks were growing so quickly the difference between this value and complete failure would be insignificant.

Section stress calculation Net-section stresses are calculated employing methods of analysis typically employed by design engineers [7]. More information is not given on the methods used. No further use of stress concentrations are used to process the values of the net section stress.

Fatigue loading The beams are subjected to a constant amplitude of four or nine hertz, with a ratio of loading of 0.1. Per test subject, the force range of the test is varied, which is shown as the net section stress range in the test data.

Test data The test data collected from the tests conducted by Bruhwiller [7] are collected in Table 4.5. Only the numbers of cycles to failure of the beam is collected, since data for crack initiation is not known. all of the failure of the members is in the constant moment zone of the beam, and crack initiation started at the rivet hole.

Table 4.5: Test data Bruhwiller

I.D.	$\Delta\sigma_{net}$	N_{ini}	N_{fail}	Failure mode	Failure zone	rivet no.
A.1	120	No data	920000	Rivet hole flange	Constant moment region	Unknown
A.2	120	No data	720000	Rivet hole flange	Constant moment region	Unknown
A.3	120	No data	970000	Rivet hole flange	Constant moment region	Unknown
A.4	90	No data	3240000	Rivet hole flange	Constant moment region	Unknown
A.5	90	No data	3040000	Rivet hole web	Constant moment region	Unknown
A.6	90	No data	1900000	Rivet hole web	Constant moment region	Unknown
B.1	79	No data	7270000	Rivet hole web	Constant moment region	Unknown
B.2	90	No data	1840000	Rivet hole web	Constant moment region	Unknown
B.3	85	No data	3590000	Rivet hole web	Constant moment region	Unknown
B.4	78	No data	4840000	Rivet hole web	Constant moment region	Unknown

The results from the tests data are collected in the scatter-plot as shown in Figure 4.6. In this figure, only one set of data is plotted, the numbers of cycles to failure. The numbers of cycles to crack initiation is not known for this source. The blue data represents 'Series A', the H-profile with additional flange. The orange data represents 'Series B', which is the build-up girder.

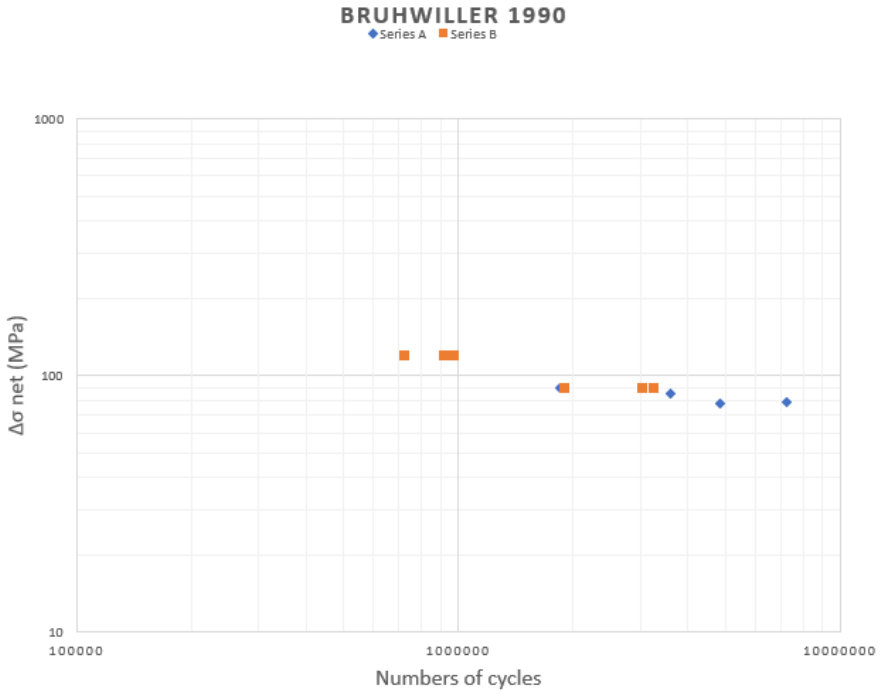

Figure 4.6: Fatigue data Bruhwiller

4.3 Test data Adamsson

The data collected in this chapter is found in the paper 'Fatigue Tests of Riveted Bridge Girders' by Adamsson in 1995 [18].

Test setup Six specimens are tested in this paper, the test objects are stringers obtained from an old dismantled railway bridge. These stringers are loaded in four-point bending. With a span of 7620 mm. Exact dimensions of the test setup are not given in the paper, the distance from the support to the point of force application is derived from pictures of the setup given in the paper.

Table 4.6: Dimensions tests Adamson

I.D	Length A [mm]	Length B [mm]	Length C [mm]
All tests	2540	2540	7620

Tested section One type of section is tested in this paper. The beam is a built-up girder from a plate 1200x9,5 with four added L profiles, connected with rivets. The cross section is shown in Figure 4.7. Rivet holes in longitudinal direction are located 43 mm from the toe of the flange and spaced 102 mm apart. Test ST1-ST7 and ST9 are in normal orientation, where test object ST8 is in inverted direction compared to the other test specimens.

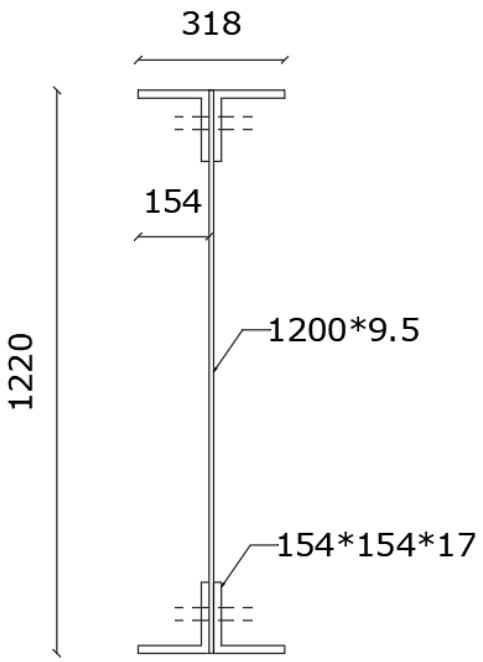

Figure 4.7: Section Adamson

Fatigue loading No information on the magnitude of the forces or minimum maximum stresses is given in the paper.

Failure Criteria Two types of data are collected in this paper. The number of cycles to the first visible crack, and failure the number of cycles to failure. Failure in these tests is assumed when one component was composedly severed by a fatigue crack, and new cracking was detected in another component.

Section stress calculation The net section stress, as shown in Table 4.7 is calculated with the use of strain gauges. These strain gauges are connected to the bottom flange of the section. From this strain the stress at the outer fibre is calculated, and with reduction of the rivet holes, the net section stress is determined. The deduction of the rivet holes only applies to the tensile side of the section, compression force is assumed to flow directly through the rivet shank [18].

Test data The data from the paper is collected in Table 4.7. The values marked with an added 's' in the beam I.D. describe an second failure mode within the beam. In these stringers, the beam had an extra area where crack initiation started, these cracks initiated in the shear zone of the beam.

Table 4.7: Test data Adamson, 1995

I.D.	$\Delta\sigma_{net}$	N_{ini}	N_{fail}	Failure mode	Failure zone	rivet no.
ST9	69	2486070	3336700	Rivet hole flange	Not specified	Not specified
ST3	73	No data	1874730	Rivet hole flange	Not specified	Not specified
ST4	69	1521450	2168570	Rivet hole web	Not specified	Not specified
ST7	66	2364230	3240180	Heel side rivet hole	Not specified	Not specified
ST8	66	7577300	2017640	No failure	N/a	Not specified
ST2	63	No data	12178930	No failure	N/a	Not specified
ST7s	61	No data	3213710	Vertical leg	Not specified	Not specified
ST8s	61	No data	10850670	Vertical leg	Not specified	Not specified
ST8i	73	No data	8073460	Gross section	Not specified	Not specified

Test data The test data is visualized in Figure 4.8. The data from the crack initiation is not known for each tested member. The known data is plotted in the figure. Data in Table 4.7 given in red is not plotted in the graph. This data is not applicable for the research since there is either no failure, or it is a different failure mode of the beam.

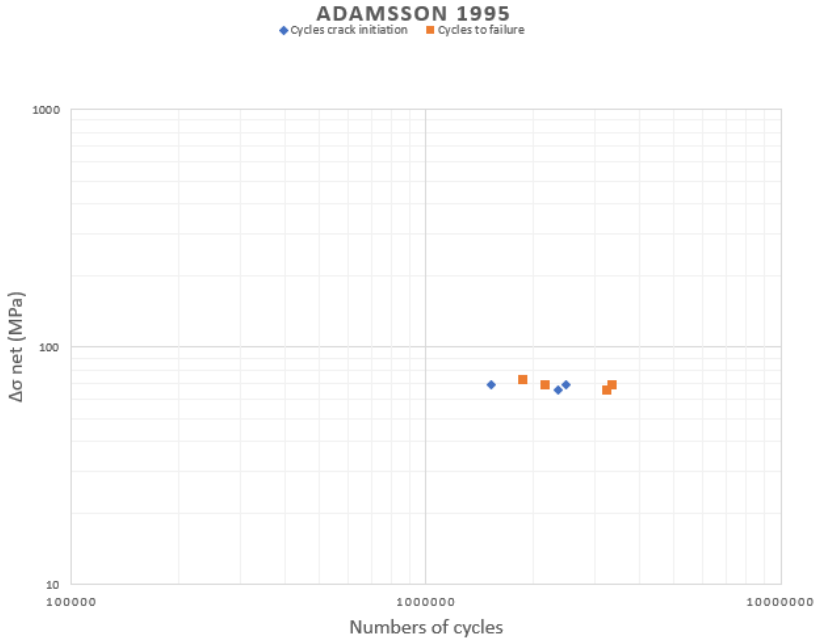

Figure 4.8: Fatigue data Adamsson

4.4 Test data Baker

The data collected in this chapter is found in the paper Fatigue of Riveted Connections by Baker in 1985[6].

Test setup The tested objects in this paper are built-up lattice girders with the chords and diagonals connected with rivets. These lattice girders are tested in a tensile test. The girders are cut longitudinal in half, so the tensile force is applied to one set of L-profiles. These L-profiles are connected, along with the with the partially cut diagonals, with rivets. The stress applied will cause stress concentrations near the rivet holes.

Tested section The tested section are 2 L-profiles 152*89*10. connected by a rivet with a partially cut-off diagonal, as in the original configuration of the beam.

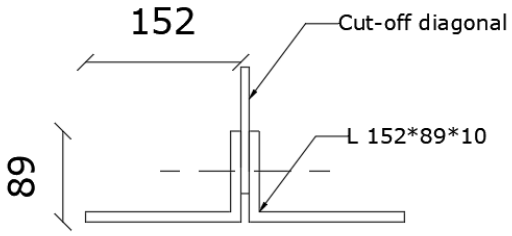

Figure 4.9: Section Baker

The rivets are located on the x-axis of the beam in groups of two rivets. the center to center distance between the two grouped rivets is 83mm, the distance in between the groups is 1016mm. The used Rivets have a diameter of 20mm.

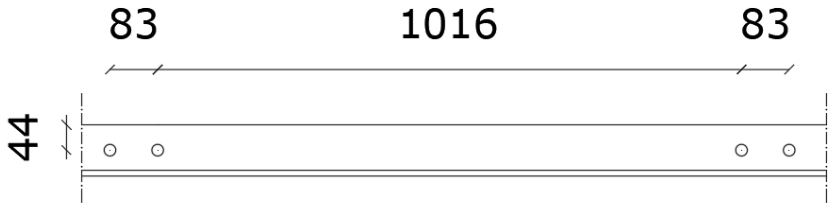

Figure 4.10: Side view Baker

Fatigue loading Testing of the members is done with a gross stress range of 138 MPa. the minimum stress in all of the tests is 20 MPa with a maximum stress of 158 MPa. The net section stress range of the type "A" members is 31 MPa - 188 MPa. The net section stress range of the type "B" members is 23 - 166 MPa

Failure criteria Two types of results are given in the research. The number of cycles to the first observed crack and the number of cycles to failure. Failure in the tests is assumed when one of the connections fractured, which causes the tests to stop automatically. For this particular data set, only the numbers of cycles to failure are given.

Section stress calculation The net section stress of the beam is calculated through the use of strain gauges. The gauges measure the strain at the gross cross section. the net section stress are derived by the ratio's between the gross section area and the net section area (and using modulus of elasticity).

Test data The collected test data is shown in Table 4.8. The tests, in contrary to the other tests, is a tensile test. The normal stress distribution over the length of the beam is constant, the location of the failed rivet is thus not of interest and not collected in the data.

Table 4.8: Test data Baker, 1985

I.D.	$\Delta\sigma_{net}$	N_{ini}	N_{fail}	Failure mode
ARS-1a	188	No Data	418500	Rivet hole web
ARS-1b	188	No Data	418500	Rivet hole web
ARS-1c	188	No Data	958300	Rivet hole web
ARS-2a	188	No Data	782300	Rivet hole web
ARS-2b	188	No Data	793600	Rivet hole web
ARS-2c	188	No Data	911800	Rivet hole web
BRS-3a	166	No Data	263100	Rivet hole web
BRS-3b	166	No Data	493300	Rivet hole web
BRS-4a	166	No Data	249100	Rivet hole web
BRS-4b	166	No Data	352800	Rivet hole web
BRS-4c	166	No Data	485200	Rivet hole web

The data is visualized in the data plot as seen in Figure 4.11.

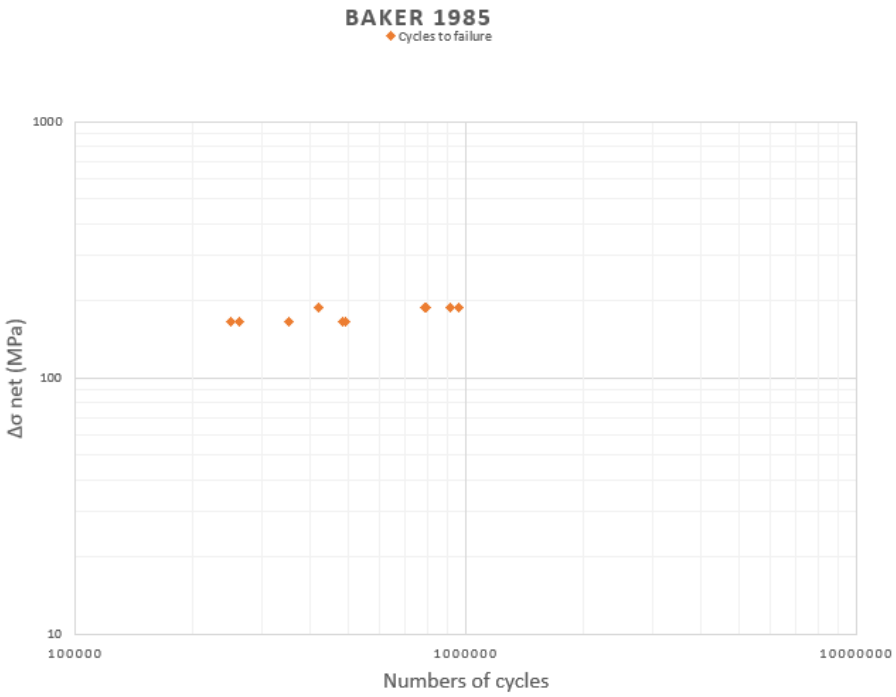

Figure 4.11: Scatterplot Baker

4.5 Test data DiBattista

The data collected in this chapter is found in the paper Fatigue of Riveted Tension Members by DiBattista in 1995 [13].

Test setup The tested members are tension diagonals retrieved from a bridge. Four diagonals were removed, and cut transversely to obtain eight specimens. only seven of these specimens are tested for one of the members was damaged during preparation. The members are tested in an axial tension fatigue test.

Tested section The tested member is a build-up beam from a flange of 356 mm in height with four L-profile 152x89x11mm connected through rivets. The rivets have a diameter of 22mm. the cross section is shown in Figure 4.12. Each test was loaded in an axial fatigue test. The net section stress is calculated through the use of strain gauges placed at mid length of the section.

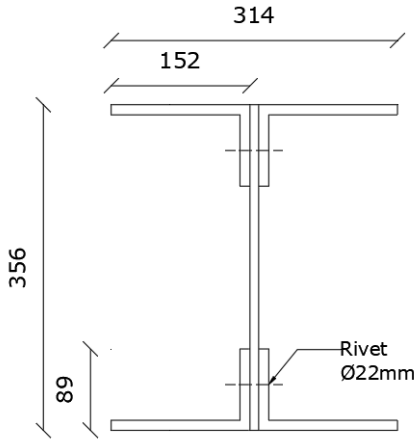

Figure 4.12: Section DiBattista

Failure criteria Two sets of data are collected, the number of cycles to crack initiation. This is defined as the first visual detected crack. Detection of the cracks is done by naked eye, or with a magnifying glass. Secondly, the number of cycles to failure. The beam is assumed to be failed when one element of the built up cross section is severely damaged and the first detection of a crack in a second element is detected.

Section stress calculation The section stress calculation is carried out through the use of strain gauges. These gauges are placed in the middle of the length of the member. Because the strain gauges are not placed in the proximity of the critical detail, crack initiation did not effect the measurements. With the strain, the gross section area stress is determined. The net section stress is calculated using the strain and the net section area of the member.

Fatigue loading The minimum loading: $\sigma_{min} = 10$ MPa for all of the tested members. No further information is given on the method of loading for these tests.

Test data collected test data is shown in Table 4.9

Table 4.9: Test data DiBattista, 1995)

I.D.	$\Delta\sigma_{net}$	N_{ini}	N_{fail}	Failure mode
BD1	73	1509710	2401580	Rivet hole flange
BD2	69	2655330	3958270	Rivet hole flange
BD3	73	2273500	Test stopped	Rivet hole flange
BD4	66	3722300	5250610	Rivet hole flange
TD1	64	1735140	1944670	Web
TD2	62	2415840	2415840	Rivet hole flange
TD3	58	2415140	2415140	Rivet hole flange

With the data plotted in Figure 4.13. Test BD3 did initiate initial cracks, however it did not reach the failure criterion of this test, this test was stopped before the beam reached complete failure.

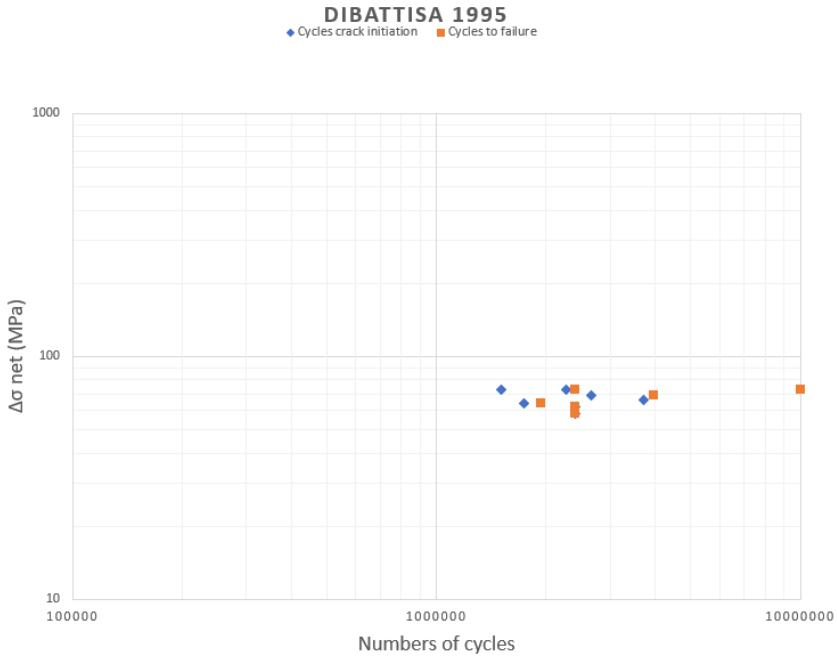

Figure 4.13: Fatigue data DiBattisa

4.6 Test data Akesson

The data collected in this chapter is found in the paper Fatigue life of Riveted Steel Bridges by Akesson in 2010 [31].

Test setup The stringers are tested with a four point bending test. The in-between distance of the load-points is 2,0 meters. The span of the test is either 4,0 or 5,0 meters. The distance for each test is indicated in the data set.

Table 4.10: Dimensions tests Akesson

I.D	Length A [mm]	Length B [mm]	Length C [mm]
6B, 7A, 12A	1000	2000	4000
2A, 3B, 5B	1500	2000	5000
4B, 5A, 10B	1500	2000	5000

Tested section The tested members all have the same cross-section. The beam is a built-up plate girder with four L-profiles connected with rivets to a plate with a height of 830mm. The connection is one row of Rivets, located 40mm from the outer fibre of the beam. The cross section is shown in Figure 4.14.

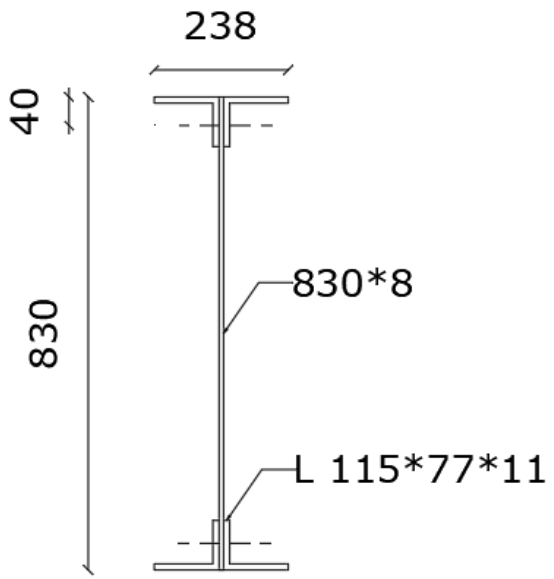

Figure 4.14: Section Akesson

Failure criteria Two types of data are found in the paper. The number of cycles to crack initiation. This is taken as the number of cycles until the first observed crack. secondly, The number of cycles to failure, which is defined as 'complete fracture of the lower tension flange' [31], where both L-profiles completely fractured.

Section stress calculation The stress of the net section area in Table 4.12 is calculated using the stress in the most outer grain of the section instead of the actual rivet location. Net section stress is calculated using the applied bending moment and the section modulus of the net section area. $\sigma = M_r/W_{net}$.

Fatigue loading This paper gives a clear description of the forces and stresses used in testing, the minimum and maximum force, with the corresponging net section area stress are given in Table 4.11.

Table 4.11: Forces and stresses tests Akesson

I.D	F_{min} [kN]	F_{max} [kN]	σ_{min} [MPa]	σ_{max} [MPa]
6B, 7A	44,1	138,3	12,8	52,8
12A	44,1	207,3	12,8	72,8
2A, 3B, 5B	29,4	213,6	12,8	92,8
4B, 5A, 10B	88,3	318,7	38,4	138,4

Test data The test data from the article is collected in Table 4.12. The data marked in red indicates that there was a run out of the test, thus no failure occurred in this stress range.

Table 4.12: Test data Akkeson, 2010

I.D.	$\Delta\sigma_{net}$	N_{ini}	N_{fail}	Failure mode	Failure zone	rivet no.
6B	40	No data	20000000	No Failure	Unknown	Unknown
7A	40	No data	20000000	No Failure	Unknown	Unknown
12A	60	No data	10000000	No Failure	Unknown	Unknown
2A	80	5893400	5995900	Rivet hole web	Unknown	Unknown
3B	80	2375500	2375500	Rivet hole web	Unknown	Unknown
5B	80	6485300	6485300	Neck rivet	Unknown	Unknown
4B	100	1637900	1637900	Rivet hole web	Unknown	Unknown
5A	100	2184900	2184900	Rivet hole web	Unknown	Unknown
10B	100	2027300	2027300	Rivet hole web	Unknown	Unknown

Figure 4.15 shows the plotted data. In this test the crack initiation and the failure of the beam are very close in value. The run out test data is not plotted since no failure occurred, and thus having no further relevance for the research.

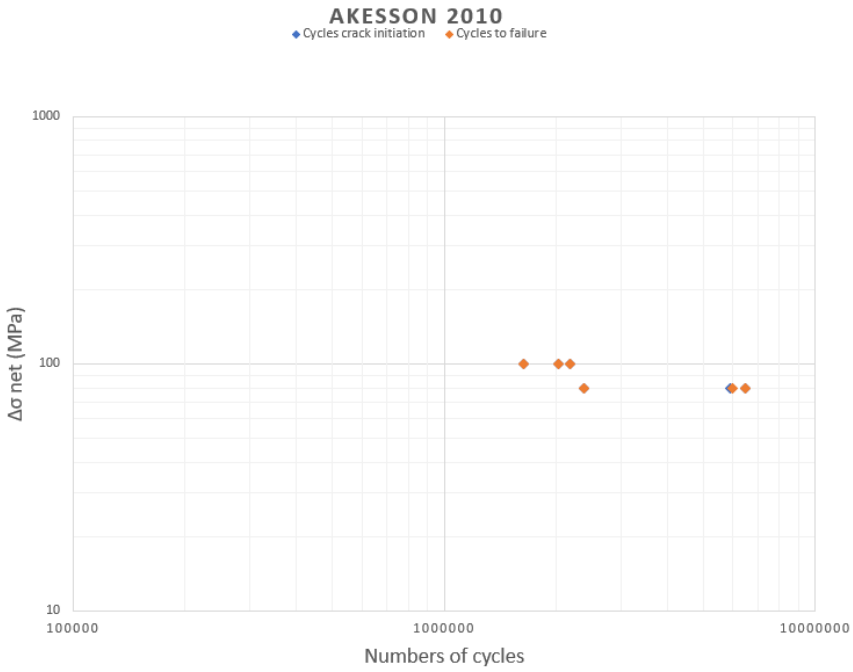

Figure 4.15: Fatigue data Akesson

4.7 Test data Al-Emrani

The data collected in this chapter is found in the paper Fatigue in Riveted Railway bridges by Al-Emrani in 2002 [3].

Test setup Test members are taken from an old railway bridge over the Vindeläven in Sweden. From this bridge 36 stringers and 9 floor-beams were detached and taken to the lab for testing. The stringers consist of four L-profiles riveted to an 8 mm thick web plate [3]. 24 of these specimens were tested in axial tension tests which showed a characteristic yield point of 256 MPa. Six stringers were tested in a four point bending test. Dimensions of the test are shown in Table 4.13.

Table 4.13: Dimensions tests Al-Emrani

I.D	Length A [mm]	Length B [mm]	Length C [mm]
All tests	2000	1250	4500

Tested section The tested section consists of a web plate with a height of 830mm and a thickness of 8mm. on this web profile four L-profiles are connected through rivets. Dimensions of these L-profiles are L115x77x11mm. The tested section is shown in Figure 4.16. The side view and test setup is shown in Figure 4.17 [3].

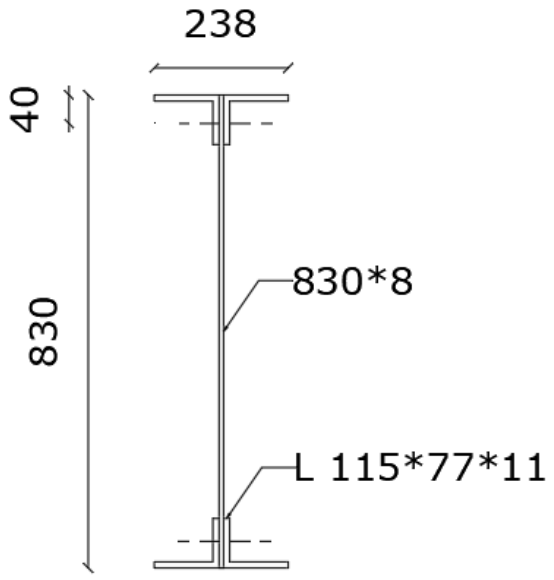

Figure 4.16: Section Al-Emrani

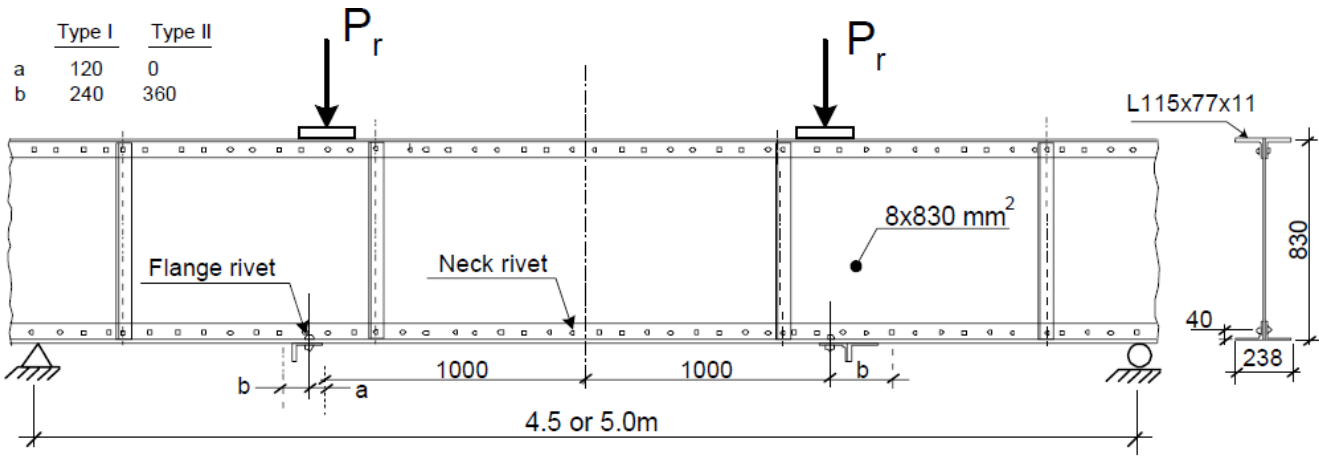

Figure 4.17: Test setup Al-Emrani

Failure criteria Three values are given in this research. The number of cycles to the first detected crack, number of cycles to fracture of the first L-profile, and total failure of the beam.

Section stress calculation The stress range is calculated in the outermost fibre of the stringer. This stress range is based on the net-section of the riveted girder, meaning the area of the rivet hole is subtracted from the gross area.

Fatigue loading Fatigue loading is described in Table ??. In this research after crack initiation stop-holes were drilled to arrest fatigue cracking. When a crack tip location as marked the test was temporarily stoppped and a holes was drilled, no further measures were taken to improve the surface [3].

Table 4.14: Loading test Al-Emrani

Stringer	Load-step 1			Load-step 2	
bla	σ_r	R	$N \cdot 10^6$	σ_r	R
1A	-	-	-	100/60	0,16
3A	-	-	-	100	0,16
12B	60	0,18	10	97	0,16
10A	60	0,20	10	97	0,20
12A	60	0,18	10	100	0,16
11B	60	0,20	20	93	0,2

Test data Paper states the crack initiation in all stringers occurred from a rivet hole. In one of these stringers (3A) crack initiation started in the flange rivet. The rest of the stringers failed in the neck rivet in the constant moment region. The failure fatigue data is shown in Table ??. No further information on the governing rivet in longitudinal direction is given in the paper.

Table 4.15: Fatigue data Al-Emrani

Stringer	σ_r	N_{detect}	N_{fract}	$N_{failure}$	**Failure mode**	**Failure zone**
1A	100 (60)	3920700	5571150	6426750	Rivet hole web	Constant moment region
3A	100	1725120	1840000	2002000	Flange rivet	Constant moment region
12B	97	5799020	5799020	$>$ 5959340	Rivet hole web	Constant moment region
10A	97	586700	$<$ 586700	704090	Rivet hole web	Constant moment region
12A	100	368500	872600	1134280	Rivet hole web	Constant moment region
11B	93	3280000	3639050	3692050	Rivet hole web	Constant moment region

The data is plotted in Figure 4.18.

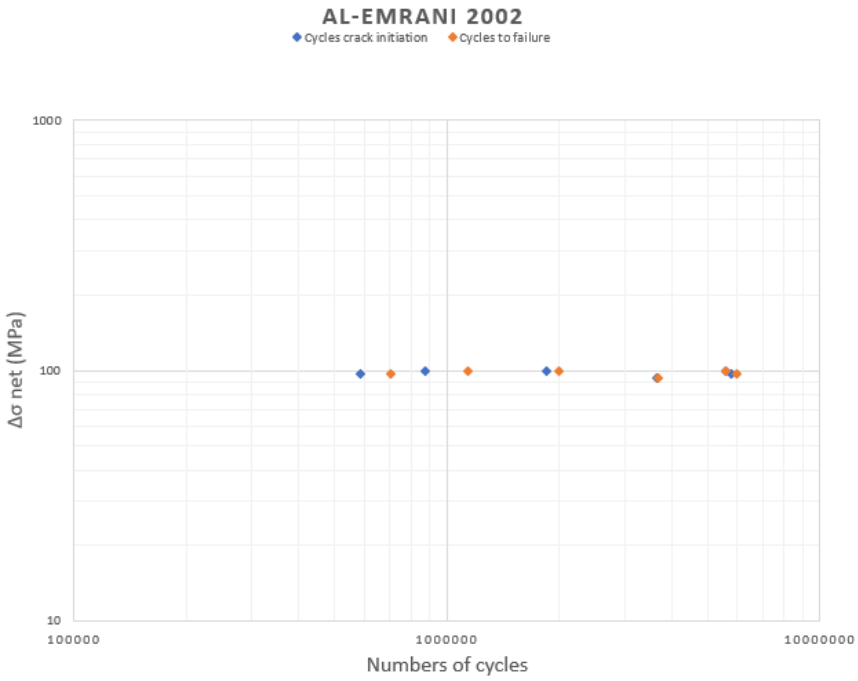

Figure 4.18: Fatigue data Al-Emrani

4.8 Test data Out

The data collected in this chapter is found in the paper Fatigue Strength of Weathered and Deteriorated Riveted Members by Out in 1984 [18].

Test setup The members tested in this paper are six built-up beams from the French Broad Ivy River Bridge. The sections are built-up from a web with a height of 1000mm and four L-profiles connected by two rows of rivets to the web. The length of the beam when cut from the bridge is 6100mm. The beams are tested in a four-point bending setup. The distance between the two load-points was 1530mm.

The state of the beams was variable, some of the flanges were severely corroded. Which reduces the thickness of the section, which causes stress concentrations. The results given in the paper separate two types of failures. One in which the corroded sections are included, and one set of data from which the failure of corroded sections is excluded. For this research, only the second set of data is relevant.

Table 4.16: Dimensions tests Out

I.D	Length A [mm]	Length B [mm]	Length C [mm]
2A, 3B, 5B	1530	2285	6100

Tested section The tested section in this paper is shown in Figure 4.19. The section height is 1000x12,7mm with four L-profiles 152x152x12,7mm. The rivet holes have a drilled diameter of 23,8mm and are spaced 152,4mm apart. Rivet hole configuration shown on the right side of Figure 4.19 [25].

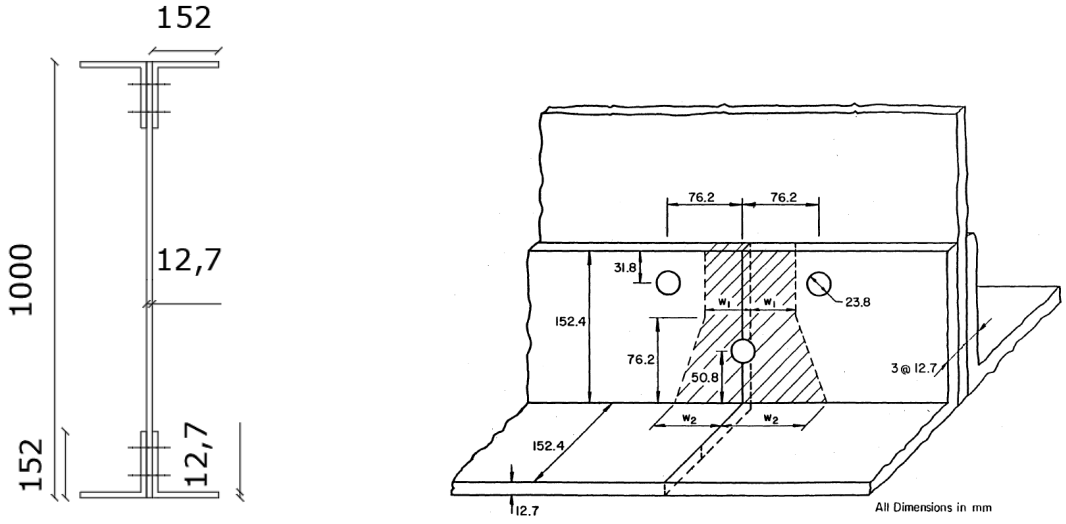

Figure 4.19: Tested section Out

Failure criteria Two sets of data are collected from this paper, the number of cycles to which the first cracks are found. And the number of cycles to complete failure of the section. A precise definition of the failure definition is not given.

Section stress calculation No specification on the methods used for the net section stress calculation is given. It is assumed the section stress range is calculated in the outer fibre of the section.

Fatigue loading The used stress ratio R used in all of the tests: $\sigma_{min}/\sigma_{max} = 0,1$

Test data The test data is shown in the Table 4.17, the data marked in red is not considered in the research. These failures did not occur due to increased stresses due to the rivet hole. Either failure because of a reduced area due to corrosion, or a change in test conditions caused the test to be stopped prematurely.

Table 4.17: Test data Out, 1984

I.D.	$\Delta\sigma_{net}$	N_{ini}	N_{fail}	Failure mode	Failure zone	rivet no.
1	75,2	3770000	4990000	Through corroded area	Constant moment zone	Not specified
2	64,8	850000	1450000	Through corroded area	Constant moment zone	Not specified
3	63,4	No data	3790000	Through corroded area	Constant moment zone	Not specified
4	57,2	1190000	7610000	Section spliced	Constant moment zone	Not specified
1	65,9	6520000	18250000	Rivet hole flange	Constant moment zone	Not specified
2	59,3	3650000	36500000	Rivet hole web	Constant moment zone	Not specified
3	56,2	1826000	38690000	Rivet hole flange	Constant moment zone	Not specified

Figure 4.20 shows the plotted fatigue data for this paper. Only the relevant tests are plotted. Sections failed due to a reduced area by corrosion are not plotted.

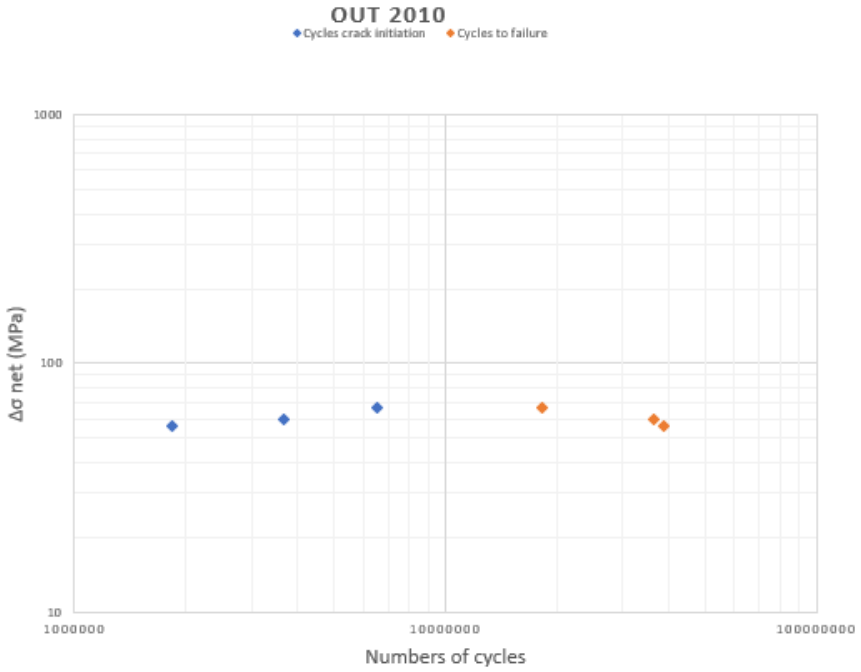

Figure 4.20: Fatigue data Out

4.9 Additional test data

The test data found here is extracted from the paper 'Fatigue assessment of riveted bridges by Tobias Larsson [20]. The original papers are not available for further processing of the data.
Fatigue Strength of Corroded Step Plates from Old Railway Bridges (Abe, 1989)

Test data The test data in Table 4.18 is retrieved from a source which collected fatigue data, no further information on dimensions is known. Only test data regarding cycles to failure is given. It is not known what the criterion for failure in this particular case is.

Table 4.18: Test data Abe, 1989

I.D.	$\Delta\sigma_{net}$	N_{ini}	N_{fail}
1	130	No data	90000
2	100	No data	100000
3	120	No data	170000
4	100	No data	450000
5	79	No data	800000
6	100	No data	1000000
7	74	No data	1100000
8	77	No data	1300000
9	81	No data	2000000

With the data plotted in Figure 4.21.

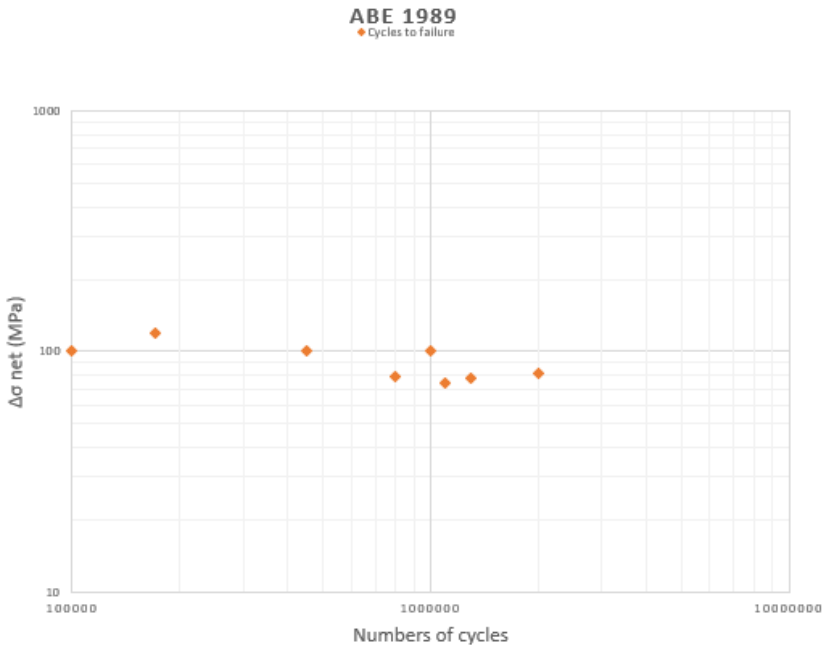

Figure 4.21: Fatigue data Abe

Application of the S-N Line Concept for the Assessment of the Remaining Fatigue Life of Old Bridges (Mang, 1993)

Test data The test data in Table 4.19 is retrieved from a source which collected fatigue data, no further information on dimensions is known. Only test data regarding cycles to failure is given. It is not known what the criterion for failure in this particular case is.

Table 4.19: Test data Mang, 1993

I.D.	$\Delta\sigma_{net}$	N_{ini}	N_{fail}	**I.D.**	$\Delta\sigma_{net}$	N_{ini}	N_{fail}
1	87	No Data	120000	**8**	140	No Data	2100000
2	130	No Data	1500000	**9**	195	No Data	650000
3	130	No Data	2000000	**10**	150	No Data	5000000
4	110	No Data	10000000	**11**	180	No Data	32000
5	180	No Data	280000	**12**	180	No Data	60000
6	140	No Data	780000	**13**	125	No Data	390000
7	140	No Data	1300000	**14**	95	No Data	2900000

With the data plotted in Figure 4.22.

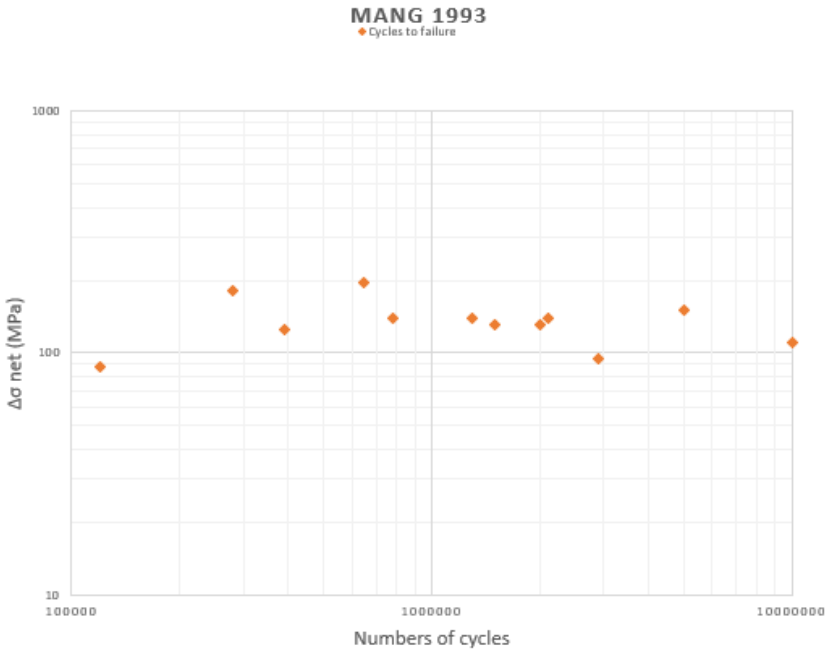

Figure 4.22: Fatigue data Mang

4.10 Complete data

In Figure 4.23 a complete set of data from earlier collected sources is combined into a single plot.

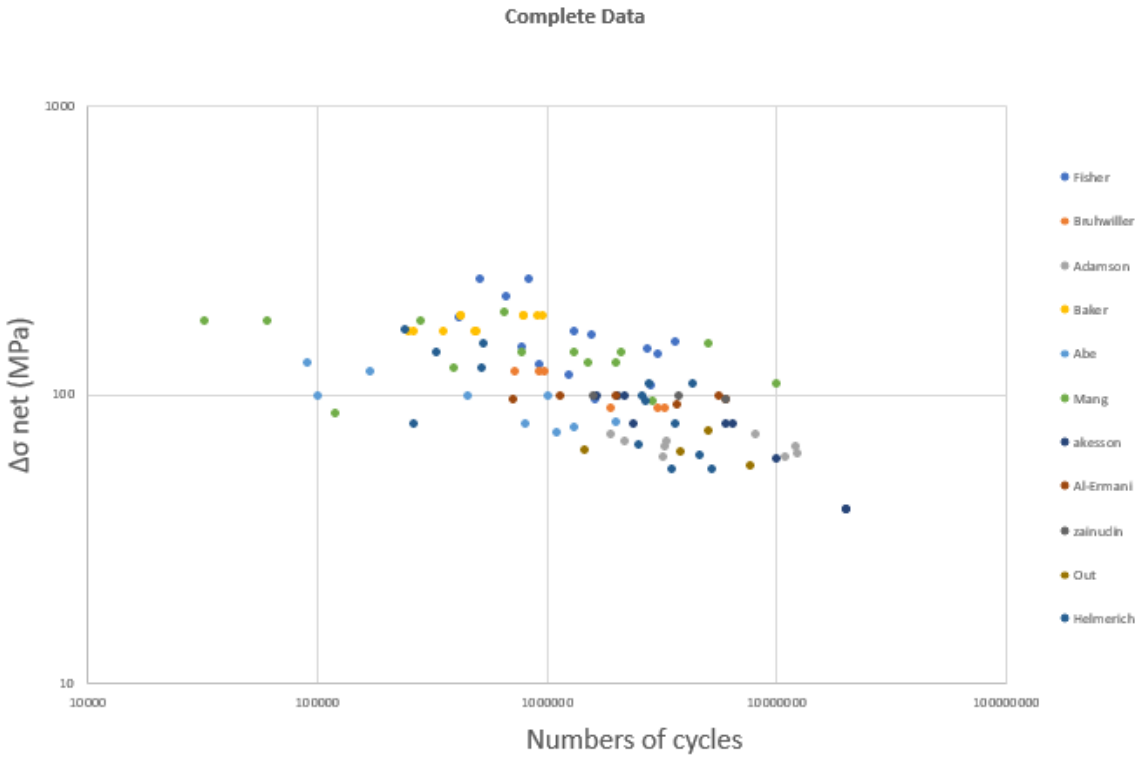

Figure 4.23: Complete data set

Bibliography

[1] *Eurocode 3: design of steel structures : part 1-5 : plated structural elements*. BSI, London, 2010. Incorporating corrigendum April 2009. 3, 13

[2] T. Adrian and V. Daniel. *Idealization of riveted joints*, volume Degree Project 2012:02. Chalmers university. 17

[3] M. Al-Emrani. Fatigue performance of stringer-to-floor-beam connections in riveted railway bridges. *Journal of Bridge Engineering*, 10(2):179–185, 2005. 45, 46

[4] ANSYS. Contact defaults in workbench and ansys. 2004. 22, 23

[5] ANSYS. Cworkbench - mechanical structure nonlinearities. 2009. VII, 23

[6] K.A. Baker and G.L. Kulak. *Fatigue Strength of Two Steel Details*. Structural engineering report. Department of Civil Engineering, University of Alberta, 1982. 38

[7] E. Bruhwiller, I.F.C. Smith, and M.A. Hirt. Fatigue and fracture of riveted bridge members. *Journal of Structural Engineering*, 116, january 1990. 32, 33

[8] F.C. Campbell. *Fatigue and fracture: understanding the basics*. ASM International, 2012. 2, 4, 6

[9] J. Carvill. *Mechanical engineer's data handbook*. Butterworth-Heinemann, 1994. 9, 10

[10] Ansys Convergence Conferences. Best practices for contact modeling using ansys. 2016. 22

[11] R.D. Cook. Finite element modeling for stress analysis. *John Wiley & Sons, ISBN: 0-471-10774-3*, 1995. V, V, V, V, 19, 20, 21

[12] B Cornell and L Darby. Correlation of anaylysis and test data to the effect of fastener load transfer on fatigue. In *6th Aircraft Design, Flight Test and Operations Meeting*, page 983, 1974. 16

[13] J.D. DiBattista, D.E.J. Adamson, and G.L. Kulak. Fatigue strength of riveted connections. *Journal of structural engineering*, 124(7):792–797, 1998. 40

[14] S. Dosman. Use and abuse of the stress severity factor. 2019. 8, 15

[15] J.W. Fisher, B.T. Yen, and D. Wang. Fatigue strength of riveted bridge members. *Journal of structural Engineering*, 116(11):2968–2981, 1990. 28

[16] T. R. Gurney. *Fatigue of welded structures*. CUP Archive, 1979. 1, 4

[17] J. Kim, J. Yoon, and B. Kang. Finite element analysis and modeling of structure with bolted joints. *Applied mathematical modelling*, 31(5):895–911, 2007. 18

[18] G.L. Kulak and D.E.J. Adamson. Fatigue tests of riveted bridge girders. 1995. 4, 35, 36, 48

[19] C. Lalanne. *Mechanical vibration and shock analysis, fatigue damage.* John Wiley & Sons, 2010. 5, 6

[20] T. Larsson. *Fatigue assessment of riveted bridges.* PhD thesis, Luleå tekniska universitet, 2009. 5, 50

[21] Y. Lee, J. Pan, R. Hathaway, and M. Barkey. *Fatigue testing and analysis: theory and practice*, volume 13. Butterworth-Heinemann, 2005. 4

[22] C. Maas. *Stress Intensity Factors of cracked riveted joints.* 2018. 13

[23] P.L. Moore and G. Booth. *The welding engineer's guide to fracture and fatigue.* Elsevier, 2014. 1

[24] C. Niu. *Airframe structural design: practical design information and data on aircraft structures.* Conmilit Press, 1988. 12, 16

[25] J.M. Out. The fatigue strength of weathered and deteriorated riveted members. 1984. 48

[26] W.D. Pilkey and D.F. Pilkey. *Peterson's stress concentration factors.* John Wiley & Sons, 2008. 10, 12

[27] J. Schijve. Fatigue of structures and materials in the 20th century and the state of the art. *International journal of fatigue*, 25(8):679–702, 2003. 4

[28] K.N. Shivakumar. *Stress concentrations for straight-shank and countersunk holes in plates subjected to tension, bending, and pin loading*, volume 3192. National Aeronautics and Space Administration, Office of Management, 1992. 12

[29] O. Sunar. Contact types and behaviours in ansys. *http://www.Mechead.com*, 1995. VII, 22

[30] T. Swift. Faa-air-90-01–repairs to damage tolerant aircraft. *Federal Aviation Administration (FAA), Atlanta, Georgia*, 1990. 15

[31] B. Åkesson. *Fatigue life of riveted steel bridges.* 01 2010. 42

Article	Girder no.	Support distance [mm]	Distance between forces [mm]	Section Height [mm]	force range [kN]	Δσ net [MPa]	Cycles crack initiation [-]	Cycles to failure [-]	Failure mode	zone	Note
Fisher 1990	**1**	7620		787,4	356	128	588000	916000	Through rivet hole	Constant moment region	
	2	7620		787,4	396	117	1094000	1237000	Through rivet hole	Constant moment region	
	3	5340		787,4	467	97	1435000	1623000	Through rivet hole	Constant moment region	
	4	5340		787,4	489	108	2630000	2836000	Through rivet hole	Constant moment region	Low temperature
	5	7620		787,4	445	144	2344000	2728000	Through rivet hole	Constant moment region	
	6	7620		787,4	423	138	2575000	3005000	Through rivet hole	Constant moment region	
	7	7620		787,4	400	147	601000	773000	Through rivet hole	Constant moment region	
	8	7920		787,4	467	166	923000	1315000	Through rivet hole	Constant moment region	
	9	7920		1562,1	187	186	0	415000	Fracture under static proof test		
	10	7920		1562,1	400	254		512000	Coverplate termination		pre existing damage (reduced section due to corrosion
	11	7920		1562,1	400	221	522000	657000	At corrosion		
	12	7920		1562,1	254	254	0	827000	At corrosion		
	13	7920		1879,6	463	153	3568000	3613000	Through rivet hole	Constant moment region	
	14	7920		1879,6	414	162	1446000	1563000	Through rivet hole	Constant moment region	Low temperature
											increased stress range from 60
Bruhwiller	**1**	2800		600		120	No data	920000	Through rivet hole	Constant moment region	Mpa after no failure
riveted built	**2**	2800		600		120	No data	720000	Through rivet hole	Constant moment region	
up girders	**3**	2800		600		120	No data	970000	Through rivet hole	Constant moment region	Net section values calculated by
	4	2800		600		90	No data	3240000	Through rivet hole	Constant moment region	methods typically employed by
	5	2800		600		90	No data	3040000	Hole in flange	Constant moment region	design engineers
											increased stress range from 60
	6	2800		600		90	No data	1900000	Through rivet hole	Constant moment region	Mpa after no failure
Rolled Girder	**1**	9780		1018		79	No data	7270000	Through rivet hole	Constant moment region	
	2	9780		1018		90	No data	1840000	Through rivet hole	Constant moment region	HEB 1000 with extra flange on
	3	9780		1018		85	No data	3590000	Through rivet hole	Constant moment region	tensile side
	4	9780		1018		78	No data	4840000	Through rivet hole	Constant moment region	
Adamson	**ST9**			1220		69	2486070	3336700	Through rivet hole		
Stringers	**ST3**			1220		73	1	1874730			initial crack not recorded
	ST4			1220		69	1521450	2168570	Through rivet hole		toe side critical detail
	ST7			1220		66	2364230	3240180	Through rivet hole		
	ST8			1220		66		12017640	No failure		
	ST2			1220		63		12178930	No Failure		
	ST7s			1220		61		3213710		Shear region	
	ST8s			1220		61		10850670		shear region	
	ST8i			1220		73	7577300	8073460			inverted position
Baker	**BkC-1s**					188		418500	cracks started at rivet holes		sigma min 31 Mpa
	BkC-1b					188		418500	cracks started at rivet holes		sigma min 31 Mpa
	BkC-1c					188		958300	cracks started at rivet holes		sigma min 31 Mpa
	BkC-2a					188		782300	cracks started at rivet holes		sigma min 31 Mpa
	BkC-2b					188		793600	cracks started at rivet holes		sigma min 31 Mpa
	BkC-2c					188		911800	cracks started at rivet holes		sigma min 31 Mpa
	Bkd-3a					166		263100	cracks started at rivet holes		sigma min 23 Mpa
	Bkd-3b					166		493300	cracks started at rivet holes		sigma min 23 Mpa
	BkD-4a					166		249100	cracks started at rivet holes		sigma min 23 Mpa
	BkD-4b					166		352800	cracks started at rivet holes		sigma min 23 Mpa
	BkD-4c					166		485200	cracks started at rivet holes		sigma min 23 Mpa
Abe	**1**					130		90000			sigma min 12 Mpa
	2					100		100000			sigma min 12 Mpa
	3					120		170000			sigma min 12 Mpa
	4					100		450000			sigma min 12 Mpa
	5					79		800000			sigma min 12 Mpa
	6					100		1000000			sigma min 12 Mpa
	7					74		1100000			sigma min 12 Mpa
	8					77		1300000			sigma min 12 Mpa
	9					81		2000000			sigma min 12 Mpa
Mang	**1**					87		120000			Test on whole bridge
full scale test	**2**					130		1500000			
	3					130		2000000			
	4					110		10000000			
	5					180		280000			
	6					140		780000			
	7					140		1300000			
	8					140		2100000			
	9					195		650000			
	10					150		5000000			
	11					180		32000			
	12					180		60000			
	13					125		390000			
	14					95		2900000			
Akesson	**A1**	5000	8300	92,2/138,3		40		20000000	No failure		
Stringers	**A2**	5000	8300	92,2/138,4		40		20000000	No failure		
	A3	4000	8300	207,3		60		10000000	No failure		
	A4	5000	8300	184,2		80	5893400	5995900			net section stress calculated at
	A5	5000	8300	184,2		80	2375500	2375500			outermost edge of beam not at
	A6	5000	8300	184,2		80	6485300	6485300			actual rivet locations
	A7	5000	8300	230,4		100	1637900	1637900			
	A8	5000	8300	230,4		100	2184900	2184900			
	A9	5000	8300	230,4		100	2027300	2027300			
Al-Ermani	**A1-1**					100	5571150	5571150			
	A1-2					100	1840000	2002000			
	A1-3					97	5799020	5959340			
	A1-4					97	586700	704090			
	A1-5					100	872600	1134280			
	A1-6					93	3639050	3692050			
Zainudin	**KAD-1**					100		3712020			
	KAD-2					100		1587110			
	KAD-3					97		5959340			
Out	**1**	6100	1530	1000		75,2	3770000	4990000	Section failed		
Corroded	**2**	6100	1530	1000		64,8	850000	1450000	Section failed		Corroded section failure
	3	6100	1530	1000		63,4		3790000	No failure		
	4	6100	1530	1000		57,2	1190000	7610000	Section spliced		
Rivet detail	**1**	6100	1530	1000		65,9	6520000	18250000	crack at rivet hole		Only cracks not affected by
	2	6100	1530	1000		59,3	3650000	36500000	crack at rivet hole		cracking of corroded section
	3	6100	1530	1000		56,2	1826000	38690000	crack at rivet hole		included
Helmerich	**10**					170		240000			Test on trusses
Truss girders	**11**					80		260000			Test on trusses
	12					140		330000			Test on trusses
	13					125		520000			Test on trusses
	14					150		530000			Test on trusses
	15					67		2517000			Test on trusses
	16					100		2600000			Test on trusses
	17					95		2700000			Test on trusses
	18					110		2800000			Test on trusses
	19					80		3600000			Test on trusses
	20					55		3500000			Test on trusses
	21					110		4300000			Test on trusses
	22					62		4600000			Test on trusses
	23					55		5180000			Test on trusses
DiBattisa	**BD1**	n/a		n/a		73	1509710	2401580	crack at rivet hole		
axial tension	**BD2**	n/a		n/a		69	2655330	3958270	crack at rivet hole		
	BD3	n/a		n/a		73	2273500	9999999	crack at rivet hole		Stress measurement by strain
	BD4	n/a		n/a		66	3722300	1	crack at rivet hole		gauges mid section
	TD1	n/a		n/a		64	1735140	1944670	crack at rivet hole		
	TD2	n/a		n/a		62	2415840	2415840			
	TD3	n/a		n/a		58	2415140	2415140			
Baker	**RS-1a**	3060		200		137,9	418500		crack at rivet hole		sigma min 20 MPa
1982	**RS-1b**	3060		200		137,9	418500		crack at rivet hole		sigma min 20 MPa
	RS-1c	3060		200		137,9	958300		crack at rivet hole		sigma min 20 MPa
	RS-2a	3060		200		137,9	782300		crack at rivet hole		sigma min 20 MPa
	RS-2b	3060		200		137,9	793600		crack at rivet hole		sigma min 20 MPa
	RS-2c	3060		200		137,9	911600		crack at rivet hole		sigma min 20 MPa
	RS-3a	3060		200		137,9	263100		crack at rivet hole		sigma min 20 MPa
	RS-3b	3060		200		137,9	496300		crack at rivet hole		sigma min 20 MPa
	RS-4a	3060		200		137,9	249100		crack at rivet hole		sigma min 20 MPa
	RS-4b	3060		200		137,9	352800		crack at rivet hole		sigma min 20 MPa
	RS-4c	3060		200		137,9	485200		crack at rivet hole		sigma min 20 MPa